1949

Calibration, validation and operation of the CMS Barrel Muon Position Monitoring System

PhD Thesis

Béni Noémi Tekla

Supervisor: Dr. Bencze György

University of Debrecen
Doctoral Committee of Natural Sciences and Information Technology
Doctoral School of Physics

Debrecen, 2019

Készült
a Debreceni Egyetem Fizikai Tudományok Doktori Iskolájának
Részecskefizika programja keretében
az Atommagkutató intézetben

Prepared at
the University of Debrecen PhD School in Physics
and the Institute for Nuclear Research

Ezen értekezést a Debreceni Egyetem Természettudományi és Informatikai Doktori Tanács Fizikai Tudományok Doktori Iskola Részecskefizika programja keretében készítettem a Debreceni Egyetem természettudományi doktori (PhD) fokozatának elnyerése céljából. Nyilatkozom arról, hogy a tézisekben leírt eredmények nem képezik más PhD disszertáció részét.
Debrecen, 2019. december 18.

Béni Noémi Tekla
jelölt

Tanúsítom, hogy Béni Noémi Tekla doktorjelölt 2006-2019 között a fent megnevezett Doktori Iskola Részecskefizika programjának keretében irányításommal végezte munkáját. Az értekezésben foglalt eredményekhez a jelölt önálló alkotó tevékenységével meghatározóan hozzájárult. Nyilatkozom továbbá arról, hogy a tézisekben leírt eredmények nem képezik más PhD disszertáció részét.
Az értekezés elfogadását javasolom.

Debrecen, 2019. december 18.

Dr. Bencze György
témavezető

CALIBRATION, VALIDATION AND OPERATION OF THE CMS BARREL MUON POSITION MONITORING SYSTEM

Értekezés a doktori (Ph.D.) fokozat megszerzése érdekében
a fizika tudományágban

Írta: Béni Noémi Tekla okleveles fizikus

Készült a Debreceni Egyetem Fizikai Tudományok Doktori Iskolája
Részecskefizika programja keretében

Témavezető: Dr. Bencze György

A doktori szigorlati bizottság:

elnök:	Dr. Zilizi Gyula	.....
tagok:	Dr. Krasznahorkay Attila	.....
	Dr. Fodor Zoltán	.....

A doktori szigorlat időpontja: 2019. április 25.

Az értekezés bírálói:

	Dr.	.....
	Dr.	.....

A bírálóbizottság:

elnök:	Dr.	.....
tagok:	Dr.	.....
	Dr.	.....
	Dr.	.....
	Dr.	.....

Az értekezés védésének időpontja: 20… . …… … .

Contents

Chapter 1

Introduction

The aim of the present thesis is to describe my work on the construction, installation, commissioning, validation and operation of the position monitoring (called also alignment) system of the Barrel Muon Spectrometer of the CMS (Compact Muon Solenoid) experiment located in the P5 experimental hall of the CERN (Conseil Européen pour la Recherche Nucléaire) LHC (Large Hadron Collider) accelerator.

The Barrel Muon Spectrometer is composed of 250 large scale (different, but typically 2.5 m x 3 m) particle detector chambers distributed over a cylindrical volume of 7 m in radius and 14 m in length. For the correct and efficient physics analysis of events recorded by the CMS experiment the positions of the barrel muon detector chambers have to be known with respect to each other with submillimeter-submilliradian precision. Since the mechanical structure of the detector is deformed by the thermal effects and the applied strong (3.8 T) magnetic field, a position monitoring system was built which is able to run permanently and determine the actual positions of the barrel muon chambers. This position information is essential for a good muon momentum resolution which is needed for all physics analyses where the final state of the created particles are muons. For example the standard model Higgs boson and Z boson mass measurement is affected by the good muon momentum measurement that is depending very much on the good geometry information of the muon detectors. Therefore the position information provided by the alignment system is used for corrections of the CMS geometry during the physics analysis.

Besides the considerable size, the large number of objects to be observed and the high precision required there are additional circumstances that make the system construction difficult. Such factors are the radiation background, the already mentioned strong magnetic field, or practical aspects like the very limited access to the elements of the system (typically once per year) and the requirement to keep the cost reasonably low. It should be underlined that one of the most demanding requirements to the position monitoring system is that it has to be absolute in the sense that it should provide the positions of the barrel muon chambers in the barrel reference and not only detect displacements. The ability of the system to provide the absolute positions of the barrel muon detector chambers is especially important at the restart of the CMS operation after the end-of-year maintenance during which the detector elements are usually moved.

The work on the barrel muon position monitoring system started in 1995. The necessary R&D work, the development of the concept and the design of the system lasted six years. The construction, installation and commissioning took another seven years. Given the complexity of the system the total construction cost of 1.3 MCHF and the time spent was regarded as reasonable and has fully been endorsed by the CMS collaboration.

The system is operational and providing measured data since 2008. This raw data is the input for the geometry reconstruction of the 6D positions of the individual detector chambers inside the barrel muon spectrometer. The reconstruction is based on the opto-geometrical model describing the elements of the position monitoring system and the connections between them. Two types of connections are used: calibrated and monitored. The calibrated connections are fix distances and orientations between some of the elements. They are measured (calibrated) once, during the construction. The monitored values are the results of the measurements during operation. In the Barrel Muon Position Monitoring system all the monitored connections are video-camera - LED pairs.

As the number of connections is significantly exceeding the number of degrees of freedom of the system, the calibrated and measured connections are composing a very robust and redundant network capable to work even in case of the failure of one or two elements and provide correct position data (local decrease of precision around the failing element is possible).

Based on the experience obtained during the first four years of work a system upgrade took place in 2013. The period of upgrade also enabled us to perform studies concerning the stability of the system by remeasurement of the critical calibrated connections.

The whole work was done by a team composed of members from the University of Debrecen, Institute for Nuclear Research alias Atomki (Debrecen), Wigner RCP (Budapest, former Researh Institute for Particle and Nuclear Physics) in collaboration with CERN and -for a dedicated task- with HEPHY (Wien, Austria). So far two PhD and 11 diploma works fully or partially dedicated to the project have been defended in Debrecen. I am the member of this collaboration since 2002 and have taken part practically in all phases of the work. In this document I include only those tasks in which my involvement was decisive.

The dissertation is organized as follows:

The first three chapters (2 to 4) are descriptive, they help to explain the tasks and problems to be solved and introduce the necessary terms and information. Thus, in the second chapter CERN, LHC and CMS are introduced very briefly. The third chapter is describing the barrel muon spectrometer to the level necessary for the understanding of the following chapters. Also, the general questions of alignment are discussed here. The fourth chapter is devoted to the detailed description of the barrel muon position monitoring system, its layout, the description of the elements of the system, the question of control, operation and the opto-geometrical reconstruction of the barrel muon chamber positions.

The following chapters are devoted to the detailed description of my work and the results included in the dissertation. In the fifth chapter the quality control of the video-sensors, in the sixth and seventh chapters the calibration of the camera-boxes and the MABs (Module for the Alignment of the Barrel, see later) are described. The eighth chapter is devoted to the validation of the system by comparing our results to other position data available in CMS. The last (ninth) chapter is examining the results of the geometrical reconstruction from the point of view of the behaviour of the barrel muon spectrometer as a deforming unit.

In Appendices A to D some useful details and additional information are included.

Chapter 2

CERN, LHC, CMS

There is a lot of widely available literature about CERN, the LHC accelerator and the CMS experiment at different levels from popular to professional, from short to very detailed that can be referred to for more information. The very brief chapter here is included mainly to introduce the terminology used later.

2.1 CERN, LHC

CERN, the European Organization for Nuclear Research [1] near Geneva, Switzerland was established by 12 European countries in 1954 not long after the Second World War to unify European scientists working on the peaceful research in nuclear and particle physics. By now this international organization with presently 23 member countries has become the largest scientific laboratory serving for the whole world. Its primary function is to provide different kinds of particle beams for experimental physicists by means of its accelerator complex.

The largest among them, the 27 km long circular accelerator, the LHC (Large Hadron Collider [2], fig. 2.1) started its operation in September 2008, with proton beams at 3.5+3.5 TeV. Then the proton energy and the luminosity increased step by step and after the planned 2013-14 long shut-down (abbreviated as LS1, see Appendix D) reached 7+7 TeV and 10^{34} $cm^{-2}s^{-1}$ respectively.

Four large experiments have been built at four interaction points of the LHC. The ATLAS (A Toroidal LHC Apparatus [3]) and CMS (see in section 2.2)

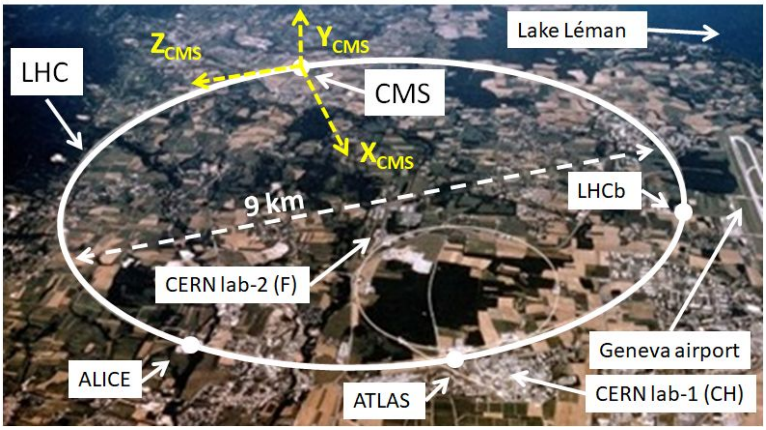

Figure 2.1. The LHC accelerator in Geneva area.

are general purpose experiments studying many different questions of particle physics. There are two specialized experiments: the LHCb (LHC-beauty [4]) investigates the b-quark related physics while ALICE (A Large Ion Collider Experiment [5]) is specialized in the heavy ion physics.

2.2 The CMS experiment

The Compact Muon Solenoid (CMS) [6–9] is one of the two general purpose detectors at the LHC accelerator. Its construction in general follows the earlier, smaller scale experiments installed on collider type accelerators. The peculiarity of CMS is the strong (3.8 T) solenoid magnet. It causes a shorter bending radius for the charged particles thus allowing of building a detector with comparatively smaller volume, in other words a compact detector (compared e.g. to ATLAS). Another pecularity of the CMS detector is the increased importance of the muon detection. A very powerful muon spectrometer with redundant triggering capabilities guarantees a highly performant trajectory measurement for the decay muons and an efficient selection of events relevant for physics studies.

The schematic drawing of the CMS experiment is shown in fig. 2.2. The inner Tracker with the Pixel detector is measuring the particle trajectories close to the collision. The Electromagnetic calorimeters are measuring the energy of photons and electrons while the Hadronic calorimeters still inside

the solenoid and at both sides around the beam pipe are measuring the energy of hadrons.

Muons leaving the solenoid are measured by the muon detectors embedded in the return yoke of the magnet.

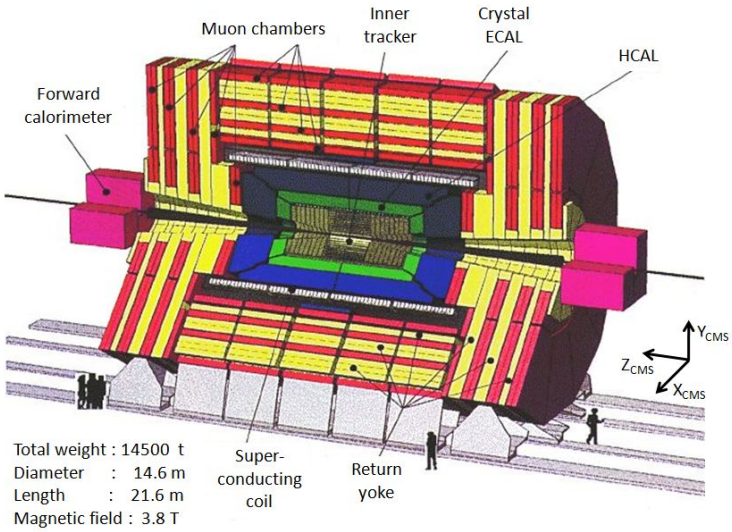

Figure 2.2. The CMS detector.

To achieve the maximum hermeticity (in other words to be able to detect all the relevant particles emerging from the collision) the central, cylindrical part of CMS called "Barrel" is closed by the Endcaps on both sides. The Barrel is composed of five wheels of ∼2.5 m width each. The central wheel is holding the full solenoid with the inner detectors inside. The barrel muon detector chambers are embedded in the iron structure of the wheels. (The barrel muon system is described in more detail in chapter 3). Each of the Endcaps is composed of three (after the LS1 four) iron disks serving as return yoke in the endcap region and carrying the Endcap Muon detector chambers. The first (innermost) disk is also holding the Endcap calorimeters. The modular construction of the CMS experiment is an important (and necessary) consequence of its compactness: the modularity makes it possible to move the big units in the experimental cavern and access the detector elements during maintenance as it is shown in fig. 2.3. These pictures are prepared by the CMS Technical Coordination group for

planning the work during the maintenance period. The heavy modules are moved on a pneumatic airpad system (details in section 10 of [7]).

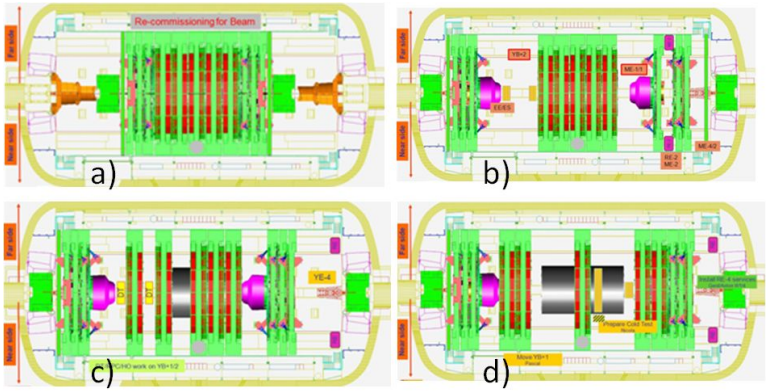

Figure 2.3. The CMS detector at different states from closed (a) to barrel open (d).

Chapter 3

The Barrel Muon Spectrometer of the CMS experiment and the muon alignment strategy

As it follows from the very brief description in section 2.2 the CMS Muon Spectrometer can be split into two different parts from construction point of view: the Barrel and the Endcap. As the geometry as well as the requirements (e.g. the spatial resolution, the number of particles to be detected or the local magnetic field) are different, the technical solutions are also different. In the Endcap region Cathode Strip Chambers (CSC) developed by an American-Russian cooperation are used. More details about the Endcap Muon Spectrometer can be found in [10]. In this chapter I concentrate on the Barrel part of the CMS Muon Spectrometer.

3.1 The Barrel Wheels

As it has been mentioned in section 2.2 the barrel part consists of five wheels. The central one is special in the sense that it holds the full solenoid magnet and the inner detectors (the full tracker with the pixel and the barrel calorimeters). It is the only fix (not movable) module of the CMS experiment centered on the beam interaction point. From the muon detection point of view it is similar to the other wheels: all of them are composed of iron slabs fixed to each other with brackets and functioning as return yoke for the solenoid magnet [11]. The barrel muon detector

chambers are inserted in the slots between the slabs. The structure of the wheels is shown in fig. 3.1.

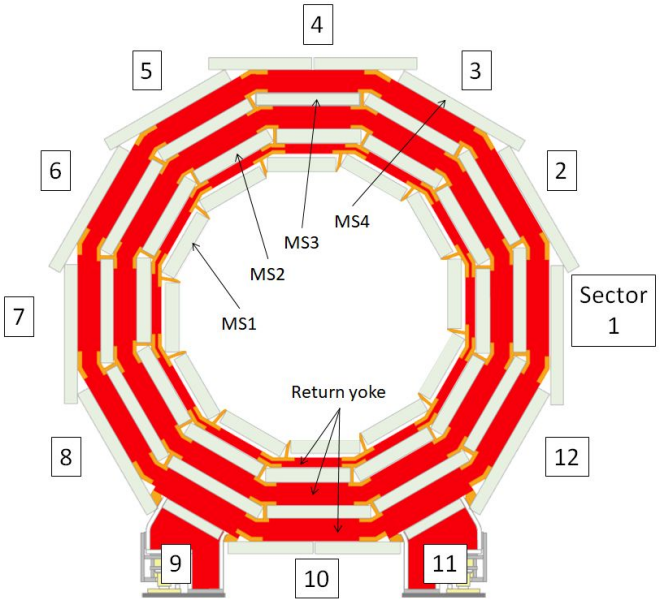

Figure 3.1. The wheel structure seen from the +Z side (MS stands for Muon Station).

Before going into more details it is important to introduce the coordinate systems and the naming conventions used in the CMS Barrel muon system.

The origo of the CMS detector is the theoretical beam interaction point at CMS. The orientations of the CMS axes are connected to the LHC as it is shown in fig. 2.1: the X_{CMS} axis is directed towards the center of LHC. The Z_{CMS} axis is tangential to the beam and oriented towards the ALICE experiment. The azimuthal coordinate ϕ is oriented from the X_{CMS} to Y_{CMS} axis.

The five wheels are named (from -Z to +Z direction) as YB-2; YB-1; YB0 (the central wheel); YB+1 and YB+2. YB stands for "Yoke" and "Barrel". The wheels are divided into twelve 30° sectors numbered from 1 (oriented in the $+X_{CMS}$ axis) to 12 growing in $+\phi$ direction. There are four muon detector chambers in each sector forming four chamber rings called "stations" starting from the innermost (station 1) to the outermost (station

4). A chamber location therefore can be described by the following set: wheel/station/sector.

In fig. 3.2 the picture of the wheel YB+1 can be seen during the installation phase. The red parts are the slabs of the return yoke carrying the Barrel Muon detector chambers that can be seen as aluminium boxes. The black structures are belonging to the Barrel Muon Position Monitoring System and will be described in full detail in chapter 4 and beyond.

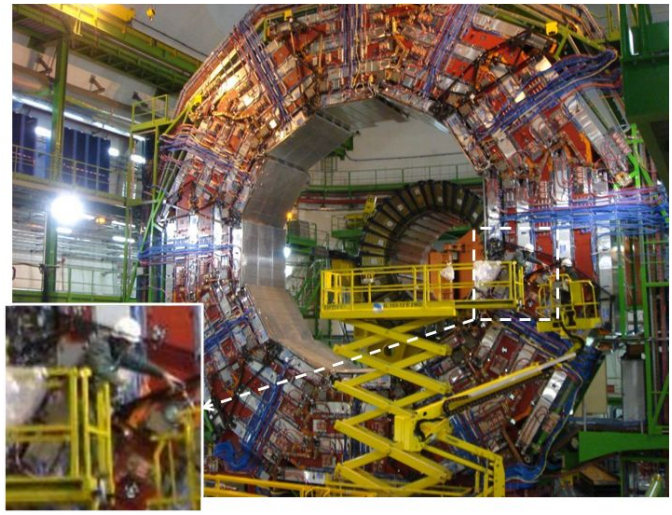

Figure 3.2. A picture from me while working on the wheel YB+1 during the installation phase.

3.2 Drift Tube chambers (DT)

The barrel muon detector chambers (called DT after “drift tube”) were designed, studied and built by an Italian-German-Spanish cooperation. As the particle rate to be detected in the barrel region is low the classical wire chamber [12] solution was a good choice. However, the special requirements following from the enhanced importance of the muon detection in CMS caused special difficulties to be solved such as the very homogenious drift velocity in the drift volume or the bunch crossing identification capability in view of the (max) 350 ns drift time compared to the designed 25 ns bunch crossing sequence.

A picture of two DT chambers on the top of each other located in the preparation hall can be seen in fig. 3.3. The chamber dimensions are as follows: in the Z_{CMS} and radial directions all the chambers are 2536 and 290 mm respectively. The chamber width (in the ϕ_{CMS} direction) varies from 1990 mm (in station 1) to the maximum width of 4190 mm in station 4. It should be noted that the station 4 chambers are not identical and the top and bottom chambers are composed of two smaller chambers placed next to each other (see on fig. 3.1). The reason is rather practical: at the bottom the wheel feet, at the top the overhead crane and the financial need to minimize the cavern height in the experimental hall forced the design to break the rotational symmetry observable for the inner stations.

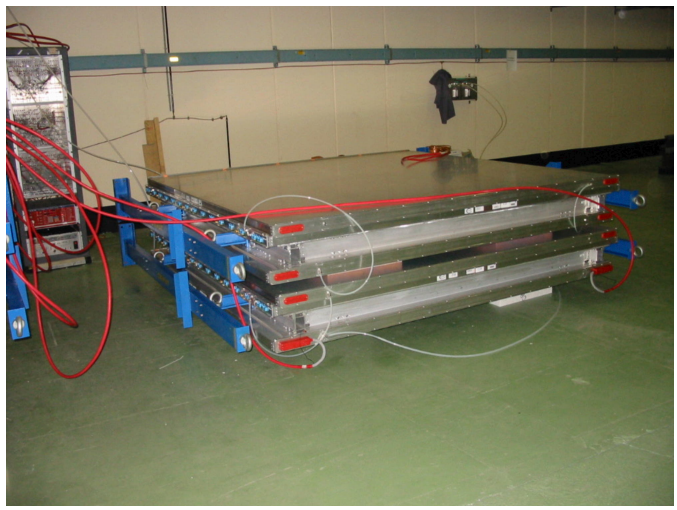

Figure 3.3. DT chambers in the preparation hall.

The r-ϕ cross section of a DT chamber is shown in fig. 3.4. Each DT chamber contains three superlayers. Each of them consisting of four layers of drift tubes staggered by half tube. The two outer superlayers are measuring the particle trajectory in ϕ direction and the lever arm (the distance between them) allows us to create a track segment inside the given muon station. The middle superlayer is rotated by 90^o to measure the particle trajectory in Z direction.

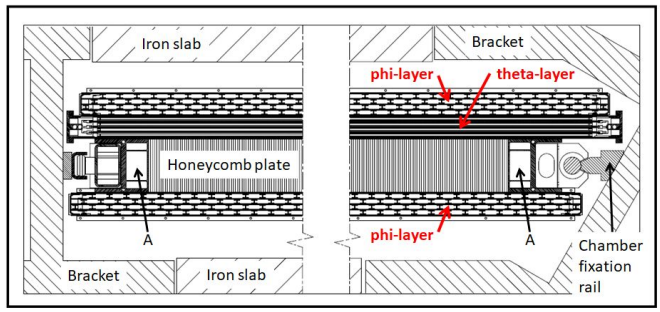

Figure 3.4. The r-ϕ cross section of the DT chamber. A: Alignment passages (discussed in chapter 4).

3.3 Muon detection in the Barrel part

3.3.1 Muon detection in a single cell

A single cell of a DT chamber is shown in fig. 3.5 ([13]).

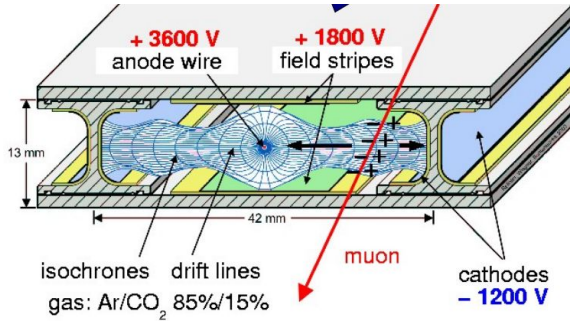

Figure 3.5. A single cell of the DT muon chamber (the picture is taken from [13]).

The primary electrons emerging from the gas atoms ionized by the crossing muon are travelling towards the anode. The time between the bunch crossing producing the muon and the anode signal is measured by a TDC (Time-Digital Converter) and - knowing the speed of drifting electrons - the muon position is calculated. This method requires stable electron drift velocity and good linearity. In the CMS DT chambers the intrinsic single event resolution is 200 μm, the deviation from linearity (optimized by the shaping electrodes) does not exceed 100 μm. The drift speed is

54 μm/ns [10] that is permanently measured by a specially designed drift velocity monitor [14].

3.3.2 Muon detection in a barrel sector

In fig. 3.6 a CMS barrel sector is shown. A muon travelling through the Barrel Muon part is creating hits in the crossed DT cells.

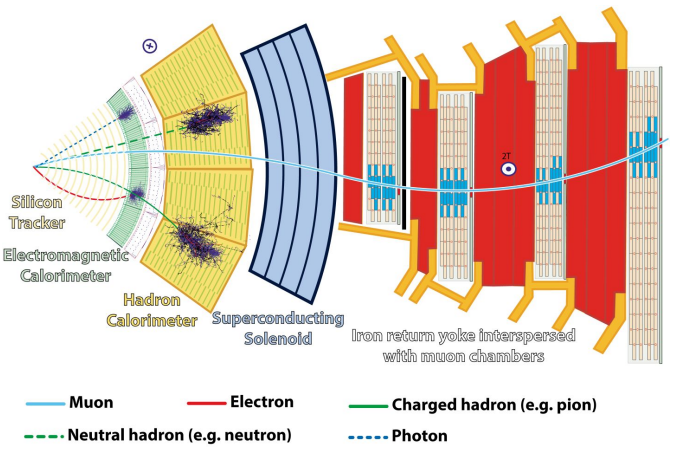

Figure 3.6. Path of particles in CMS.

In ideal case the number of hits is 48. There are many factors, however, that might reduce this number. The single cell efficiency is close to but not 100 %. The muon sometimes can only cross three stations (or even two in case of a low momentum muon or at the Barrel-Endcap transition region). Often the hit cannot be unambiguously identified due to the presence of correlated (event-related) and noncorrelated (radiation) background. These effects had been studied in a dedicated R&D program at CERN called RD5 [15–17] and resulted in the design of a robust and redundant Barrel Muon spectrometer that is able to work efficienly despite the mentioned disturbing factors.

Now we can return to the question of the single cell resolution. It can be derived from the requirement to the global resolution of the Barrel Muon spectrometer. The generally accepted 100 μm value in r-ϕ direction is comparable to the contribution of the multiple scattering up to the transversal momentum (P_T) of 200 GeV/c. At higher momenta, where the global fit of muon and tracker information gives the best performance, the muon detector contribution to the error is of the same order as the one from the tracker. The 100 μm chamber resolution may be achieved by 8

track points measured in the two outer (ϕ) super layers, if the single wire resolution is better than 250 μm [10].

3.4 The muon alignment strategy in CMS

In all the experimental setups where particle trajectories are measured by a series of position sensitive particle detectors located along the particle path the task of alignment naturally occurs. The errors of the detector installation have to be corrected to get the maximum precision in trajectory determination. The process is generally called "alignment" though the detectors are usually not moved after installation but the information on their real positions are used for correction during the physics analysis. As an example the alignment of the muon chambers is clearly improving the dimuon mass resolution as it is explained in [53].

The simplest way to align the detectors is to use straight, preferably high momentum tracks to calculate of both signs. In smaller fix target experiments this takes a short (typically few minutes) data taking time only and the achievable precision is well below the resolution of the detectors to be aligned. The track based alignment is also used in large experiments. In CMS the strategy is first to align the detectors of the Central Tracker with tracks. Then selected particles (typically muons of both signs with $>$50 GeV energy) are propagated to the muon system and used to correct the positions of the muon chambers by minimizing the residuals between the propagated tracks and the muon hits in the muon chambers.

In large experiments, however, there are several factors that make the track based alignment insufficient, especially in the muon part of the detector. These are the possible movements of the detectors during the running period, the difficulty to collect sufficient quantity of tracks in reasonable time (especially in the barrel region), large quantity of material between the tracker and muon system, presence of magnetic field and -as a consequence of these factors- long time (years) to gain enough experience to develop the track based algorithm into a powerful tool. To avoid degradation of physics analysis due to missing or imperfect alignment the CMS collaboration decided from the beginning to build a hardware system that can measure the positions of the muon chambers and follow their movements independently of physics data.

The hardware and track-based alignment methods are not only alternative solutions but also complementing each other [53]:

- The hardware alignment can be operated even when the accelerator is not working. So it is able to provide the starting positions of the chambers before the first physics run. The track-based alignment needs considerable time to collect enough quantity of usable tracks before the alignment algorithm can be applied. It has to be assumed that during the track collection time there are no significant movements in the muon system. This proof can be obtained from the hardware alignment which is capable to detect the position changes quickly and continuously.

- The hardware alignment accuracy has a natural limit due to systematic errors coming from the calibration and statistical (measurement) errors. There are systematic errors as well in the case of the track-based alignment (e.g. the not sufficiently precise knowledge of the magnetic field) but they can be reduced by time and by tuning the algorithm. Therefore in long term the track-based method can give more accurate data.

- The hardware system as a direct measuring tool can be useful for the track-based method in two ways:

  - it can help to develop and tune the track-based algorithm by providing the position values for comparison,

  - The track-based method is not equally accurate for all the 6D dimensions, some of them are less precise (called weak mode). The hardware system can provide additional information on these degrees of freedom.

To complete the information on the track-based alignment in CMS, two additional studies should be mentioned [50]. These studies are using tracks not emerging from collisions. In the first method cosmic rays are used to align the CMS detectors. This method is extremely useful but has only limited capability due to the limited angle of the incoming rays and the low particle rate. The second method is using the beam-halo (muons arriving in parallel with the accelerator beam but outside the beam pipe). Obviously, the first method is more applicable for the barrel, the second for the endcap region. It should be noted that collection of cosmic or beam halo tracks require special trigger conditions.

The harware alignment system is split into three subsystems: the Endcap, the Link and the Barrel.

The role of the Endcap Muon Position Monitoring system [10, 18] is twofold: it determines the positions of the Encap Muon chambers in both (positive and negative) Endcaps and connects the two Endcap Muon systems to each other. As the Endcap chambers are partially overlapping there is a possibility to align the adjacent chambers to each other by tracks. Therefore the Endcap Muon Position Monitoring system locates only a few chambers along six radial lines crossing the endcap disks. Another six long lines (called transfer lines) are connecting the two Endcaps through the Barrel. Crosshair type laser beam is used to make the connections between the objects to be observed and a specially designed light detector frame composed of four linear CCD sensors is detecting the arms of the crosshair beam. The system is completed by proximity sensors to measure the distances between the Endcap disks and the innermost disk to the Barrel. The Endcap system is built and maintained by a collaboration of several American universities with the Fermi National Accelerator Laboratory (FNAL, Illinois, USA).

The role of the Link System [10, 19] is to connect the Barrel and Endcap Muon systems to each other and to the Central Tracker. The system is also based on laser beams. Transparent sensors are used to detect the laser light. The Link System is also containing additional sensors: proximity distance meters and tilt sensors, this latter to detect the deviation from vertical at μrad precision. The system is developed and maintained by the University of Cantabria (Santander, Spain) in collaboration with CIEMAT (Madrid, Spain).

The barrel part of the hardware alignment or as it is called by its full name, the Barrel Muon Position Monitoring System which is the subject of the next chapters is providing the positions of the barrel muon chambers in its own coordinate system and following their movements as a stand-alone system. It is connected to the Endcap and Link to locate the full barrel w.r.t. the endcap or the Tracker but this task can also be solved by tracks which is a much simpler task than to align all the 250 chambers individually.

Chapter 4

The Barrel Muon Position Monitoring System

The following sections of this chapter are devoted to the detailed description of the Barrel Muon Position Monitoring System.

4.1 The requirements

As it has been described in the previous chapters the aim of the Barrel Muon Position Monitoring System is to determine the 6D (3 translational and 3 rotational) positions of the 250 DT chambers with respect to each other and monitor their movements during the CMS operation. There are three important parameters to be determined before the system design starts: the measurement range, the system precision and the duration of the measurement.

4.1.1 Range of the measurement

The measurement range can be determined by the estimation of the maximum deviation of the monitored elements from their nominal (designed) positions. In the case of the CMS Barrel wheels the expected deformation was calculated by finite element analysis [11] leading to few mm values shown in fig. 4.1. Similar (in fact smaller) values can be expected for movements due to switching the magnetic field on and off or the thermal dilatation. The difference between the central wheel and the outer ones is caused by the large weight of the solenoid and the inner detectors. There

is also a third factor to be taken into account when the necessary range of measurement is estimated: the opening and closing of the CMS detector. Despite the huge dimensions of the objects to be moved and adjusted at CMS closing the repeability of a few mm is feasible in all directions. As a conclusion we can state that the range of measurement does not have to exceed ±1-2 cm.

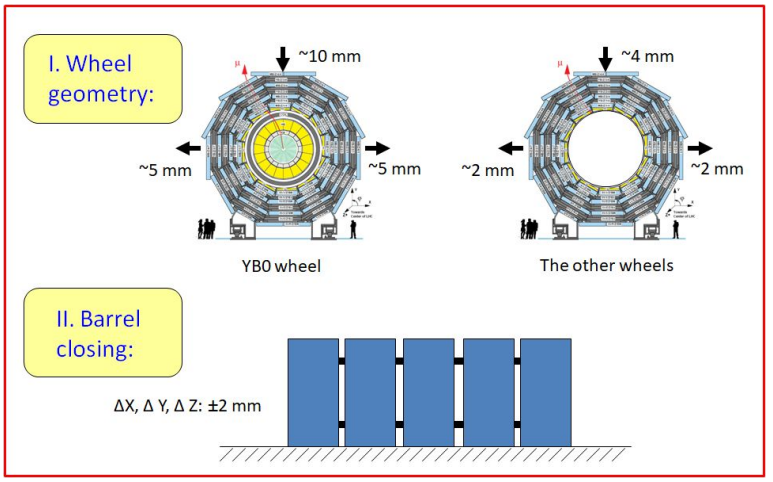

Figure 4.1. Wheel deformations: expected deviations from the nominal values [11].

4.1.2 Precision

As usual, the precision is determined by two types of errors: the accuracy is connected to the systematic errors of the equipment, while the resolution is the summary statistical error of the measurements performed by the system. As we will see later, due to the huge number of elements to be calibrated the precision is dominated by the systematic errors, the resolution is at least by one order of magnitude better. So the requirement formulated in this subsection sets a limit to the acceptable calibration errors.

The required precision can be derived from misalignment studies [20–22] carried out at the early phase of the system design. There are three consequences of the misalignment: degraded trigger efficiency, difficulties to match the trajectory of the same muon in the tracker and the muon spectrometer and finally the error in the momentum measurement. Among these the most critical from precision point of view is the muon momentum

measurement, which is essential in particulal for the Higgs and Z boson analysis.

Three error sources of the muon momentum measurement, namely the intrinsic DT chamber resolution, the multiple scattering and the misalignment were investigated and compared at different P_T values and for all the four muon stations. As an example, the result of the misalignment studies concerning the MB1 station chambers is shown in fig. 4.2. The left drawing is showing the P_T error depending on the misalignment for different momenta. The right picture shows the relative degradation of the P_T measurement w.r.t. a perfectly aligned MB1 chamber.

Based on these studies the accuracy requirement in the ϕ direction can be formulated as follows:

- MS1 and MS2 aligned better than 300 μm,
- MS3 and MS4 aligned to 500 μm.

In the other coordinates the requirement is less demanding, in R and Z the misalignment error should not exceed 1 mm.

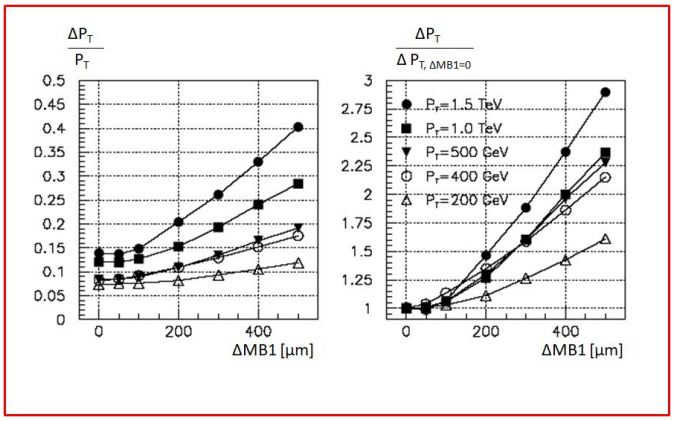

Figure 4.2. Degradation of the muon momentum measurement due to misalignment for MB1 chambers [22].

4.1.3 Duration of the measurement

Fortunately this parameter is a relaxed one as in normal circumstances the movements are very slow. The magnet ramp up or ramp down time is several hours, the warm up period after switching on all the CMS electronics

is also measured in hours or even days. So even several hours for a full measurement cycle of the Barrel Muon Position Monitoring System is fully acceptable (though of course the shorter the better). On the other hand this practical question is more important than it seems at the first glance as the number of measurements to be executed is very high. Therefore some parallel work is necessary during the operation that requires a certain multiplication of measurement channels.

4.2 The system layout

4.2.1 The design and its concept

The system (presented in detail in [10, 23]) is schematically shown in fig. 4.3. Here we give a brief description, more details will be added in the subsequent sections.

The system contains 36 large rigid carbon fiber structures called MABs (Module of the Alignment of the Barrel), 12 rigid long rods called Z-bars and the 250 DT chambers equipped with LED light sources as objects to be monitored. These LEDs are observed by small video-cameras fixed on the MABs. Azimuthally the system can be divided in 12 planes. Six of them (at 60^o from each other) called "active plane"s are containing 4 MABs (two on both sides of the YB0 wheel, two at both edges of the barrel). The 6 intermediary planes called "passive plane"s are containing only 2 MABs at the outer side of YB+1 and YB-1 wheels. The Z-bars are fixed to the central (YB0) wheel in the active planes. They also contain LED sources observed by cameras fixed on the MABs. The diagonal lines inside the MB1 and outside the MB4 stations are also LED-camera connections. The LEDs for the diagonal connections are located on the active MABs, the cameras are installed on the MABs of the passive planes.

The concept behind the system design can be characterized as follows:

- The system is composed of few (three) types of elements only: the DT chambers themselves holding LEDs, and two types of rigid structures: the MABs holding video-sensors and LEDs, and the Z-bars holding LEDs only.

- All the connections to be measured during the operation are performed by LEDs (as light sources) and 2D video-sensors (as light detectors).

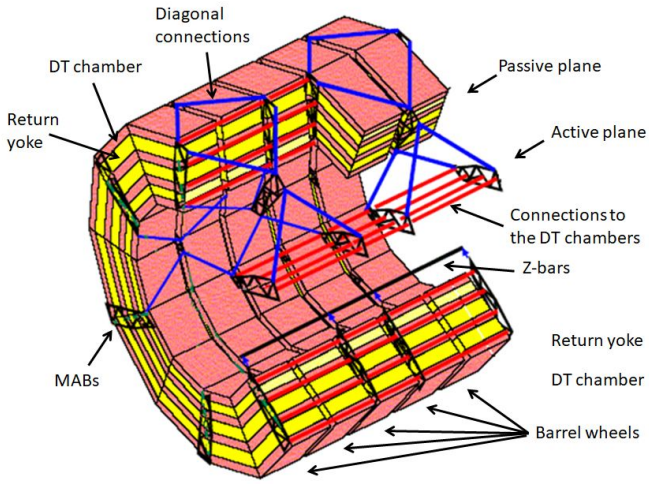

Figure 4.3. Schematic view of the Barrel Muon Position Monitoring System.

– The required precision of the system is achieved by a network-like connection scheme and a high level redundancy.

– All the permanent connections are mechanically fixed on rigid structures and calibrated. Therefore no extra precision is needed during the production of the elements, the accuracy is guaranteed by precise calibration. In order to minimize the systematic errors the calibration is performed in conditions very close to the situation (geometry, environment) in which the given element is intended to be used later.

4.2.2 The optical connections and their functions

The primary function of the Z-bars is to measure the relative movements of the outer wheels in Z_{CMS} direction, in other words the shrinking and expansion of the full barrel when the magnet is on or off.

The diagonal connections were designed to reinforce the redundancy of the position measurement in case of large temperature changes in the CMS cavern causing thermal dilatation of the DT chambers exceeding the tolerable measurement errors. Fortunately the temperature in the cavern is very stable and varies only within 2-3 °C that has made the diagonal connections less important.

More words are needed to show the role and strength of the connections through the DT chambers. In fig. 4.4 a simple setup is shown to explain the essence of the DT connections.

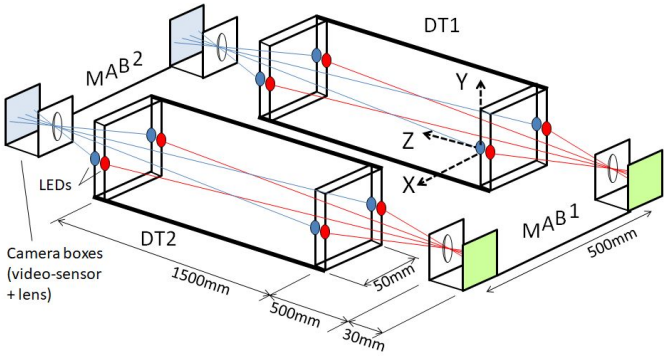

Figure 4.4. Explanation to the connections through the DT chambers (drawing not to scale, the dimensions are given in the figure).

The system consists of four rigid elements: two boxes representing the DTs and two camera holders representing the MABs. These simplified DTs contain two forks with 4 LEDs each (2 are seen from the left, 2 from the right). The simplified MABs are equipped with 2 camera-boxes. The camera-box is a lens-sensor assembly described in subsection 4.3.2.

Let us imagine that the task is to mesure the 6D positions of the DT2 in the coordinate system attached to DT1. There are 16 LEDs altogether seen by the cameras (4 by each). The rigid elements are calibrated so the distances and orientations within the rigid bodies are known. This simple setup has 18 unknowns (DT2, MAB1, MAB2), 32 measured and 68(!) calibrated values. The details of the analysis of this simple test setup are given in Appendix A. The dimensions and the precision of calibrations are corresponding to those in the Barrel Muon Position Monitoring System. In this setup the redundancy is not very high (32 measurements compared to 18 degrees of freedom), nevertheless the location and orientation of DT2 can be determined by the precision given in table 4.1 taken from Appendix A.

The results shown in table 4.1 confirm the power of the proposed position monitoring system: a $\sim$2 m large object located at half meter from the reference can be positioned by the fraction of mm (including the impact of the rotations). A deeper analysis can reveal the fact that the precision is

Precision of the DT2 X coordinate	71	μm
Precision of the DT2 Y coordinate	170	μm
Precision of the DT2 Z coordinate	687	μm
Precision of the DT2 rotation around X-axis	0.11	mrad
Precision of the DT2 rotation around Y-axis	0.10	mrad
Precision of the DT2 rotation around Z-axis	0.86	mrad

Table 4.1. The accuracy of the determination of the DT2 chamber position.

not uniform. This follows from the asimmetry of the arrangement and can easily be interpreted.

It should be noted (see in Appendix A) that the calculation also gives us the 6D positions of the two MABs in the same coordinate system though this is not the aim of the position monitoring system. The knowledge of the MAB positions, however, is extremely useful for the system validation and different studies as it will be seen in chapter 8. It should also be noted that the strength of the measurement is determined mainly by the quality of the calibration of the two sides of the forks w.r.t each other and the fact that the Test-DT is measured from two opposite sides.

The DT connections in the Barrel Muon Position Monitoring System are built up in the same way. Thanks to the construction of the forks (see in subsection 4.3.1) the LEDs in the far forks are not blocked by the close ones so the same camera can observe two or three chambers located behind each other as it is shown schematically in fig. 4.5. In azimuthal direction each MAB is connecting two adjacent sectors as it is shown on the photo of sectors 1 and 2 connected by a common MAB (fig. 4.6).

Finally, there is one more strong constraint: the connection network is forming a closed ring that makes the system much more rigid.

4.2.3 The system design in numbers

The characteristic numbers concerning the system design are given in table 4.2.

Figure 4.5. Optical connection scheme in active and passive planes. 1) MAB; 2) Single camera-box; 3) DT chamber; 4) Chamber LED holder (fork); 5) Double camera-box; 6) Z-bar (on the vacuum tank); 7) Z camera-box; 8) Z LED holder

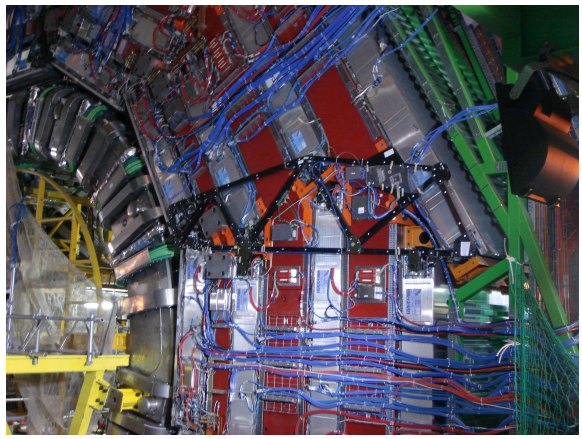

Figure 4.6. The photo of the MAB between sectors 1 and 2 on wheel YB+2.

Item	Quantity
DTs	250
DT forks	1000
MABs	36
Camera boxes	600
LEDs	10432
Z-bars	12
Degrees of freedom to be measured	1710
Calibrated constants	∼33000

Table 4.2. The system in numbers

4.3 Elements of the system

4.3.1 The DT chamber as element of the system

As it was explained in subsection 3.3.1 the DT chambers measure the distances between the crossing muons and the anode wires of the drift cells. Therefore the position monitoring system -in principle- should monitor the anode wire positions of the DT chambers. This, however, is not possible as the number of wires is close to 200000 ([10] p.51) and they are sealed in the chamber box. On the other hand, the DT chamber can be considered as a rigid body deforming only within the requested monitoring accuracy (due to gravity as the chambers are installed in different orientations and the thermal dilatation). The wire positions are measured during the chamber construction w.r.t. outside reference objects called corner blocks (see later) that can be seen and measured after the chamber closure. In fact the wire position measurement w.r.t the corner blocks is the first step in the calibration of the DT chambers as elements of the position monitoring system.

Each superlayer contains four corner blocks (one at each corner) as it can be seen on the left side in fig. 4.7. The corner blocks are precisely ($<$20 μm) machined objects. The blind holes shown in black on the technical drawing (seen on the right side of fig. 4.7) are so called survey holes used during the next calibration step of the DT chambers.

The corner blocks are carrying the information about the anode wires but they are not observable during the CMS operation and would not be practical to make them observable. Instead, an additional element

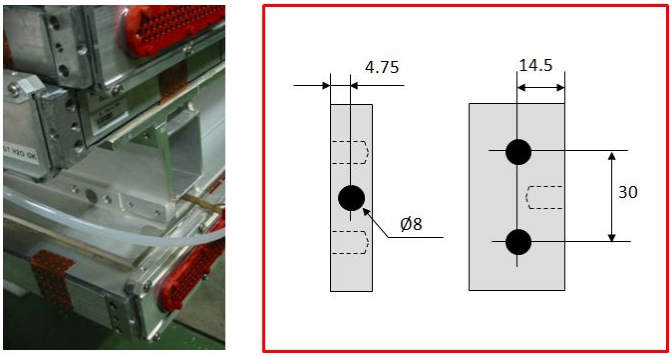

Figure 4.7. Corner blocks on the DT chambers. Left: the photo; right: the technical drawing.

containing LED light sources and called fork shown in fig. 4.8 has been constructed and installed on the DT chambers (four forks per chamber). The arms of the forks with the LEDs are located inside the long tubes called alignment passages on both sides of the honeycomb structure (see also fig. 3.4). As there are LEDs on both sides of the arms, the forks can be observed from both ends of the passage.

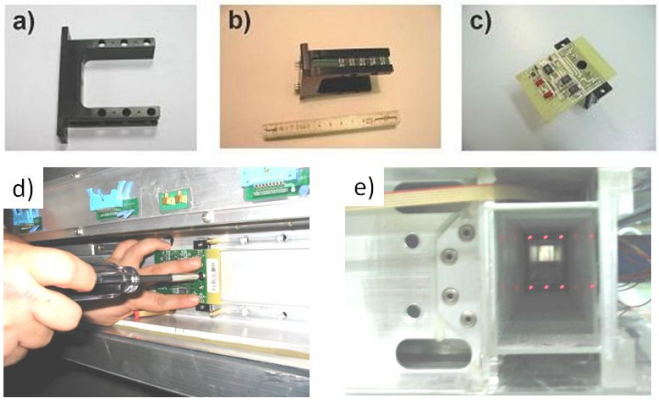

Figure 4.8. The fork: a) the fork mechanics; b) mounted LEDs; c) mounted electronics; d) fork installation on the DT; e) fork operation [23]

The fork driver electronics based on PIC16F84 microcontroller is mounted on the back of the fork mechanics (see fig. 4.8c). Its function is to switch the LEDs on and off in arbitrary configuration and setting the intensity of the emitted light by adjusting the LED currents. This unit is connected to the

DT control and readout board through an I^2C bus. Thus during the CMS operation the fork-LEDs are activated through the DT control system.

The fork mechanics was designed at the Institute for Particle and Nuclear Physics (RMKI, Budapest, Hungary, predecessor of the Wigner RCP). The driver electronics was designed and produced at the University of Debrecen in collaboration with Atomki.

Each fork is containing 10 LEDs. The choice of the LED was based on the following considerations:

- sufficiently large brightness
- narrow spatial light distribution
- large dynamic range
- narrow spectral range
- small emitting surface

The LED chosen was the FH1011 from Stanley Electric Co., Ltd. (Japan). Its image and the spectral distribution of the emitted light are shown in fig. 4.9. The detailed characteristics can be found in [24].

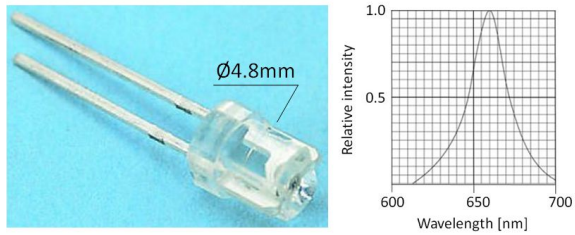

Figure 4.9. The STANLEY FH1011 LED and the spectral distribution of the emitted light.

In order not to increase the cumulative systematic error of the position monitoring system the requirement to the knowledge of the LED positions is $\leq$15 μm in the coordinate system of the fork. This can be achieved by calibration of all the forks. The fork design, production and calibration is described in full detail in [23].

The next and last step in the preparation of the DT chambers as elements of the position monitoring system is the chamber calibration i.e. the

measurement of the positions of the LED forks w.r.t the corner blocks. This step is also described in detail in [23].

It seems useful to summarize the main points described in this subsection:

The anode wires of the DTs are not observable for position monitoring. The position measurements are performed by observing LEDs installed on the DTs. The connection between the positions of the anode wires and the LEDs is established by calibration steps: the wire positions w.r.t the corner blocks, LED positions in the forks and finally the forks w.r.t the corner blocks.

4.3.2 Camera-boxes

The camera-boxes are video-cameras specifically designed for the position monitoring system. The factors to be taken into account during the design were the simplicity, reliability, small size, light weight, ability to operate in magnetic field up to 1.7 T (field in saturated iron), radiation hardness up to 10^{11} neutrons/cm^2 (according to estimations in chapter 10 of [10]), minimum cabling, ability to send the video-signal up to 7 m distance without signal loss or additional noise and finally tolerable price in view of the large number of cameras in the system (600 plus spare).

The camera-box is containing two components: a 2D light detector and a lens. The sensor chosen was the VV5402 CMOS analog black&white sensor from the VLS Vision Ltd [25]). The sensor parameters and settings are listed in table 4.3. The electronic part of the sensor was designed (adapting the original factory design to our needs) and assembled at Atomki. The sensor chip mounted on the driver electronics can be seen in fig. 4.10a. The assembled camera-box and the box mounted on the MAB are shown in fig. 4.10b, c.

Number of pixels	384 x 287
Pixel size	12 x 12 μm^2
Sensitive area	4.66 x 3.54 mm ^{2}
DC power	8 - 12 V
Automatic gain	off
Sensitivity control	off
Correction	linear

Table 4.3. The parameters and settings of the 2D video-sensor

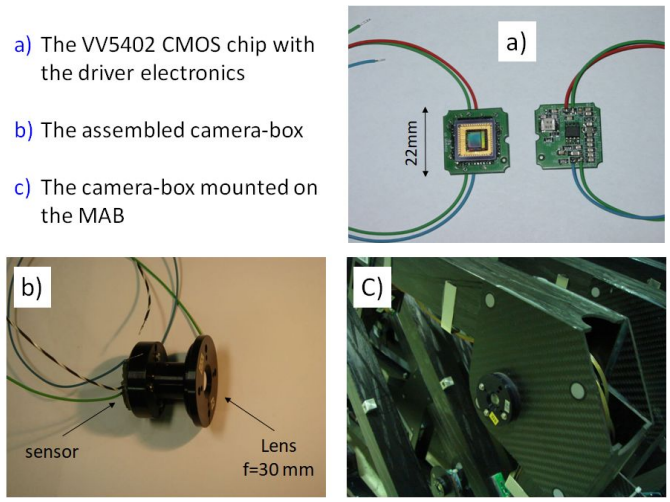

Figure 4.10. The camera-box.

The lens is a plano-convex singlet made of BK7 glass that is fully sufficient for the given LED spectrum (see in fig. 4.9). The focal length is 30mm for the DT-connections, 20 mm for the Z-bar connection and 70 mm for the diagonal lines. There are a few specially designed DT chambers installed at the chimneys of the cryogenic equipment of the solenoid. At these locations f=20mm lenses are used.

Though the camera-box seems to be a very simple object, several factors had to be taken into account during the finalization of the design. Mechanically it had to be in agreement with the MAB design. This fact can explain the shape of the camera-box: it had to fit in the corresponding cylinder on the MAB.

Optically there are several arguments to be taken into account. First, the LED is not a point source (see fig. 4.11a). Also. the forks to be observed by the same camera are located at different distances from 0.5 to 7 m (see e.g. fig. 4.5). On the other hand we do not want to reproduce the exact image of the LED source but obtain a light spot that can be associated with the LED location. Studies have shown that these aims can be achieved by placing the sensor exactly in the back focal plane of the lens and using a small ($\varnothing$3 mm) diaphragm behind the lens. The LED image seen by the camera designed this way is shown in fig. 4.11b.

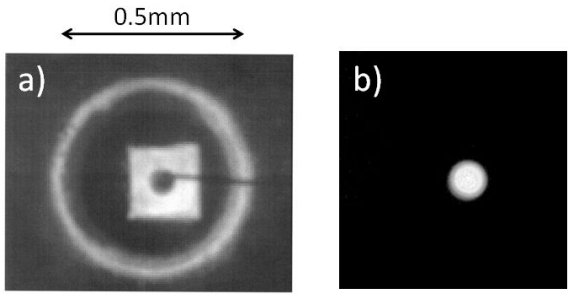

Figure 4.11. a) emitting surface of the LED; b) Image of the LED seen by the camera-box at 0.5 m distance

4.3.3 MABs

The 36 MABs are the most visible and impressive objects of the Barrel Muon Position Monitoring system. They can be seen on many pictures taken from the barrel part of CMS and generate questions at the visitors during the maintenance period when CMS is open and the MABs can be seen. The name MAB is an abbreviation and stands for "Module for the Alignment of the Barrel".

The main function of the MABs is to hold the camera-boxes in fix positions. The MABs in the active planes are holding also the LED holders used in diagonal connections. In addition, all the MABs are equipped with so called survey target holders and temperature & humidity sensors. The survey target holders are used for housing precisely machined plugs during the MAB calibration and installation for position measurements by survey methods. More information on this item is given in chapter 8 and in Appendix B. The temperature & humidity sensors (4 sensors per MAB, located close to the DT chambers) are giving a detailed map of the enviromental parameters during the CMS operation. The sensor element is the SHT15 sensor manufactured by Sensirion (Switzerland) shown in fig. 4.13. More information on this item is given in chapter 9.

Before going into more details we have to introduce the naming conventions for the MABs. The MABs are numbered indicating the wheel-gap and the MAB-sector. The wheel-gap is the gap between the barrel wheels or between the outer wheel and the endcap and numbered as -3; -2; -1; +1; +2; +3. The MAB-sector starts at $\phi = 15$ degree (between the DT-sectors 1 and 2) and numbered from 1 to 12. As an example MAB +3_1 is located

on the positive side of CMS in the gap between the YB+2 wheel and the positive endcap and azimuthally between the DT-sectors 1 and 2 (this MAB is shown in fig. 4.6).

The MABs are made of carbonfiber material glued together with araldite. They were designed at CERN, the production was made at the Institute of Mechanics of Materials and Geostructures S.A (Penteli, North-Athens region, Greece) under CERN's supervision.

The MAB shape is determined by the geometry of the barrel muon system. The camera-boxes are fixed on the nodes or camera holding plates located against each alignment passage.

The most important requirement to the MAB is to be rigid and free from any short or long term deformation. Talking about rigidity it must be noted that all the MABs are installed in the X_{CMS}-Y_{CMS} plane which is very close to vertical (the deviation is coming from the fact that the LHC tunnel at the CMS location is incined by 0.74 degree with the + side up). Therefore there is no special need to reinforce the MAB structure against deformations outside its plane. The situation, however, is completely different in ϕ direction as the MABs are installed at very different angles. On the other hand, all the MABs are calibrated at the same angle (see in chapter 7). So the MAB should be extremely rigid against rotation around the axis perpendicular to its plane. The simulation of the full position monitoring system has shown that the camera positions with respect to each other on the same MAB should not change by more than 100 μm and 100 μrad. Finite element calculations during the design and a special rigidity test have confirmed the correctness of the design and the quality of the material used for production. The MABs are fixed on the outer (non-IP) side of the barrel wheels at three points allowing free (tensionless) movement of the MABs even if the wheel is deforming.

The MAB shape is following the wheel structure and the locations of the DT chambers inside the wheels. As it was explained in subsection 4.2.2 the MABs are connecting two adjacent sectors i.e. the $+\phi$-side alignment passages of the DTs of a sector to the -ϕ-side passages of the next sector. There is a node at each of the mentioned passages containing a camera-box. The outer ($\pm$3) MABs are holding a single camera-box, the inner MABs are holding double cameras composed of two single camera-boxes installed back to each other (see schematically in fig. 4.5).

As the inner part of the barrel muon system (stations MS1 to MS3) has a rotational sysmmetry, the camera-boxes in inner part of the MABs are located at the same positions for all the MABs. The outer part (MS4) is different depending on the MAB-sector. It was possible during the MAB design to keep only two basic MAB-shapes: the "straight" and the "croissant" (fig. 4.12). The croissant-MABs are located at MAB-sectors 4, 5, 6, 7, 8, 10. The rest of the MABs is of straight type.

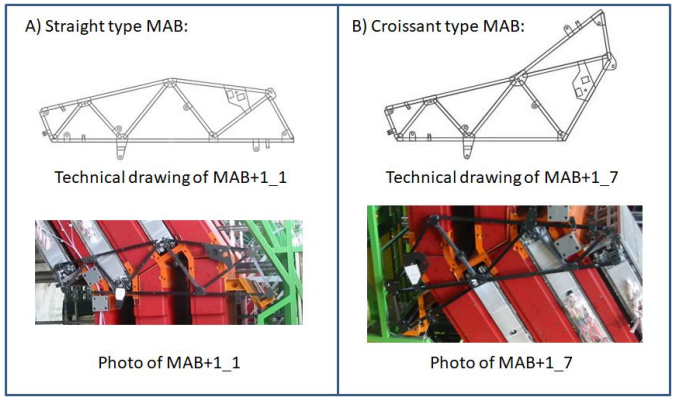

Figure 4.12. The basic MAB-shapes. (The photos were taken during the test-installation of some MABs in 2005).

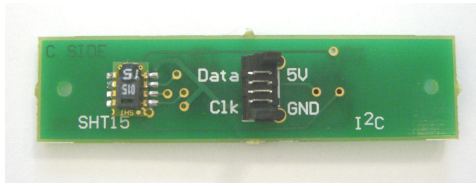

Figure 4.13. The SHT15 Temperature and Relative Humidity sensor.

From system network point of view the MABs are floating bodies in the sense that the result of the reconstruction of the DT positions is independent from the 6D positions of the MABs (of course all the cameras should remain in the range of observation).

4.3.4 Z-bars

The Z-bars are ⌀8 mm carbon composite rods of ∼5.3 m length fixed at one end to the vacuum tank of the solenoid at YB0 otherwise freely sliding in the Z_{CMS} direction in a tube installed along the vacuum tank (see fig. 4.14A)

under the MABs of the active planes. The total number of Z-bars is 12 (6 on the positive and 6 on the negative side). A LED holder shown in fig. 4.14B and C is installed at both ends of each rod.

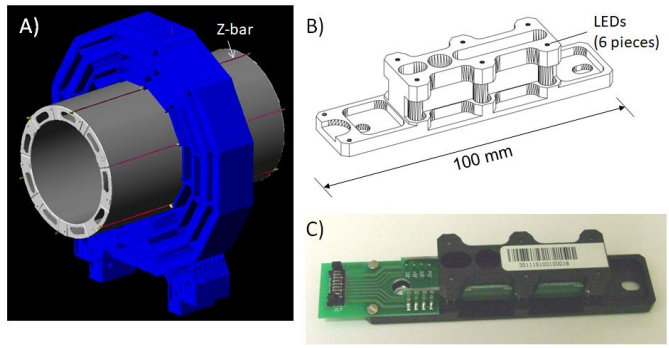

Figure 4.14. The Z-bars: A) Z-bars on the vactank - conceptual drawing; B) LED holder technical drawing; C) LED holder photo

All the Z-bar LED holders and the bars themselves were calibrated in the construction phase of the project. In practice -as it has been mentioned in subsection 4.2.2- the Z-bars are used for relative measurements only to follow the movements of the outer (± 2) wheels in Z_{CMS} direction due to magnetic forces. These movements will be analysed in chapter 9.

4.3.5 System electronics

From electronics point of view the Barrel Muon Position Monitoring System is controlled and the measured data from the cameras and the temparature&humidity sensors are collected by a local network of minicomputers called Board PCs [54] schematically shown in fig. 4.15. The Board PC (see the photo in fig. **??**) is following the PC/104 standard [26]. The core module, the power card and the frame grabber are purchased units, the Custom interface and the Video-multiplexer are designed and built in Atomki. Each MAB is served by one such PC and the 36 Board PCs are connected to the master computer located in the control room (called USC hall) of the CMS experiment about 90 m away from the experimental cavern (called UXC hall). The schematic view of the PC-network is shown in fig. 4.17.

As it has been mentioned in subsection 4.3.1 the fork-LEDs on the DTs are activated by the main workstation through the DT control channel and powered by the DT electronics unit called minicrate [27]

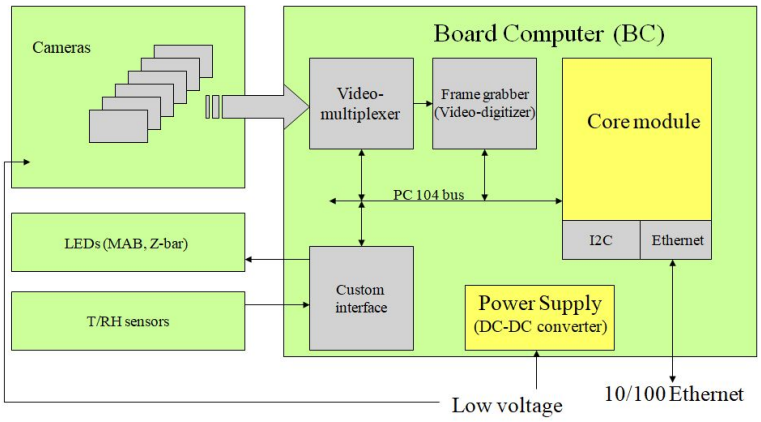

Figure 4.15. The schematics of the Board PC.

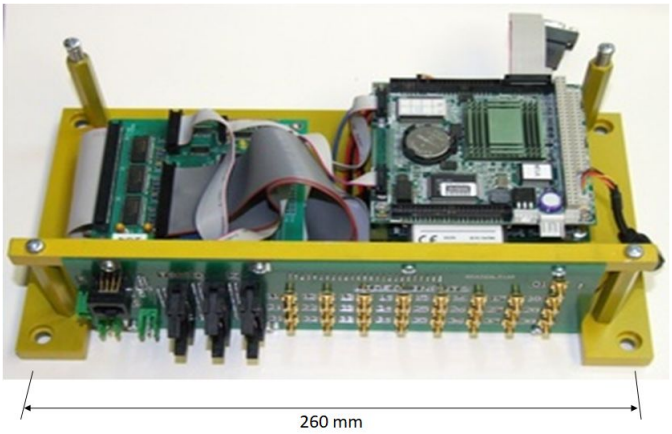

Figure 4.16. The photo of the Board PC.

4.4 Measurement and image evaluation

The measurement in the Barrel Muon Position Monitoring System is a snapshot of a LED image taken by a camera-box. Then the image is digitized and –after a careful quality control– the centroid of the LED-image is calculated. The details of the process including the control and

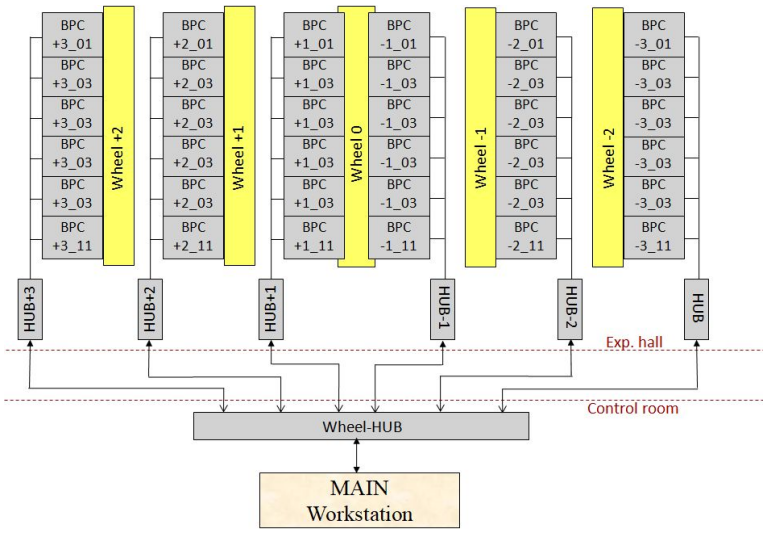

Figure 4.17. The schematics of the PC network.

data flow scheme are described in [58]. In this section the problems of the measurement steps are discussed mainly following the work described in [23].

4.4.1 Required accuracy of the centroid determination

The camera-boxes are observing LEDs located at different distances from ∼0.5 to ∼7 m corresponding to magnification between ∼17 and ∼270. The error in the centroid definition is also magnified the same way. The most significant measurement from the DT position point of view, however, is the measurement of the closest fork. (The longer distance measurements are more relevant for the determination of the angular position of the chamber and are usually reinforced by the measurement of the same DT from the opposite side.) It follows from the system design that each DT is measured at least in one point from close distance. If we would like to keep the error of the close measurement below 10 μm then the error of the centroid definition should not exceed 0.6 μm i.e. 0.05 % of the 12 μm sensor pixel size (see table 4.3).

The centroid definition depends on the algorithm of the calculation. Besides this fact there are two more effects limiting the accuracy of the measurement

from hardware point of view: the statistical noise and the so-called pixel-effect.

4.4.2 The centroid calculation algorithm

The steps of the centroid determination algorithm are described in full detail in [23]. Here we briefly list the main steps of the algorithm. First the full image is digitized on a 8-bit scale, i.e. between 0 (dark pixel) and 255 (saturated pixel). In the next step the algorithm is looking for the area of maximal intensity in the image. Then the contiguous spot and its border-line is determined. This area, associated with the image of the LED is marked by a rectangular frame around the border line called green box (after the colour of the rectangular on the display). The pixels outside the green box are not taken into account. The pixels inside the green box but below the predetermined threshold are set to zero. As the last step the weighted average in 2D is calculated inside the green box. The average X and Y values are taken as coordinates of the LED-image in the coordinate system of the sensor.

4.4.3 The statistical noise

This question was studied in [31], [32] and [23]. The effect can be illustrated by fig. 4.18 ([31]) showing the calculated centroids of subsequent images taken during the period of ∼1 minute at unchanged conditions. In [32] the statistical fluctuations were investigated by a simple setup consisting of a standard camera-box with f=30 mm lens observing a LED placed at 567 mm distance from the camera-box. 1000 single pictures have been taken and the centroid was calculated for each image individually. The distribution of the centroid values (along the long direction of the sensor) is shown in the left part of fig. 4.19. The same 1000 images were then distributed in 20 groups of 50 images each. The 50 centroids in each group were averaged. The distribution of the averaged centroids is shown on the right side of fig. 4.19.

The conclusion of this study is that the statistical noise can be kept below the required centroid determination accuracy by averaging up to 50 images. Repeated tests and calculations using the centroid definition algorithm described in 4.4.2 have shown that a good accuracy can already be achieved by averaging ∼20 images. This fact has an important consequence as the time needed for a full measurement cycle can be reduced by ∼60 %.

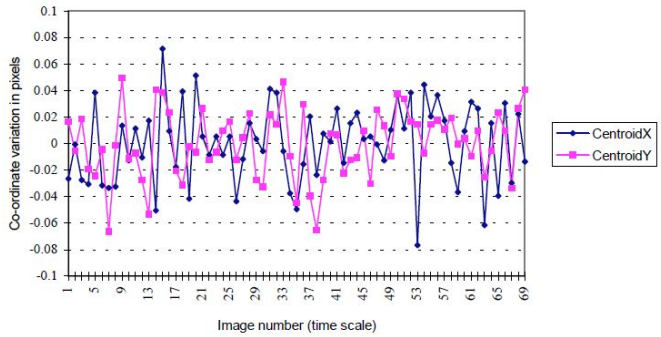

Figure 4.18. Statistical fluctuations of the centroid of single images (full horizontal scale: few minutes) [31]

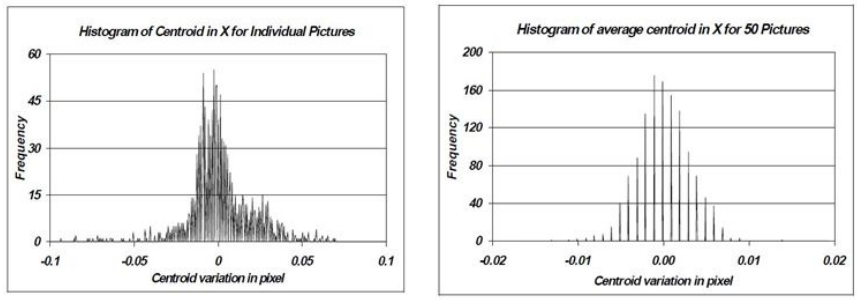

Figure 4.19. The statistical noise of the centroid detection. Left: distribution of 1000 individual centroids. Right: distribution of the centroids calculated as the average of 50 images

4.4.4 The pixel-effect and the threshold

It has been observed at the very beginning of the project (and generally known in the vision metrology) that an oscillation occurs with a period corresponding to the width of a pixel as the image sweeps across the sensor surface. This effect called pixel-effect was demonstrated by a simple setup shown in fig. 4.20 [31] originally aimed to be used to measure the linearity of the centroid detection w.r.t the displacement of the light source.

Moving the LED light source by 1 mm (corresponding to the movement of the image on the sensor by $\sim$4 pixels) the effect could clearly be demonstrated as it can be seen in fig. 4.21. Later this effect was studied in more detail [33] and sevaral methods have been proposed to minimize the error.

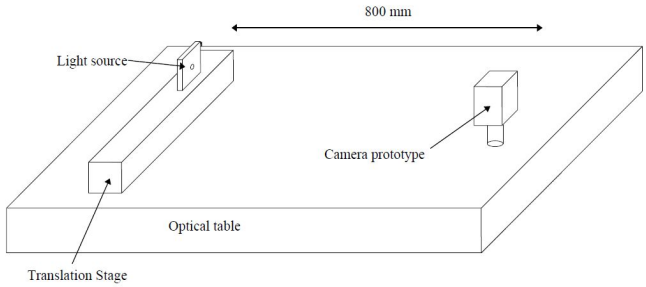

Figure 4.20. Linearity test setup

Finally, the effect was studied by simulation of the centroid definition at different locations of the LED image w.r.t the pixel-structure of the sensor [34]. It has been shown that the pixel-effect is connected to the treshold during the calculation of the centroid. The sensor has a dark current signal which has to be eliminated by applying a threshold during the digitization of the image. The higher this threshold the bigger is the pixel effect because pixels with the intesity close to the threshold can be or not be taken into account as part of the image depending on the area of the pixel illuminated. To keep the noise caused by this effect below the requirements a threshold of $\leq$10 on the 255 (8 bit) scale is sufficient if the maximum intensity of the image is close to saturation.

The final conclusion of this section can be summarized as follows:

- The required accuracy of the centroid-determination is $\leq$5 % of the pixel size ($\leq$0.6 μm).

- The centre of the LED-image should be close to saturation (close to 255 on the 8-bit scale). This can be set by the LED current for the given distance.

- The statistical noise can be kept below $\pm$0.6 % of the pixel size (0.07 mm) by averaging 20 to 50 images. This fact, however, has an impact on the operation speed of the system when a large number of LED-images have to be taken and evaluated

- The pixel-effect can be kept below $\pm$2 % of the pixel size ($\leq$0.24 μm) if the cut threshold of the 8-bit image digitization is $\leq$10.

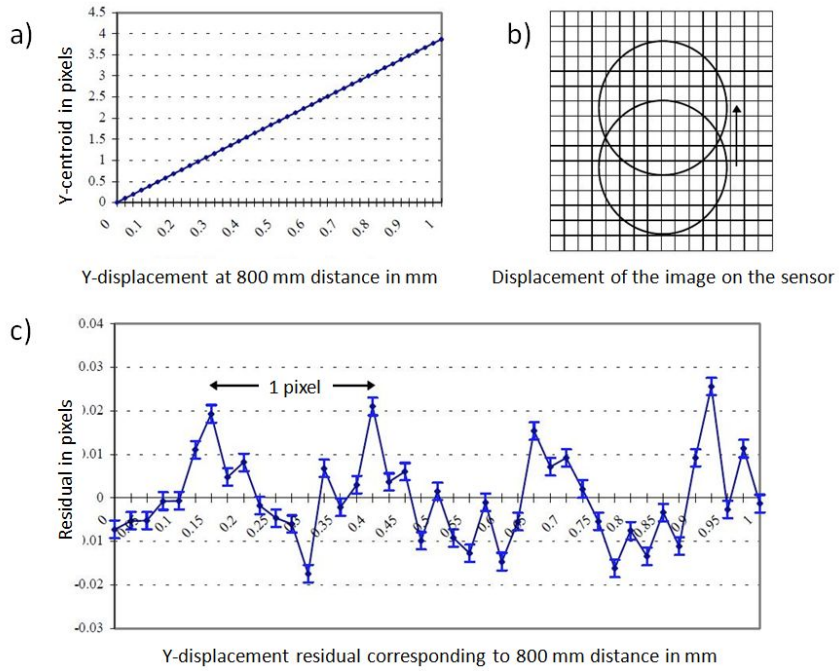

Figure 4.21. Pixel-effect [31].

– The centre-of-mass algorithm is giving a simple and precise enough determination of the spot centre that can be associated with the location of the image of the LED light source.

– As the "LED location" and the "spot centre" can depend on several factors, the same settings and methods have to be used at all the steps of the project: at the calibration of individual items like the forks or the camera-boxes, at the calibration of more complex objects like the DTs or MABs and at the operation of the full system at CMS.

– In the COCOA-model (see in subsection 4.4.5) of any measurement (used for calibration or for system operation) the measurement accuracy parameter should be set to 0.5 μm.

4.4.5 Opto-geometrical reconstruction

The 6D positions of the DT chambers are calculated from all the input data provided by the Position Monitoring System:

- measured data (centroid positions of the LED-images),
- calibration data for all the calibrated elements stored in the alignment database,
- the error of the calibration for each calibrated value
- the nominal positions of the DTs that are not very far from the real ones and could be used as starting positions to be corrected,
- the connection network (which LED is observed by which camera),
- the error of the camera-measurement including the precision of the algorithm used to determine the centroids.

The calculation, called opto-geometrical reconstruction is performed using a special software package developed by the muon alignment group during the R&D and construction phase of the muon alignment project. The first version called SIMULGEO [28] already contained the main features of the package. The considerably revised new version, called COCOA (CMS Object-oriented Code for Optical Alignment [29]) is used for all the calculations in the project requiring position reconstruction from calibrated and measured data. As we will see in the following chapters, it was also used during the calibration of the elements and at the system validation. COCOA was also used for the analysis of the small setup discussed in subsection 4.2.2. The COCOA is part of the general CMS analysis software framework called CMSSW.

As in the case of any complex software, the correct and efficient usage of COCOA requires considerable practice. A starting guidance can be found in [29] and [30]. As the software is primarily developed for the CMS alignment application it contains several basic optical and optoelectronic elements used by the muon alignment. The presently available basic elements are as follows: laser, cross-hair laser, source, lens, pinhole, mirror, cube splitter, plate splitter, optical square, modified rhomboid prism, sensor2D, COPS, distance-meter, distance-target, tilt-meter. Most of the elements is used by the link and endcap alignment. The barrel system including both the calibration tasks and the opto-geometrical reconstruction of the DT positions is using only three basic elements:

- source: point-source of light
- pinhole: diaphragm of point-like aperture

– sensor2D: 2D light detector

For different studies and comparisons described in chapter 8 the distance-meters and the distance-targets are used as well.

The COCOA-models of the full Barrel muon alignment system and all the calibration setups are composed of these three basic elements. For example the camera box is a composition of a pinhole and a sensor2D (see more in chapter 6). The MAB is composed of camera-boxes. Therefore the MAB is a composed object containing objects that are also composed.

Formally the COCOA model is a text file containing all the input data listed above in a strict form using key words. Each degree of freedom of each object has to be declared whether it is UNK (unknown), CAL (calibrated with some error) or FIX (known with no error). Depending on the selected option COCOA can perform different calculations but in general it gives the values of the UNK degrees of freedom with their errors. The calculation itself is an iterative process using matrix operations and ending with the best fit for the given UNK parameter that is most consistent with the calibrated and measured data in the least square sense. The iteration stops when the correction of the new iteration is below a predetermined limit. The error values of UNK parameters are calculated from the calibration and measurement errors.

COCOA is a very powerful tool to perform opto-geometrical calculations for a large variety of optical setups. It should be noted, however, that COCOA has to be used with extreme care. This is especially true if the number of objects is large. In this case the calculation may stop at wrong local minimum. There are three ways to avoid this problem: a) give starting values for the UNK parameters (especially for angles) close to the expected results; b) try to perform the calibrations as precisely as possible; c) always check the result carefully.

Chapter 5

Quality control of the video-sensors

The measurement of the DT chamber positions is based on the determination of the centroids of the LED images seen by the camera-boxes. In section 4.4 the centroid calculation algorithm, the statistical noise and the so-called pixel effect were analysed as those factors that may influence the precision of the centroid determination. These error sources are independent of the sensor quality and are present even in the case of a perfect sensor. Unfortunately this is never the case, especially if the sensor used is not specifically designed for metrology applications. In this chapter the influence of the imperfectness of the sensor on the centroid determination is investigated. There are three factors to be studied:

- the gain uniformity (in other words the fluctuation of the gain from pixel to pixel at homogenous illumination),
- the dark current (in other words the detected signal for each pixel when there is no illumination),
- the defected pixels (in other words the number and position of pixels with zero or maximum output independently of the incident light).

This task was solved in the following way:

- As the first step these error sources were studied by simulation an the criteria for the tolerance against these factors were formulated.
- As the second step a calibration bench was constructed to measure these parameters for each sensor.

– As the third step all the sensors were measured and the measured data evaluated.

– As the fourth step sensors fulfilling the criteria formulated during the first step were selected for further usage.

In the following sections the steps listed above are described in detail.

At this point we should note that in normal conditions these properties usually do not change during the life-time of the sensor. In our application, however, the radiation background could -in principle- damage the sensor and cause defected pixels during the operation. As it was mentioned in subsection 4.3.2 this effect had been investigated and the chosen sensor type successfully passed the tests from this point of view.

5.1 Simulation of the impact of the sensor quality on the centroid determination

5.1.1 Simulation of the light spot and its detection

In order to simulate the intensity distribution inside the LED image, at the same time keep the statistical character of this distribution, the simulated spot was generated by Monte-Carlo method using 10^7 photons that is close to the reality. The intensity-distribution inside the spot is similar to a truncated Gaussian due to the fact that often the central part of the image is saturated. In fig. 5.1 a real and a simulated spot is compared. This spot-generation method was already applied in [23] to study the pixel-effect described in subsection 4.4.4.

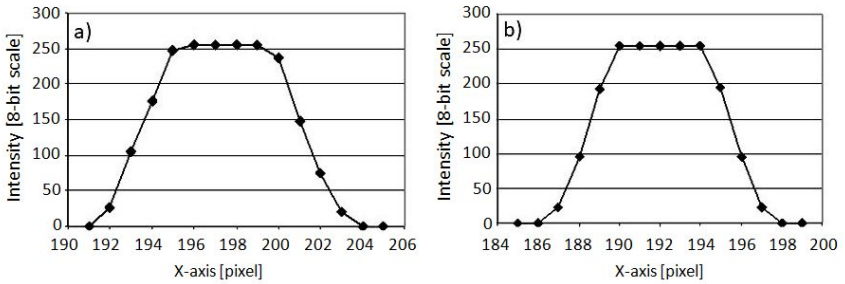

Figure 5.1. Comparison of the intensity distributions in X-direction for a real (a) and a simulated (b) light-spot.

The sensor response was also simulated by the program by adding adjustable dark current and gain values for each pixel and including defected (insensitive or saturated) pixels. For the centroid determination the algorithm described in subsection 4.4.2 was used.

5.1.2 Simulation of the gain uniformity

To simulate the impact of the gain fluctuation on the centroid determination the same (simulated) light spot was deteted by a (simulated) sensor in which the gain fluctuated around the mean value following a gaussian distribution. The standard deviation was changed and at each value the simulation was repeated 20 times and the result averaged. The dependence of the centroid on the gain fluctuation is shown in fig.s 5.2 and 5.3. The unit on the horizontal axis is the standard deviation expressed as the percentage of the mean gain value.

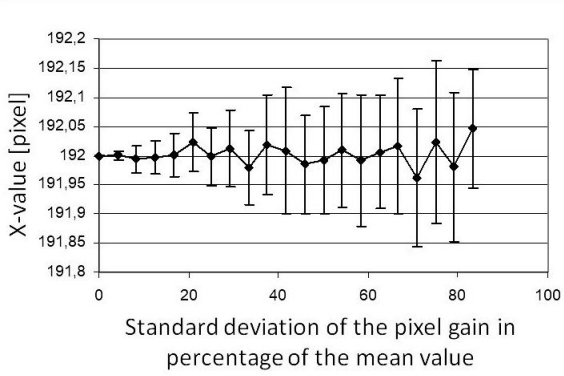

Figure 5.2. Simulation of the centroid position at different deviations in the pixel gain, X-direction.

It is clearly seen that the accuracy of the centroid determination is degrading with the increase of the gain fluctuation. On the other hand, sensors with relative standard deviation not exceeding $\sim$15 % do not show any degradation so those sensors can surely be used in the position monitoring system.

5.1.3 Simulation of the dark current

This question is connected to the pixel-effect discussed in subsection 4.4.4. It was shown that the cut threshold in the centroid calculation algorithm

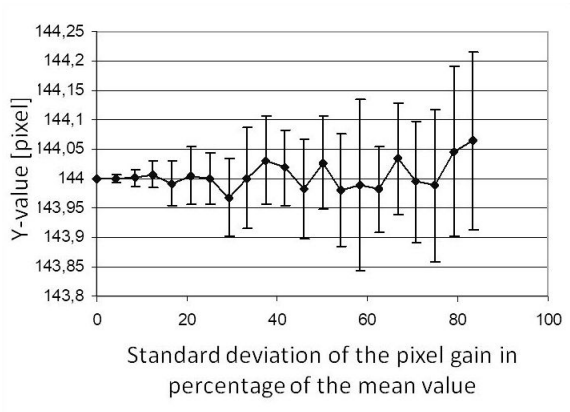

Figure 5.3. Simulation of the centroid position at different deviations in the pixel gain, Y-direction.

should be below 10 which is the upper limit to keep the pixel-effect at the tolerable level. On the other hand, this threshold has a minimum value determined by the noise of the dark current (the signal produced by a non-illuminated pixel).

This noise was also simulated to quantify the minimal value of the cut threshold. Five images were generated with and five without dark current at the same predetermined centroid of X=192; Y=144 at the generation step. Preliminary measurements have shown that the dark current signal generally does not exceed 1-2 on the 8-bit scale. So in the simulation the dark current signal of each pixel was set to a random value between 0 and 2.

The centroid obtained for the same light spot in the presence and without noise are compared in the table 5.1. The table gives the values of the mean and standard deviation in pixel units for both cases.

Five images with noise				Five images without noise			
Mean		St. deviation		Mean		St. deviation	
X	Y	DeltaX	DeltaY	X	Y	DeltaX	DeltaY
191.998	144.001	0.010	0.004	192.000	143.999	0.001	0.001

Table 5.1. Simulation of the dark current effect (see text).

Though the dark current considerably increases the error of the centroid determination w.r.t. the noiseless sensor, the absolute value of the error is still negligibly small. This means that we could -in principle- even decrease

the cut threshold and set somewnere in the 3 to 10 range. In practice, however, it was kept and fixed at 10.

5.1.4 Simulation of the defected pixels

It cannot be excluded, especially in the case of a general purpose low cost sensor that it contains one of even more insensitive (in extreme case fully dark or saturated) pixels. Their presence can cause significant error in the centroid definition. To study this effect a real LED-image was modified by simulated dark or saturated pixels. The defect was moved across the image step by step and the variation of the centroid w.r.t the original one was calculated. The calculations were performed for scans in both X and Y directions but -as the results were very similar- only the X scanning direction is shown.

In figs 5.4 to 5.7 four different cases are seen: single dark, single saturated, double dark and double saturated pixel-failures. As the line of movement of the failing pixel(s) is not exactly crossing the centre of the spot, some effect is also seen in Y-direction but its quantity can be neglected. The X-curves can easily be interpreted. The dark pixel is not causing any error if it is located outside or in the centre of the light spot. The error is maximal at the slope of the spot intensity distribution. The saturated pixels, on the other hand, cause the maximum error outside the spot and do not cause error in the area where the spot itself is also saturated.

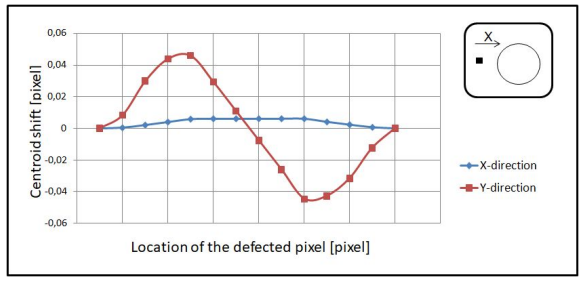

Figure 5.4. Centroid variation in the presence of a dark pixel scanned in X-direction.

As it is seen from the curves quantitatively even one defected pixel (dark or saturated) can cause an error in the centroid definition exceeding the tolerable 1-2% of a pixel size therefore such sensors should not be used in the system and have to be rejected.

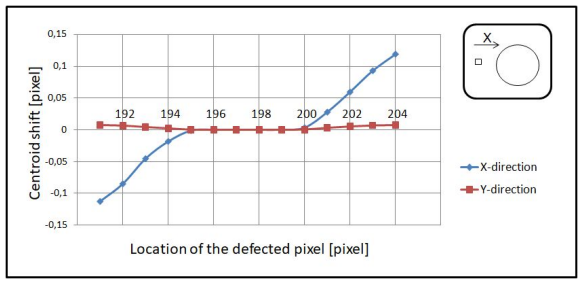

Figure 5.5. Centroid variation in the presence of a saturated pixel scanned in X-direction.

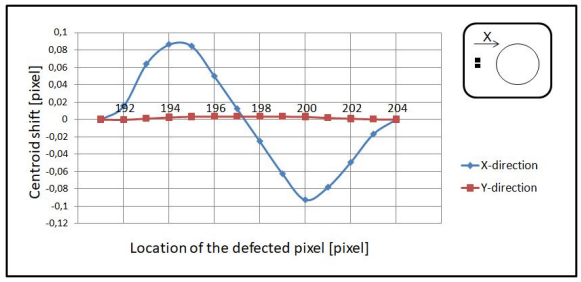

Figure 5.6. Centroid variation in the presence of a double dark pixel scanned in X-direction.

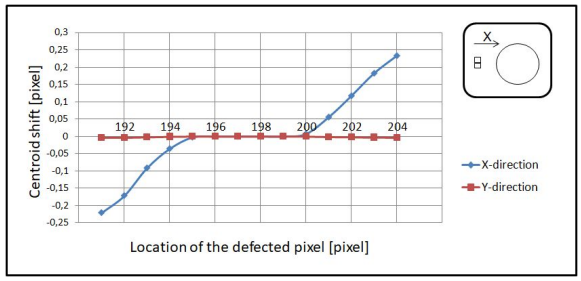

Figure 5.7. Centroid variation in the presence of a double saturated pixel scanned in X-direction.

It should be mentioned that the pixel-failure in the sensor is not the only source of this type of defect. During the assembly steps the sensor can be damaged, scratch, drop of glue or nonremovable dirt can cause similar problems. These sensors have to be rejected as well.

5.2 The quality control setup

As it follows from the preceeding subsections a quality check and preselection is required to avoid the usage of sensors having non-uniform gain, large dark current or containing local defects. To perform the quality control a test setup was assembled at the University of Debrecen in collaboration with Atomki. The drawing of the optical part is shown in fig. 5.8. The photo of the setup and its parts can be seen in fig. 5.9.

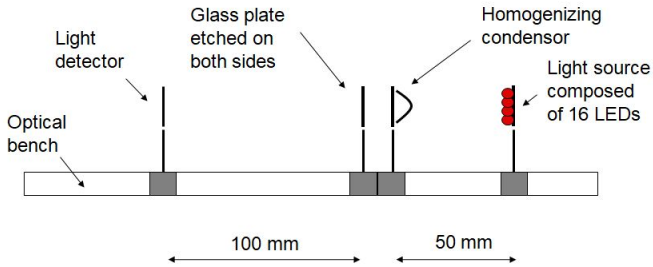

Figure 5.8. Schematic drawing of the optical part of the setup used for sensor QC measurements.

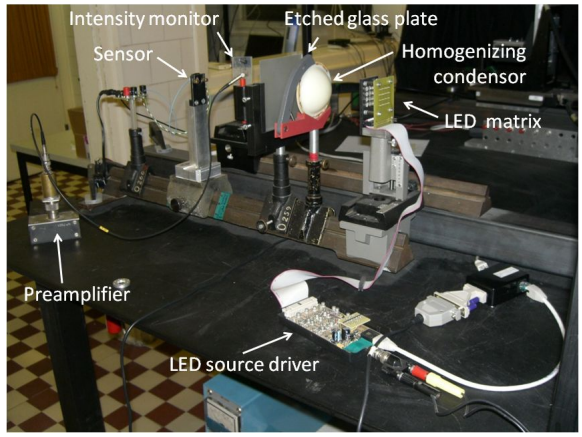

Figure 5.9. Picture of the setup and its parts used for sensor QC measurements.

The principle of the setup is quite simple: the sensor is illuminated by homogenious light and the response is recorded. The selection of good and bad sensors is based on the analysis of the recorded images.

In practice, however, considerable attention had to be paid to the technical details to get valuable results. As we are intending to measure few bit differences on the 8-bit (0 to 255) scale the requirement to the uniformity of the light distribution had to be of the same order of magnitude, i.e. the intensity-variation of the illuminating light over the full sensor surface ($\sim$4x5 mm^2) had to be kept below $\sim$1 % for all the illuminating intensities. This was achieved by a light source composed of a 4x4 LED matrix. The current of each LED could be adjusted by a digitally controllable electronic unit designed in Atomki for this task. After a preliminary test of 69 LEDs 16 of them having similar output light intensity v.s. the LED current characteristics (seen in fig. 5.10) were selected to be used in the light source matrix. The "Det_current" in fig. 5.10 is the current generated in the light detector measuring the intensity. These characteristics were recorded in the database and used to tune the LEDs for each illuminating intensity.

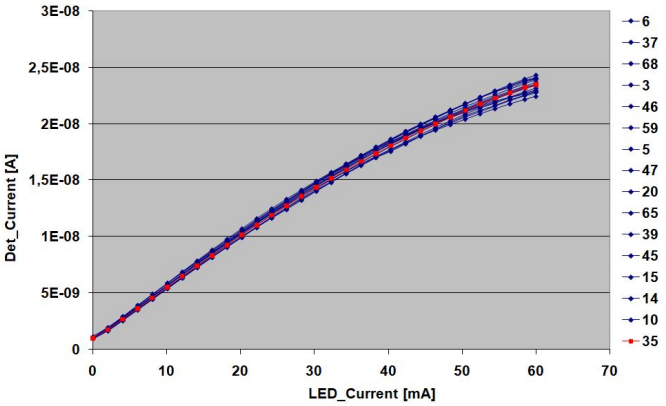

Figure 5.10. Intensity v.s. current characteristics of the LEDs selected for the light source of the sensor quality check setup.

The light of the LED-matrix was then further homogenized by a double scatterer indicated in fig. 5.8 as "Homogenizing condensor" and "Glass plate etched on both sides". The intensity at the designed location of the sensors was measured by a scanning light detector. As the light was expremely weak an electrometer preamplifier NV-822A with electrometer amplifier and filter NV-822B designed by Atomki was used. By tuning the LED currents the necessary uniformity could be achieved as it is seen in fig. 5.11 shown as an example for 30 mA LED current. Setting the LED current to a certain value means setting of LED No. 35 (marked by red colour in fig. 5.10 and well representing the average characteristics) to the given current and adjust the

other LEDs to the current giving the same intensity using the characteristic curves.

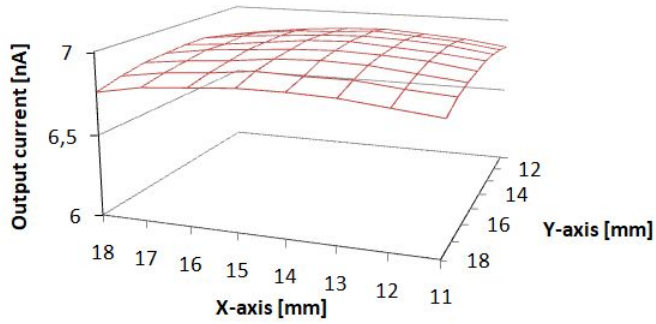

Figure 5.11. Light intensity distribution at the sensor plane (reference-LED current: 30 mA).

5.3 The quality control measurement

In view of the large quantity of sensors (>600) to be checked the sensor holder was designed to allow a rapid sensor changement and electrical connection. To make the measurement semi-automatic, I developed a software package to control the setup, perform the measurement and store the data for further analysis [56]. Essential part of the software package is the rapid analysis display showing the summary information about the sensor after the measurement.

The quality control measurement of the video-sensors consisted of the following steps:

1. Fixation of the sensor, entry of the sensor ID number (requested by the control program)

2. The LED currents are set to 0 mA and 10 images are recorded.

3. The LED currents are set to different values between 5 and 60 mA in 5 mA steps and 10 images are recorded at each value.

Steps 2. and 3. are automatically executed by the control program after the entry of the sensor ID.

As an example, the data display of the sensor quality control measurement for sensor No. 226 at 40 mA LED current is shown in fig. 5.12. The details of the display panel can be explained with the help of figs 5.13 to 5.17.

The top left part (fig. 5.13) contains the sensor ID, the led current and the output current of the light detector. The artificially coloured 2D picture shows the measured intensity of each pixel. The curves on the right and at the bottom show the average intensity in the given row or column respectively.

The top right part (fig. 5.14) is showing the noise (the sigma of the intensity variation of the 10 images) pixel by pixel.

The main statistical characteristics of the 10 images are given in fig. 5.15.

The bottom left part (fig. 5.16) is showing the distribution of pixels within 1 sigma, between 1 and 2 sigma and above 2 sigma w.r.t. the average intensity.

Finally, the bottom right part (fig. 5.17) is showing the pixel intensity distribution histogram.

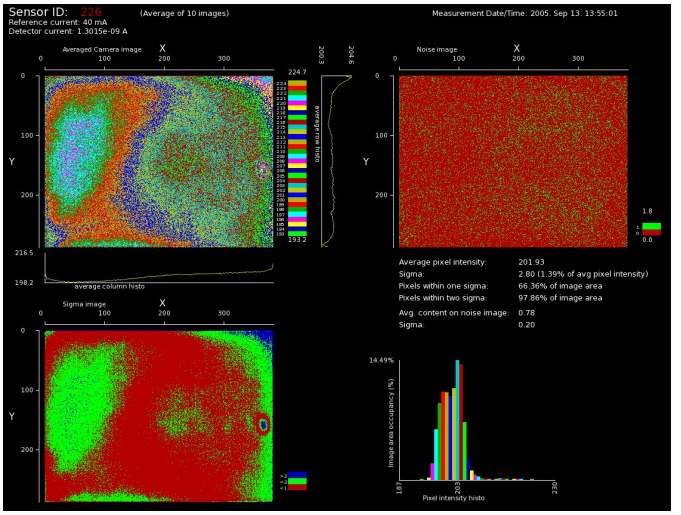

Figure 5.12. Sensor-data display example: distributions and statistics calculated from 10 images taken by sensor 226 at 40 mA LED current.

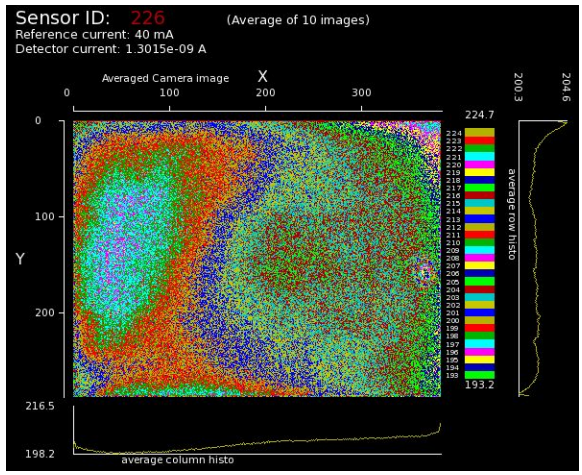

Figure 5.13. Sensor-data display, top left part: gain uniformity - artificially colored picture and histograms next to the image show the gain pixel by pixel and the average intensity in the given row or column respectively.

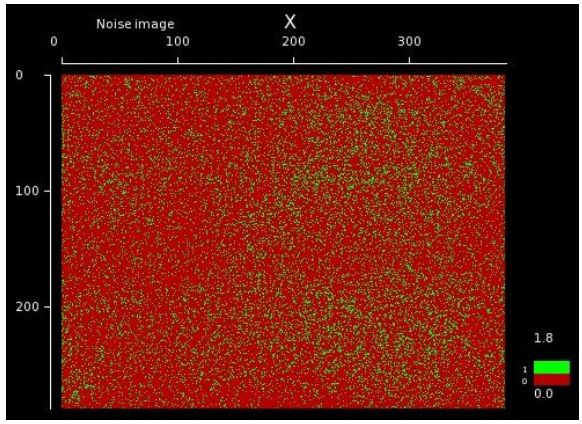

Figure 5.14. Sensor-data display, top right part: noise distribution of the 10 images.

5.4 Selection criteria and statistics

The practical aim of the sensor quality control is to select the “good” sensors for further usage in the position monitoring system and reject the “bad” ones. The choice must be based on a set of objective parameters

Average pixel intensity:	201.93
Sigma:	2.80 (1.39% of avg pixel intensity)
Pixels within one sigma:	66.36% of image area
Pixels within two sigma:	97.86% of image area
Avg. content on noise image:	0.78
Sigma:	0.20

Figure 5.15. Sensor-data display, middle right part: Summary of the main statistical characteristics.

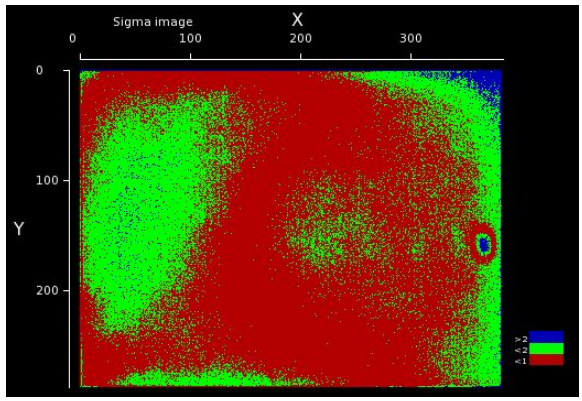

Figure 5.16. Sensor-data display, bottom left part: sigma distribution of the pixel intensity (a local defect is clearly visible on the right part of the image).

followed from studies described in section 5.1 and, at the same time, from the circumstances in which the sensors are used.

Based on the studies three general selection parameters can be formulated:

- Gain uniformity: the standard deviation should be <15 % of the average gain (subsection 5.1.2).
- Dark current: the output signal of each nonilluminated pixel should be: <10 on 8 bit scale (subsection 5.1.3).
- Defected pixels: no defected (permanently empty or saturated) pixels are accepted (subsection 5.1.4).

The final statistics of the sensor quality control measurements is given in table 5.2.

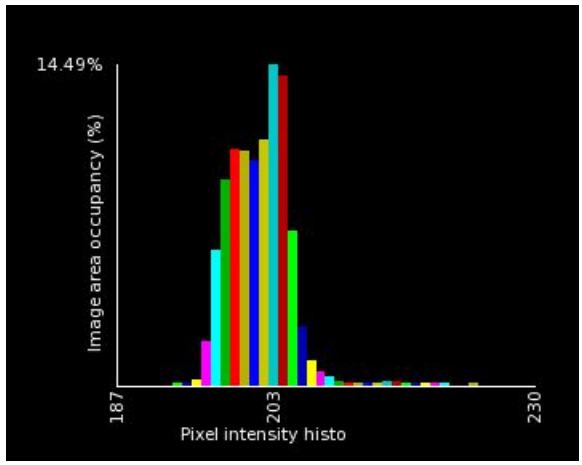

Figure 5.17. Sensor-data display, bottom right part: pixel intensity distribution histogram (same colors as on the image on top left).

Sensors tested (pieces)	712
Passed	611 (85%)
Not functioning	24
Out of criteria or dirty	77

Table 5.2. Statistics of the videosensor QC test

The table shows the importance of the QC of the videosensors as 15 % of the sensors had to be rejected.

The measured sensors were hermetically packed to avoid any dirt and were sent to CERN for the assembly of the camera-boxes.

Chapter 6

Calibration of the camera-boxes

The active measuring elements in the Barrel Muon Position Monitoring system are the camera-boxes described in subsection 4.3.2. Though the mechanical parts were produced with CNC machine and the assembly was made with maximum care the achievable accuracy was not enough and the camera-boxes had to be individually calibrated. In this chapter the required accuracy, the calibration method and setup [56], the measurements and the results are discussed.

6.1 Required precision of the camera-box calibration

A camera-box contains two elements: a lens (with a small diagraphm behind) and a 2D video-sensor. In fig. 6.1 an ideal camera-box and the relevant coordinates are shown. The sensor coordinate sysem is attached to the sensitive surface. The origo is the middle point of the central pixel, the X and Y axes are parallel to the pixel rows and columns. The sensitive side of the sensor is oriented in the +Z direction.

The presence of the diaphragm, the narrow spectral bandwidth of the LED-light and the fact that the camera-boxes installed in the position monitoring system are used in paraxial mode only allow us to describe the camera-boxes using the geometro-optical approximation. In this case the origo of the camera-box coordinate system is the pinhole representing the lens and the diaphragm. The axes are parallel to those of the sensor.

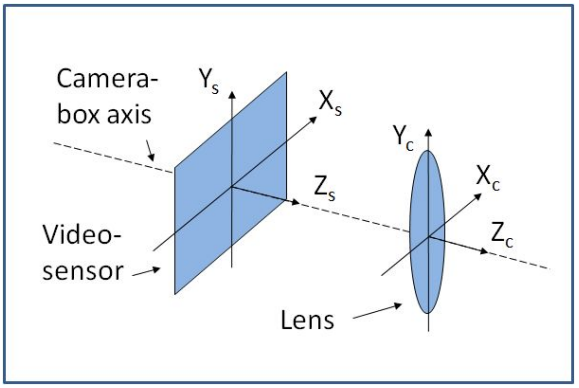

Figure 6.1. The coordinate system of the box (c) and the sensor (s).

In reality the sensor surface is not necessarily perpendicular to the camera-box axis and the sensor to lens distance is varying within the tolerance of the camera body production and the camera-box assembly. In the language of COCOA (subsection 4.4.5) the camera-box has three internal parameters:

- pinhole-sensor distance along the camera-box optical axis,
- rotation of the sensor around the camera-box X-axis,
- rotation of the sensor around the camera-box Y-axis.

The calibration task is to measure these internal parameters for each camera-box used in the position monitoring system. It should be underlined that the deviation of the internal parameters from the nominal ones do not cause any detection error if they are perfectly known. The calibration error (mismeasurement of the internal parameters), however, is leading to a misdetermination of the centroid location in the position monitoring system as it is shown schematically in figs. 6.2 and 6.3. This effect is maximal for the LEDs located on the closest fork w.r.t. the camera-box. For this case the typical values for the distances and angles marked on the figures are given in table 6.1.

As the expected deviations from the nominal values and the expected errors are small we can investigate the sensor-distance and the tilt errors separately with the help of figs. 6.2 and 6.3.

In the case of the sensor-pinhole distance mismeasurement (fig. 6.2) the error in the LED-position measurement is expressed by formule 6.1:

D	~550 mm
h	< 40 mm
Z_{sm}	~ 30 mm
$\lvert Z_{sr} - Z_{sm} \rvert$	± 0.1 mm
$\lvert \alpha \rvert$	<50 mrad

Table 6.1. Typical values for the distances and angles on figs. 6.2 and 6.3.

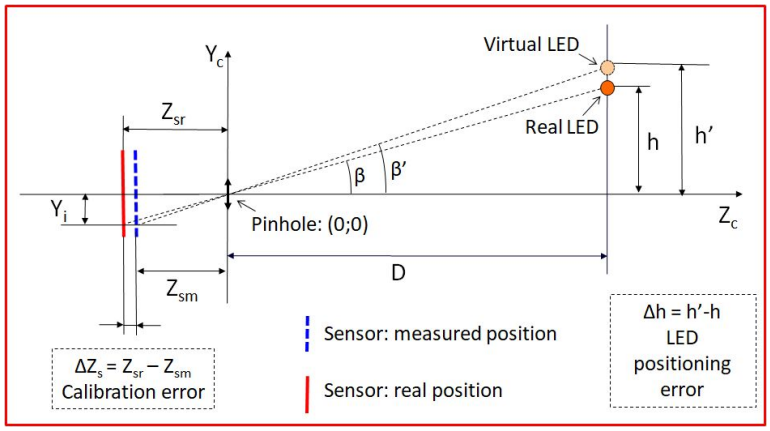

Figure 6.2. The impact of the sensor-pinhole distance mismeasurement on the LED positioning - explanation

$$\Delta h = h' - h = h * \left(\frac{Z_{sr}}{Z_{sm}} - 1 \right) \tag{6.1}$$

If we want to keep the LED-positioning error within the range of <20 μm then using the values from table 6.1 we can get the required calibration accuracy (fig. 6.2) concerning the pinhole-sensor distance:

$$Max.distance - error = Z_{sr} - Z_{sm} = Z_{sm} \frac{\Delta h - h}{h} < 10\ \mu m \tag{6.2}$$

In the case of the sensor-tilt mismeasurement (see fig. 6.3) the error in the LED-position measurement is expressed by formule 6.3:

$$\Delta h = h' - h = D * tg\beta * \left(\frac{cos\alpha' * tg\beta}{cos\alpha - sin\alpha * tg\beta + sin\alpha' * tg\beta} - 1 \right) \tag{6.3}$$

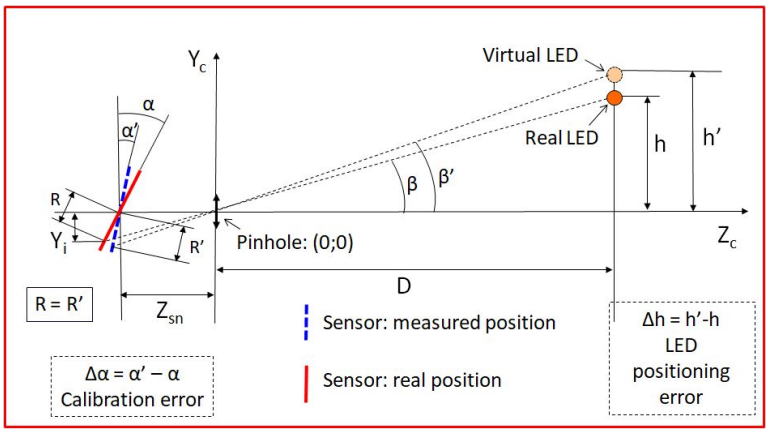

Figure 6.3. The impact of the sensor-tilt mismeasurement on the LED positioning - explanation.

The estimation of the permitted maximum tilt-error is more sophysticated as the effect depends not only on the absolute value of the sensor tilt (α) but also on the sign of the tilt as it is illustrated in fig. 6.4. It should be noted that there is no error if the light ray is parallel to the camera-box axis and if it is perpendicular to the sensor.

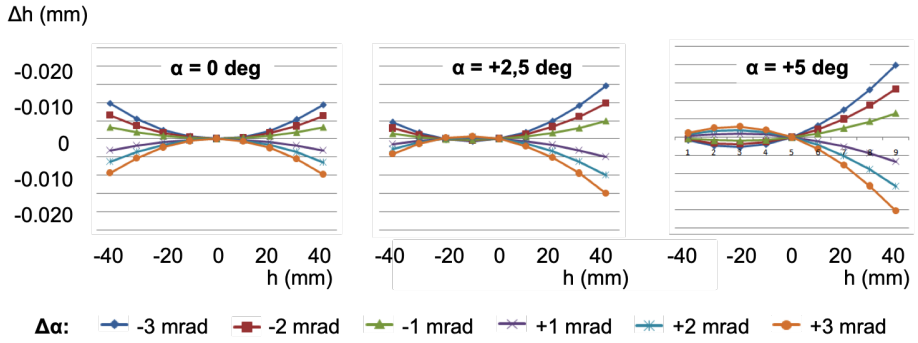

Figure 6.4. The impact of the sensor-tilt mismeasurement on the LED positioning at different tilt and tilt-error values.

The camera-box design, production and assembly could guarantee that the sensor tilt is not exceeding few deg (section 6.5). As it can be seen in fig. 6.4. even in the worst case a calibration performed within the error of $|\Delta\alpha| \leq$3-4 mrad can keep the LED positioning error within the $|\Delta h| <$20 μm range.

6.2 The calibration principle and the bench model

Two difficulties have to be overcome when we attempt to measure the internal parameters of the camera-boxes. The first is quantitative: the requirement to the precision is very high: <10 μm and <3-4 mrad for the distance and tilt respectively. The second problem is rather practical: the lens-diaphragm and the sensor itself are extended and structured objects as it can be seen in fig. 6.5. There is no object or detail that could be precisely associated with the sensitive surface of the sensor or the principal plane of the lens.

Therefore an alternative, indirect way had to be chosen. In the position monitoring system the camera-box with known internal parameters is measuring the light sources installed on the DT chambers. As we saw in subsection 4.2.2 this type of measurement is redundant so -in principle- could determine more parameters than just the chamber positions. If we use a similar and precisely known (measured) setup then the internal parameters of the camera-boxes could be measured and calculated by COCOA from the camera-box response. The principle of the proposed method is shown in fig. 6.6.

Figure 6.5. The inner structure of the camera-box.

The COCOA-model of the setup contains three objects: Front plate, Back plate and the camera-box. Both plates contain several light sources. The model of the camera-box was already discussed in section 6.1. The source positions inside the plates and the plate positions w.r.t. each other are known (see later in sections 6.3 and 6.4). The unknown parameters are the three internal parameters of the camera-box and the box location w.r.t. the plates.

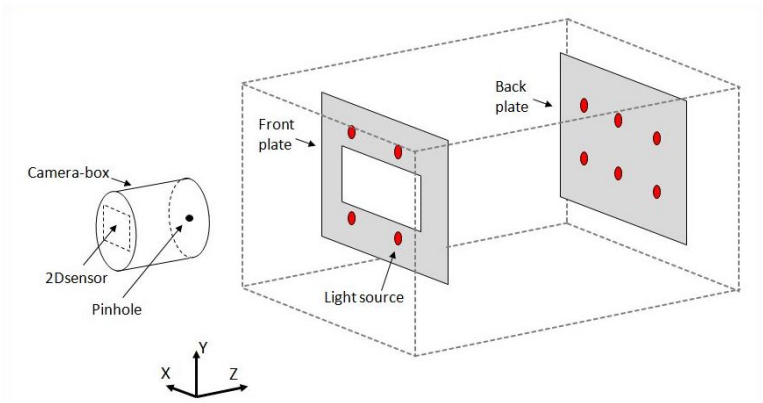

Figure 6.6. The principle of the camera-box calibration measurement.

The model was tested by COCOA-simulation at different input parameters varying the distances between the three objects and the number and configuration of the light sources. The following considerations helped to minimize the possible variations and choose the perspective directions:

- The angle of visibility of the camera-box is ± 4.4 and ± 3.8 degree in X and Y respectively. Light sources beyond these angles are not visible. On the other hand, it is worthwile to put sources close to the angle limit to increase the lever arm of the measurement.
- The front plate hole must be large enough not to block the light from the outer sources on the back plate. This limits the number and arrangement of sources on the front plate.
- As the number of the camera-boxes to be calibrated is high ($\sim$600 pieces) and the calibration bench should not deform during this period it must be robust, compact and of moderate size.

These considerations and the comparison of the achievable accuracy for the internal parameters at different configurations led to the final choice of the setup schematically shown in fig. 6.7. The COCOA-simulation gave the following results for the precision for the internal parameters:

- accuracy of the pinhole to sensor distance measurement: 5.5 μm
- accuracy of the measurement of the sensor tilt around the X-axis: 2.8 mrad

– accuracy of the measurement of the sensor tilt around the Y-axis: 2.3 mrad

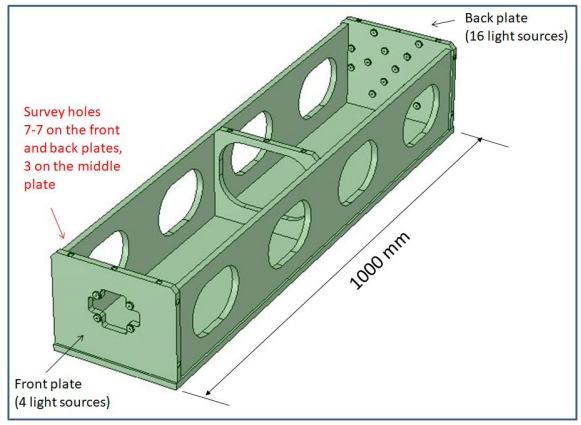

Figure 6.7. The 3D drawing of the setup chosen for the camera-box calibration.

These values are fully compatible with the requirements formulated in section 6.1 and allow to keep the LED position mismeasurement below the tolerable level even if all the errors are present. The difference in the tilt accuracy in X and Y is explained by the fact that the X-dimension of the sensor is larger giving a bigger lever arm.

As it was pointed out above, the setup is also providing -as byproduct- the camera-box position in the bench coordinate system. The accuracy in this setup is $\sim$150 μm in translation, 0.3 mrad in rotation around X;Y and 0.1 mrad in rotation around Z (the optical axis). This question becomes important for the MAB calibration (chapter 7).

6.3 The optical fiber etalon for calibration

Before going into details of the design of the camera-box calibration tool a method described in [23] has to be introduced. This method, giving a solution to the question how to realize a point-like light source was already used for the calibration of the forks and the DT chambers.

The calibration is based on the observation of light sources with precisely known location. As we saw earlier the LEDs used in the project are not point-like sources therefore they are not suitable for the calibration

task. The solution developed by our group is based on the usage of illuminated optical fibers. The standardized fiber light source is a 50/125 μm core/cladding optical cable fixed in a plate containing reference holes measurable by survey methods. These elements are illustrated in fig. 6.8. During the plate assembly the plug is glued in the fiber-hole of the calibration plate, then the nose of the fiber connector is inserted in the hole of the plug and the connector is glued in the plate.

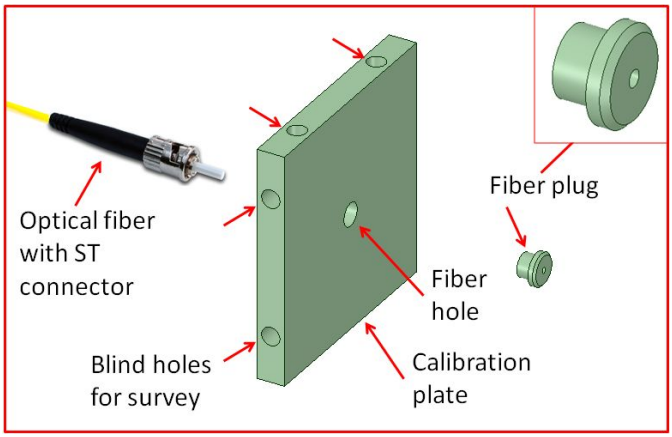

Figure 6.8. The principle of the fiber-etalon tool.

The optical fiber is illuminated by a LED equipped with an optical fiber connector. Such LEDs are available on the market. Our choice has fallen on the HFBR-1414T from Agilent [35] shown in fig. 6.9 and the equivalent AMP 269110-2 LED emitting incoherent but narrow band light at 820 nm and equipped with standard ST-type fiber connector.

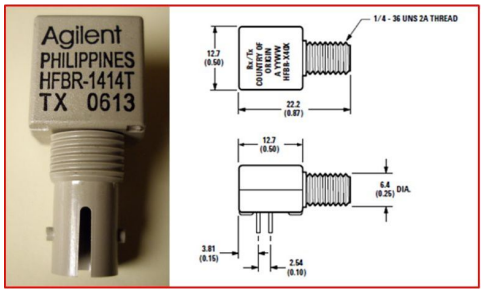

Figure 6.9. The Agilent HFBR-1414T LED and its dimensions

The next step is the measurement (calibration) of the assembled plate in a metrology laboratory where the centre of the fiber is related to the blind holes with micrometer precision.

6.4 The calibration bench design and construction

The setup shown in fig. 6.7 was built at CERN. The technical drawing of the plates is shown in fig. 6.10. After the plate production the optical fibers were glued and the plates were measured in the CERN metrology laboratory: the positions of the illuminated fibers and the survey hole axes at 2 and 10 mm from the surface were measured with several μm precision in the plate coordinate system. Then the bench was assembled and the relative orientations of the plates were measured by photogrammetry. The measurement was performed by the CERN Survey group [36]. The photo of the assembled bench equipped with retroreflective survey targets is seen in fig. 6.11. Though the middle plate is not relevant for the calibration it was also measured by survey to detect any deformation if later the bench had to be recalibrated by survey. Fortunately this did not have to happen during the operation of the calibration bench.

The fully equipped bench can be seen in fig. 6.12. It was installed in the CMS Alignment laboratory at CERN. (The laboratory will be introduced in chapter 7.) Here we can already mention that the temperature in this laboratory is stable within 3-4 deg so the thermal dilatation of the camera-box calibration bench made of AlMgSi alloy is negligible.

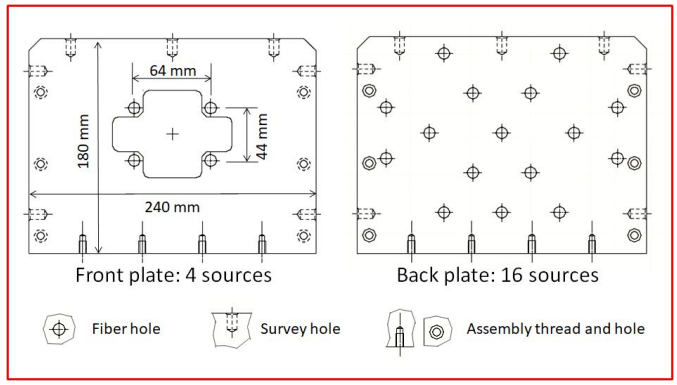

Figure 6.10. The technical drawing of the plates.

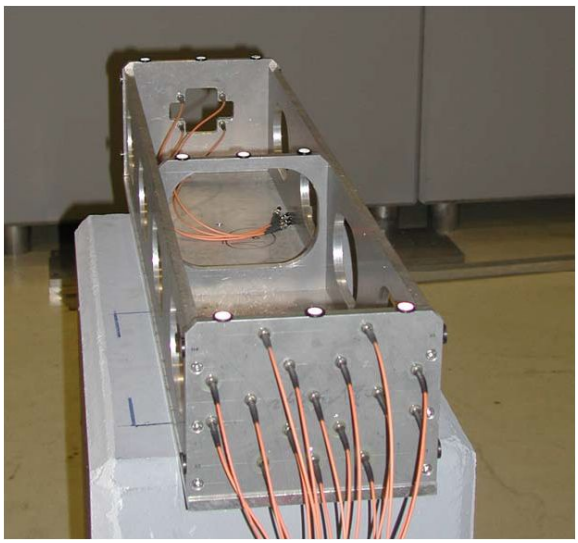

Figure 6.11. The mechanically assembled camera calibration bench with survey targets.

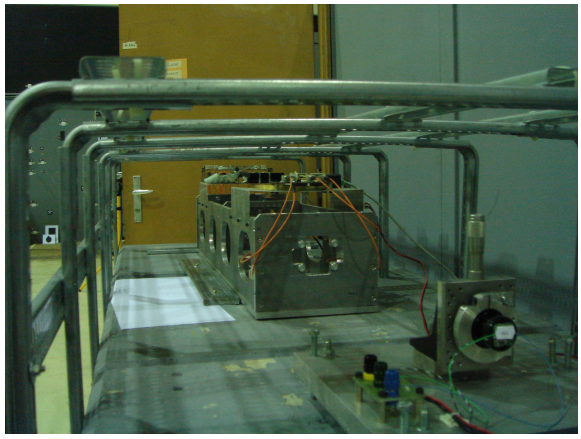

Figure 6.12. The camera calibration bench in operation.

The electronic part of the camera-box calibration bench is composed of two units connected to the main bench control PC via ethernet. The first unit is a microcontroller based card switching on and off the LEDs on the front and back plate of the bench. This type of unit called PIConNET was developed and produced by Atomki and the University of Debrecen and was also used during the 2006 magnet test of CMS in the surface hall [55]. The LED

current was optimized and fixed once and kept at the same value during the full period of the bench usage. The task of the second unit is to read out the camera images and calculate the centroid values. For this purpose a Board PC (subsection 4.3.5) was used.

I developed a JAVA-based software running on the main control PC to control the bench and automatize the measurement. The control panel in fig. 6.13 is showing the status after the measurement of the LEDs on the back panel.

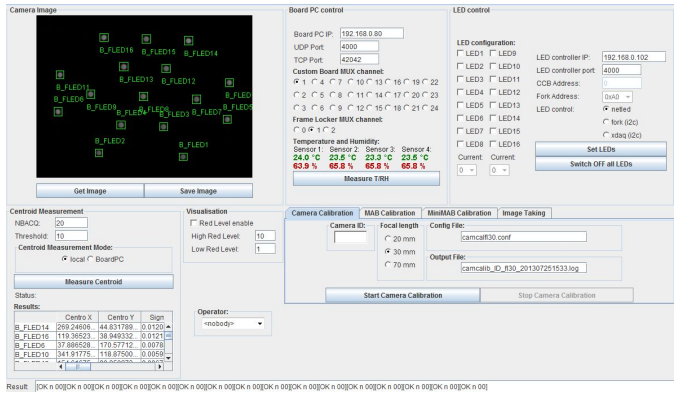

Figure 6.13. The control panel of the camera-box calibration, showing the status after the measurement of the camera-box No. 161 illuminated by the LEDs on the back panel.

6.5 Bench operation and results

The camera-box calibration bench was most intensively used in the period of 2004 to 2008 preceeding the MAB assembly. The bench itself is fully operational up to today and it was used several times after the CMS installation period to calibrate replacement camera-boxes.

The calibration of a camera-box is composed of the following steps:

- Fixation of the camera-box in the camera-box holder. No precision is required, e.g. the approximate orientation around the box-axis is sufficient.
- The front-LEDs are switched on (all at the same time) and 20 camera-images are recorded following the experience described in section 4.4.

– Then the back-LEDs are switched on (all at the same time) and 20 camera-images are recorded.

The measurement software is able to identify all LEDs on the recorded image and calculate their centroid values based on 20 avareged images according to the method described in subsections 4.4.2 and 4.4.3. The corresponding green boxes and the LED identification numbers are indicated on the control panel (fig. 6.13) to help in the work of the operator. The centroids are stored in the Barrel Muon Alignment Database.

The internal parameters of the camera-boxes are calculated offline using

– the COCOA model of the setup,

– the LED location data within the front and back panels obtained from the CERN metrology laboratory,

– the plate locatons w.r.t. each other obtained from the survey measurement of the bench,

– the centroids of the LED images obtained from the camera calibration measurement.

The results of the camera-box calibration are summarized in fig. 6.14, 6.15 and 6.16 using the example of the 30 mm camera-boxes.

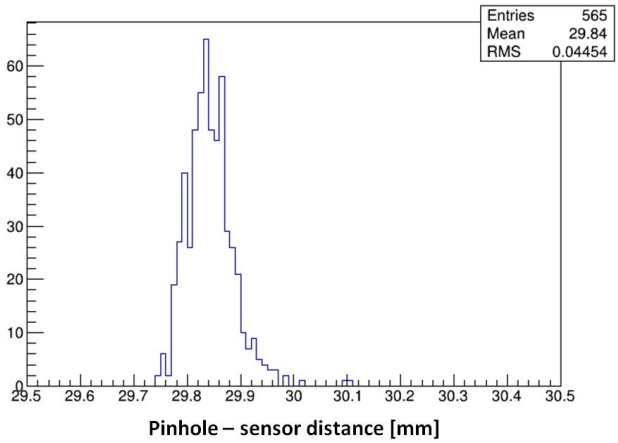

Figure 6.14. Histogram of the pinhole-sensor distances for the nominally f=30 mm camera-boxes.

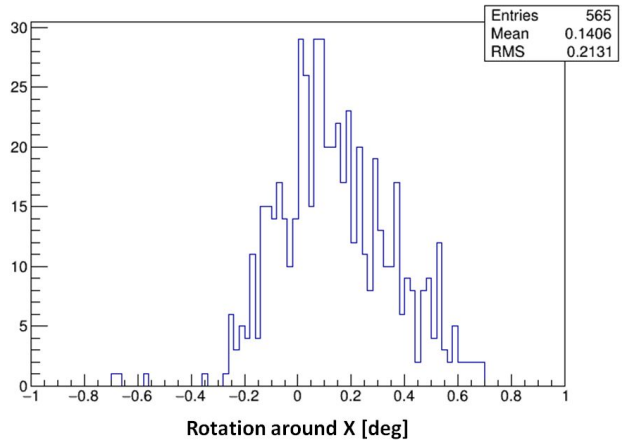

Figure 6.15. Histogram of the sensor rotations around the X-axis for the nominally f=30 mm camera-boxes.

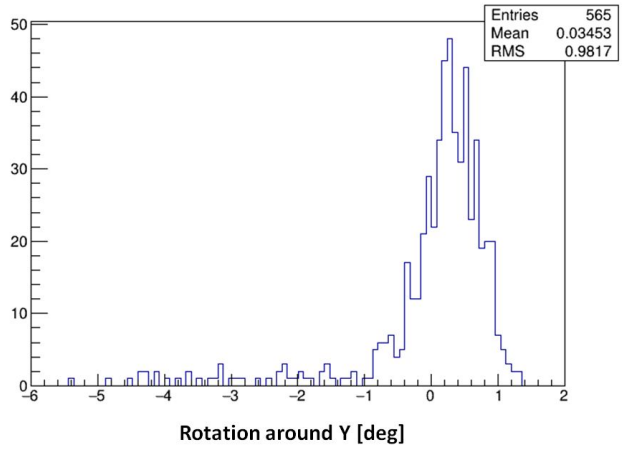

Figure 6.16. Histogram of the sensor rotations around the Y-axis distances for the nominally f=30 mm camera-boxes.

The conclusion is that the camera-boxes are suitable for the project (this is also valid for the boxes with other focal length). The precision of the camera-box production and assembly is in general more then sufficient for the project. The tail on the negative side of fig. 6.16 can be explained

-without going into details- by the technology of the assembly but even those cameras could be used.

Chapter 7

Calibration of the MABs

The MABs (subsection 4.3.3) are the camera-box holders in the Barrel Muon Position Monitoring System. During the MAB assembly the camera-boxes are fixed on the MABs and electrically connected to the MAB patch-panel. After this step the MABs are fully operational. The construction can guarantee the rigidity and stability of the assembled MABs but -as usual in this project- the precision of the knowledge of the camera-box positions and orientations are not sufficient. The task of the MAB calibration is to measure these parameters.

As we saw in section 6.2 the camera-box calibration setup is able also to measure the location and orientation of the camera-box in the calibration bench coordinates. In principle the same method can be used here as well. The difficulties come from the fact that the MAB is a large (about 4 m long) object containing from 9 to 17 camera-boxes to be calibrated w.r.t. a coordinate system attached to the MAB body. Also, the camera-box calibration bench was optimized to measure the internal parameters of the camera-boxes. In the case of the MAB calibration the aim is to optimize (maximalize) the precision of the location of the camera-boxes for which the internal parameters are already known.

In this chapter first we discuss the requirements then the design of the calibration setup and finally the operation of the bench and the results of the calibration.

7.1 MAB calibration requirements

In order to determine the necessary accuracy of the MAB calibration a COCOA simulation of the full position monitoring system has to be performed at different MAB calibration input data. This simulation permits us to study the accuracy of the determination of the chamber positions at different precisions of the MAB calibration. The simulation of the full system was performed at the early phase of the project [37] and concluded with the following result: in order to achieve the required precision of the position monitoring system the position and orientation of the cameras on the MABs have to be determined with <100 μm, <100 μrad accuracy.

7.2 Principle of the MAB calibration

As throughout this project there is no direct way to measure the locations and orientations of the camera-boxes with respect to the MAB body. Instead, an indirect method illustrated in fig. 7.1 has been proposed. The elements of the calibration bench are the MAB itself with mounted camera-boxes and a set of so-called calibration plates containing optical fiber etalon sources (used already for the camera-box calibration and described in section 6.3). The calibration plates are containing also photogrammetry targets for survey-measurements. The locations of light sources w.r.t the photogrammetry targets are measured in metrology laboratory with <5 μm accuracy. The MABs are also equipped with photogrammetry targets. The calibration steps are as follows:

- The photogrammetry targets of the MAB body are measured in the coordinate system of the calibration bench.
- The photogrammetry targets of the calibration plates are also measured in the coordinate system of the calibration bench.
- The images of the light sources are recorded by the camera-boxes.
- The 6D coordinates of the camera-boxes w.r.t the MAB body are calculated offline using the metrology lab measurement data, results of the photogrammetry measurements (MAB, plates), the internal parameters of the camera-boxes and the centroids of the the camera-box images taken from the light sources of the MAB calibration bench.

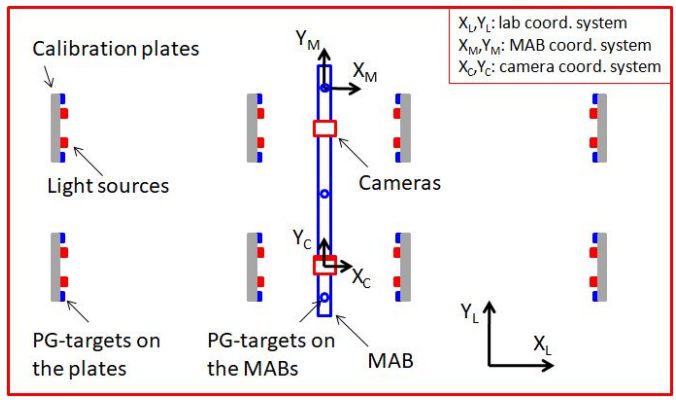

Figure 7.1. The principle of the MAB calibration (see text, PG = photogrammetry).

7.3 Design of the MAB calibration setup

The MAB calibration bench has been designed according to the principle discussed in 7.2. It was the result of a long optimization process that included several aspects:

- the required accuracy of the calibration,
- the bench rigitdity, stability and variability (the MABs are different in shape),
- logistical aspects (to bring in, fix and remove the MABs),
- give enough room for the photogrammetry measurements.

The photo of the bench constructed in the CMS Alignment Laboratory in one of the experimental halls of the CERN ISR ring is shown in fig. 7.2. The size of the bench is 11x7 m^2.

The metallic MAB fixation stand in the middle part can hold all the types of MABs: inner, outer, straight-shaped, croissant-shaped, left, right. The MABs are attached to the bench in the same stressless way as on the CMS wheels. The rest of the construction is fixed on concrete blocks.

The arrangement of the bench can be discussed using the schematic drawing in fig. 7.3. The drawing shows an inner MAB (with camera-boxes on both sides). The four camera-lines are corresponding to chamber stations 1 to 4. (In reality there are two camera-boxes at each station looking at the adjacent

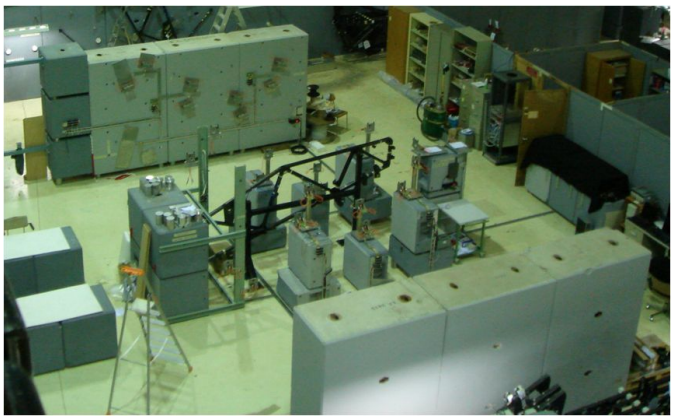

Figure 7.2. The overall picture of the MAB calibration bench built in the CMS Alignment Laboratory at the CERN ISR ring.

sectors.) There are four walls numberred as 000 to 300. Each of the walls contains calibration plates. Each camera-box is calibrated by two plates, one close and one far plate (fig 7.4) similarly to the camera-box calibration process. The close plates are located at 800 mm from the camera-boxes and contain 8 fiber etalon light sources. As the camera-boxes are rotated by + or -15 deg around the longitudinal axis of the MAB, usually 5 to 6 sources can only be seen and used for calibration, which is fully sufficient. The large hole in the centre of the close plate assures the visibility of the far plate located at 4000 mm distance from the close plate. The far plates contain four sources and their orientations follow the rotations of the camera-boxes.

As the camera-box locations for the three inner stations are identical for all the MABs this part of the bench is fixed permanently. The camera-box locations for the fourth station, however, are varying from MAB to MAB. Therefore this part is mobile, the plates can be mounted at several predetermined positions. As 24 (the so-called active) MABs are also containing Z-camera-boxes looking at the Z-bars, their calibration is performed by two additional (called Z) plate pairs (for left and right mounted MABs respectively).

As it has aready been mentioned the calibration plates contain survey holes to insert the targets for photogrammetry measurements. The plates equipped with photogrammetry targets are shown in fig. 7.4. The geometry of all the plates is precisely known as all the sources and survey holes had

been measured with <5 μm precision at the CERN metrology laboratory before their installation on the bench [38], [39].

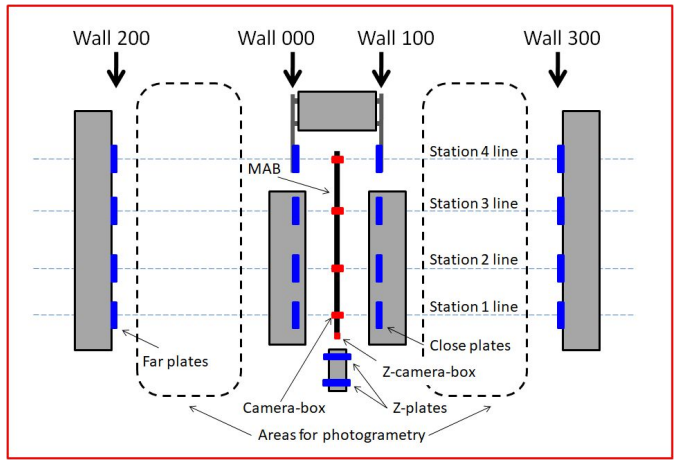

Figure 7.3. The schematic drawing of the MAB calibration bench.

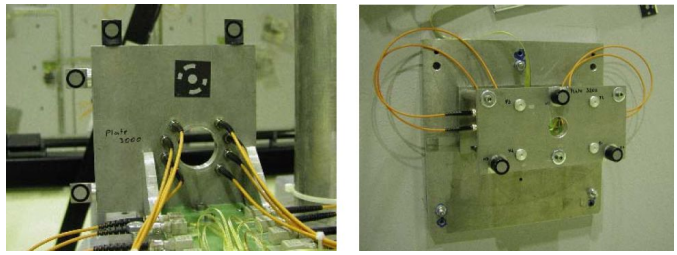

Figure 7.4. MAB calibration plates equipped with photogrammetry targets (left: close plate right: far plate)

The control and data acquisition for the full bench containing 16 close, 16 far and 4 z-plates (216 fiber etalon light sources altogether) and 9 to 17 cameraboxes to be calibrated was built according to the scheme shown in fig. 7.5. The concept is very similar to that for the camera-box calibration bench: the LEDs on the plates are switched on and off via PIConNET-s, the camera images are grabbed and the temperature sensors are read out by a Board PC. Therefore I adapted the DAQ and control software of the camerabox bench according to the needs of the MAB calibration task.

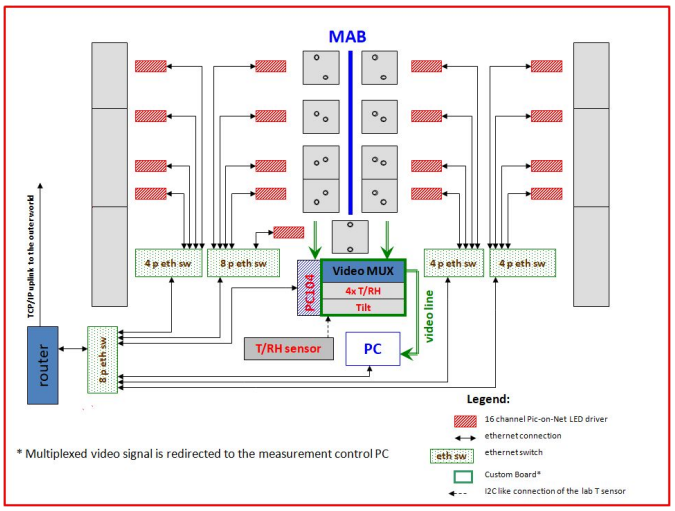

Figure 7.5. Schematic view of the MAB bench control and DAQ.

7.4 Accuracy of the calibration measurement

The achievable precision of the MAB calibration bench was simulated by COCOA. As the bench contains 16 identical branches it was enough to simulate only one of them.

The typical error of the photogrammetry measurement of a single target is 0.1mm per coordinate [40]. The precision of the knowledge of the internal parameters of the camera-boxes were already known (see chapter 6). These errors and the full geometry were indtroduced in the COCOA-model of the setup. The results of the simulation summarized in table 7.1 show that the designed calibration bench is fulfilling the requirements formulated in section 7.1.

7.5 Operation of the MAB calibration setup

The operation of the MAB calibration bench consists of the following steps:

- The MAB to be calibrated is mounted on the MAB stand and the cameras are connected to the DAQ system.
- The full bench (all the plates and the MAB body) are measured by photogrammetry.

Input:	
camera-box lens-sensor distance error	8 μm
camera-box sensor tilt error	3 mrad
Photogrammetry error	100 μm
Resulting accuracy:	
camera-box X;Y	<60 μm
camera-box Z	<250 μm
camera-box rotX, rotY	<75 μrad
camera-box rotZ	<150 μrad

Table 7.1. Simulation of the accuracy of the MAB calibration bench: input and results

- All the relevant LEDs are switched on one by one and the images are recorded by the cameras (20 images are taken from each LED following the experience described in section 4.4). It is a crucial point that both sides of the inner MABs are measured in the same bench and in a sigle step. This establishes a rigid connection between the two sides of the MAB.
- The photogrammetry measurement is repeated again to make sure that no movement occured during the camera operation step.
- The MAB is disconnected and removed from the bench.

The calibration of one MAB takes about 2-3 hours. The photogrammetry measurements and the camera images are evaluated and the camera-box positions and orientations w.r.t. the MAB body are calculated offline.

The first operation of the MAB calibration bench took place in 2006 when 12 MABs were calibrated [40]. The aim of the 2006 calibration campaign was twofold: to test the bench and the calibration method in practice and to provide several MABs for the 2006 magnet test performed in the surface experimental hall. The real calibration of the MABs were performed during the installation phase of the experiment in 2007 when all the 36 MABs were measured [41], [42]. The calibration constants are stored in the alignment database.

Chapter 8

System validation

The construction and installation of the Barrel Muon Position Monitoring System was completed in 2009 and the system was able to provide data since the first moment of CMS operation. The next logical step is to validate the system measurements i.e. make sure that the chamber positions provided by the system are corresponding to the real positions within the allowed error [60].

The best way to validate any measurement is to perform an independent, already validated measurement and compare the results. Fortunately there is such independent measurement available in CMS. Survey methods (briefly introduced in Appendix B) are widely used at CERN to measure the positions of elements in the accelerators and experiments. The survey measurement is a daily practice also at the CMS experiment during the installation and maintenance periods.

Unfortunately there are three limiting factors to be taken into account when considering to use these measurements as reference:

- The survey measurements are performed at open detector, on each wheel separately and often several months earlier then the CMS closure during which the wheels are moved and adjusted.

- The photogrammetry measurements are far from being complete due to lack of visibilitiy of one or another element (e.g. the measurement point is hidden under cables).

– The accuracy of the photogrammetry is not better then ±0.3 mm (in sigma) at such a large surface like a CMS wheel. For less visible points it might reach ±1 mm (see section 8.2).

Still, there are two possibilities to use the survey measurements for validation:

– The wheel YB0 is not moving so the positions of the DT chambers and MABs on this wheel remain the same before and after closure. Therefore the survey measurements at open detector can be used for comparison. Important remark: this is valid only until the first magnet operation. As for the MABs there is some danger that some of the MABs are touched between the survey measurements and the CMS closure (especially at the bottom part) but this can be detected when the MAB positions are compared. The details of the YB0 comparison are described in section 8.1.

– The DT chambers are no longer visible after the CMS closure. But the outer ends of the MABs can still be seen at least partially. A special study extending the validation beyond the wheel YB0 and based on the visibility of the outer parts of the MABs is described in section 8.2.

8.1 YB0 comparison

8.1.1 Validation with YB0 MABs

In the first calculation devoted to validation the MABs located on both sides of the wheel YB0 were used.

Each MAB contains survey reference target points that can be seen by photogrammetry. Initially five such points (schematically shown in fig. 8.1) were installed on each MAB and calibrated during the MAB calibration step. In the Long Shutdown 1 (LS1) period more target holders have been added. Their role will be discussed later in section 8.2.

Target point denoted as 7001 is the origo of the MAB coordinate system by definition. This point can directly be measured by Survey group and calculated by analysis, therefore this target point is best suitable for comparison.

There are 12 MABs installed on the wheel YB0. The origo points are well distributed over the YB0 wheel as it can be seen in fig. 8.2 a) where the

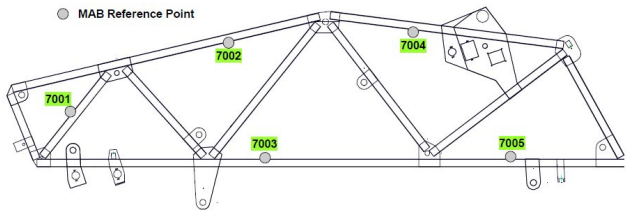

Figure 8.1. Survey reference points on the MABs.

origo point areas are shown by red circle. The MABs on the negative side are located at ∼2.5 m distance behind the ones shown in the figure.

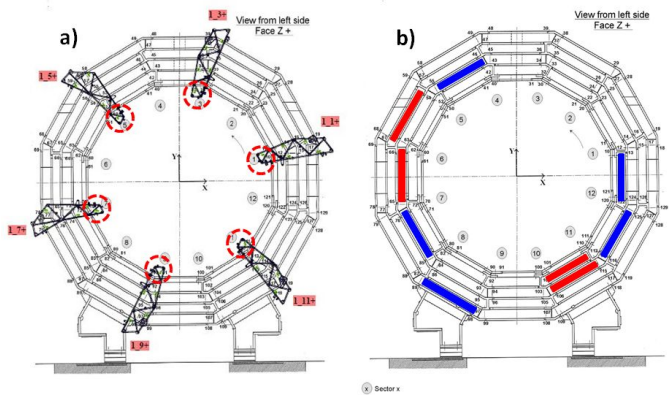

Figure 8.2. a) MABs on YB0 positive side. The areas of the MAB origo are marked with red dotted circle. b) Chambers included in the validation study. (Red: targets on the positive side, blue: targets on the negative side)

The survey measurements used for comparison were performed in the period between January 2008 and February 2009 ([43], [44]). Unfortunately two MABs (-1_3 and +1_3) could not be measured by Survey so finally 10 points were used for validation, 5 on each side of the wheel. This data was compared to the results of the run 152 of the Position Monitoring System. The run 152 took place on 8th July 2009 at 0T field, before the first turn on of the CMS magnet after the CMS closure.

To make the two sets of data for the MAB origo points directly comparable, first the Monitoring System data has to be transformed into the Survey data set using the least square criteria. This can be done in several ways, but in our case the COCOA tool offers a very simple and elegant solution

to find the coordinate transformation parameters for the best fit for the two data sets. The method is explained in more detail in Appendix C. After this step the two data sets are directly comparable and the residuals can be calculated.

The results of the YB0 MAB comparison are summarized in table 8.1.

MAB	X [mm]	Y [mm]	Z [mm]
1_1+	1.185	0.157	-0.249
1_5+	0.611	-0.633	-1.265
1_7+	-1.842	0.364	-0.041
1_9+	0.059	0.243	-0.195
1_11+	1.432	0.053	0.222
1_1-	0.180	0.723	-0.015
1_5-	0.648	-0.737	1.552
1_7-	-2.129	-0.423	-0.491
1_9-	-0.690	0.160	-0.286
1_11-	0.547	0.094	0.769
Sigma	1.201	0.459	0.751

Table 8.1. Residuals between the Position monitoring and Survey

The conclusions will be discussed in section 8.3.

8.1.2 Validation with YB0 chambers

A series of survey measurements performed during the LS1 between 2013 and 2015 [45] has given a new possibility to make the validation study more complete. The reasons to restrict this study to YB0 objects remained the same but this time several muon chambers were also measured by Survey that could be used for comparison.

During the survey measurements photogrammetry targets are inserted in the survey sockets of the barrel muon chambers as shown in fig. 8.3. In ideal case a chamber could be equipped with eight targets: four of them are seen from YB0 positive side the other four from the negative side. Unfortunately in most of the cases the number of usable targets was very limited. Finally only 28 targets could be used. There was no chamber seen from both sides as it can be deduced from fig. 8.2b) where the chambers participating in the validation study are shown. Chambers in red or blue indicate that the

targets could be seen from the positive or negative side only. Still, this quantity was enough to perform validity calculations.

Figure 8.3. Part of the barrel muion chamber equipped with a photogrammetry test-target.

For comparison with Survey the run 6325 has been chosen. This measurement was taken on the 16th of March 2015. It was the first complete run after the CMS closure but still before the first magnet operation. To make the analysis data directly comparable with Survey the chamber positions obtained from the analysis were recalculated using the chamber calibration data to locate the target points the same way as the Survey document does. Then the corner block positions obtained by the Monitoring System were fitted to the Survey data using COCOA and the residuals were calculated.

The results are presented in fig 8.4. The conclusions will be discussed in section 8.3.

8.2 Comparison at closed detector

Validation studies described in the section 8.1 were restricted to wheel YB0 measured by Survey at open detector. During the LS1 stop a joint project was launched in collaboration with the survey group to extend the validation to the full barrel and to try to perform both measurements at the same time. The idea was to create target points that could be observed by survey even after the CMS closure. Of course these new points had to be on object(s) that could also be measured by the Position monitoring system. The obvious choice was to install additional survey target holders on the outer part of the MABs.

All the 36 MABs were equipped with new outer survey target-holders (fig. 8.5) and calibrated w.r.t. the old ones during LS1.

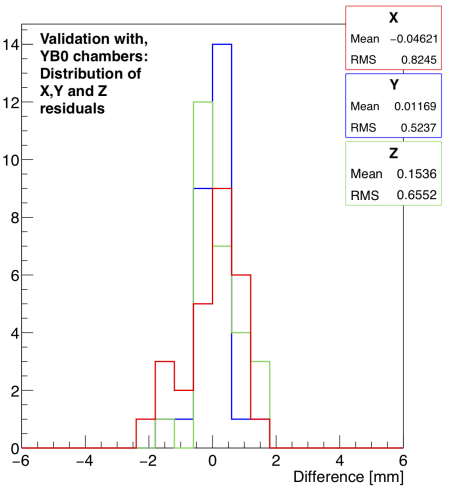

Figure 8.4. Comparison of YB0 chambers: histogram of the differences between analysis and survey.

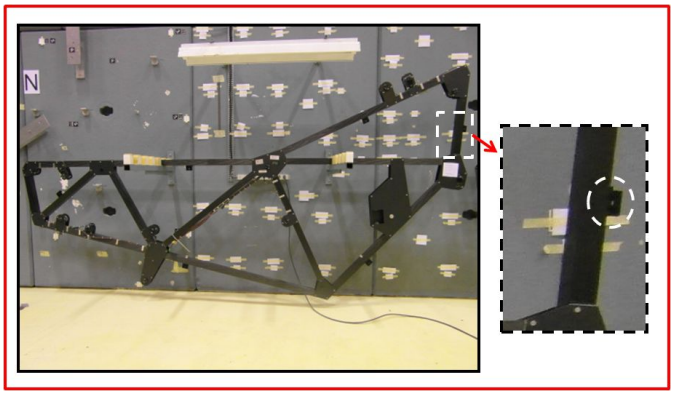

Figure 8.5. A croissant type MAB in the CMS alignment lab equipped with outer survey target holder.

Due to very limited visibility at closed CMS only part of the outer targets could be observed by Survey. The real situation is shown on fig. 8.6. Finally 16 targets could be seen at all by Survey and only 13 of them could be used for the validation calculations. The distribution of the measured points over the CMS barrel is shown in fig. 8.7.

The validation study followed the usual scheme:

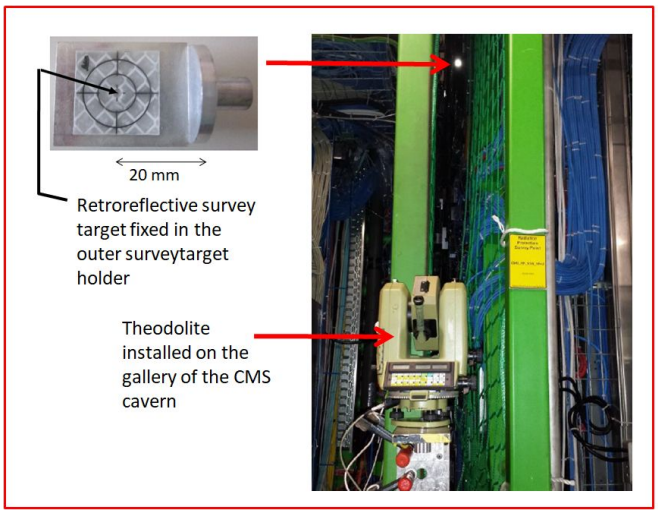

Figure 8.6. Visibility of an outer survey target at closed CMS.

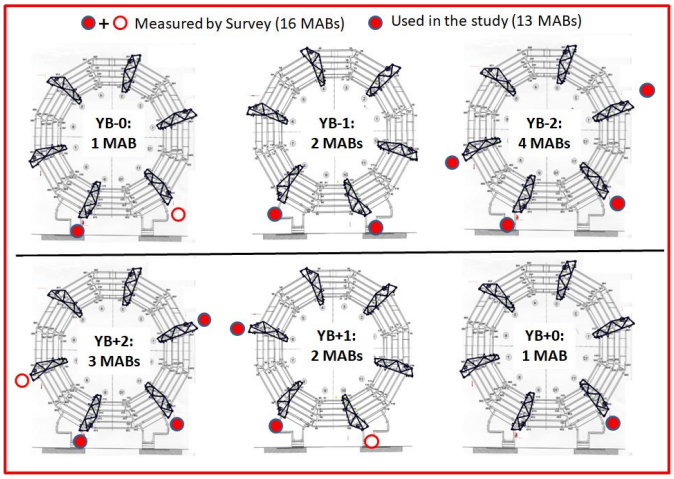

Figure 8.7. Distribution of the outer targets measured by Survey.

– Survey measurement: The outer targets were measured by Survey on the 16th and 17th June 2015 and reported in [47]. The accuracy of the survey measurement was ±1 mm in sigma as theodolite was used and the angle of visibility was very narrow.

– Run 6544 data: Run 6544 taken on 14 June 2015 has been chosen for comparison. During the three days between the data taking by the Monitoring System and Survey the CMS magnet was permanently off.

– Calculation of the outer target positions from analysis: This step is new compared to the procedure in subsection 8.1.1. There the origo-targets were compared and the positions of those targets are directly obtained from the analysis. In the present case the positions of the outer targets are calculated using the MAB origo, MAB orientation and the MAB calibration data.

– Best fit to survey: The analysis-points expressed in the analysys coordinate system are transformed in the Survey system.

– Calculation of residuals: The coordinates obtained by analysis and survey are compared.

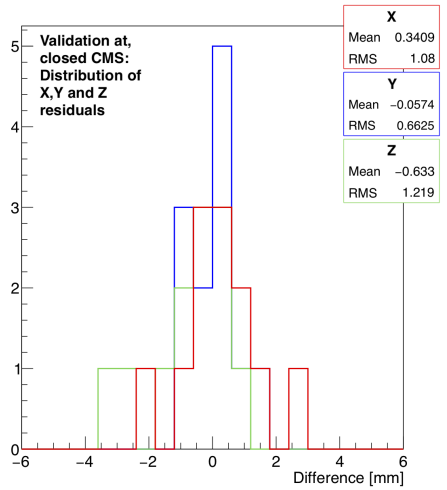

Figure 8.8. Comparison at closed CMS: histogram of the differences between analysis and survey.

The results are summarized in fig 8.8. The conclusions are discussed in section 8.3.

8.3 Validation: discussion and summary

In chapter 8 three studies have been described. The aim of these studies was to proove that the Barrel Muon Position Monitoring System is providing the correct positions of the Barrel muon chambers (and the MABs as byproduct). To obtain the real accuracy of the system an independent measuring tool which is at least one order of magnitude better in precision should have been used. However, the only available tool for comparison, the Survey measurement is in the same range of accuracy than the system to be validated. Therfore the conservative formulation of the aim was to show that the difference is not exceeding 1mm in sigma.

Though the studies were performed at different times and conditions, they can be treated as a single measurement. In total 51 points (153 coordinate values) well spread over the volume of the barrel muon system and located on different objects (MABs, chambers) were used. The summarized residual distributions are shown in fig. 8.9.

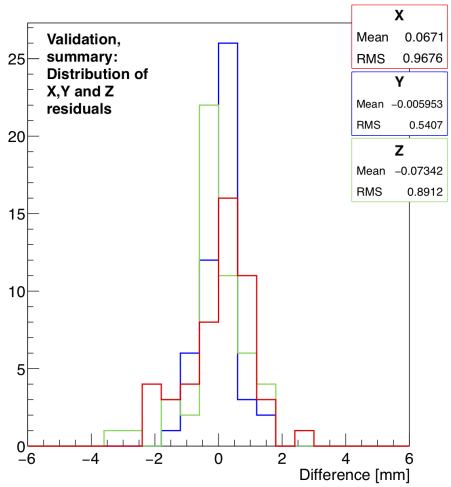

Figure 8.9. Histogram of the summarized differences between analysis and survey.

The calculated positions for all the 51 points (153 coordinates) are in excellent coincidence with the survey values for all the points. The standard deviations shown in the figures (0.97 mm in X, 0.548 mm in Y, 0.905 mm

in Z) can be regarded as conservative values characterizing the accuracy of the Barrel Muon Position Monitoring System.

These results are validating not only the system as a whole. They also validate the concept, the design (especially the sufficient degree of redundancy), all the calibration steps, the performance of the measurement, preparation of the raw data including the necessary quality control where each measured LED-image is carefully weighted and the data analysis including the opto-geometrical model of the system.

Chapter 9

Muon barrel spectrometer deformation studies

The primary function of the Barrel Muon Position Monitoring System is to provide data about the 6D positions of the barrel muon chambers. On the other hand, the evolution of the chamber positions with time and the comparison with the magnet operation or the variation of the enviromental parameters can help us to draw some conclusions about the behaviour of the barrel system as a mechanical unit [59].

In principle -knowing the barrel design- this behaviour could be simulated and calculated by standard methods like finite element analysis. It was done during the design and construction phase of the barrel wheels [11] at the level of necessity for the design. For submillimeter level of accuracy, however, all the input parameters (materials used, joints, map of the magnetic field, etc) would have been necessary to be known with high precision which is practically impossible not talking about the dynamics of the changes. Therefore the primary source to study the barrel construction is the data obtained by the Position Monitoring System.

In this chapter first the real and ideal positions are compared and the possible influence of the enviromental parameters is investigated. Then the behaviour of the barrel muon structure is analysed by comparison of data taken at different times and conditions.

9.1 Comparison of the ideal and real chamber positions

The ideal (or nominal) barrel muon system is a massless structure composed and assembled of elements with the designed dimensions without tolerance error. The expected deviation of the real structure from the nominal values was already studied during the design phase [11]. It was shown by finite element calculations that the wheel structures deform by several millimeters under influence of gravity alone (see fig. 4.1 for details) even if the other parameters (size of parts, accuracy of the assembly, etc) are ideal. The information about the expected deviation from the ideal (nominal) position was used in subsection 4.1.1 to determine the required range of measurements for the Barrel Muon Position Monitoring System. As the wheels are the support structures of the barrel muon chambers the wheel deformations have primary impact on the chamber positions. On the other hand, measuring the real chamber positions and comparing them to the nominal positions the wheel deformations can be measured.

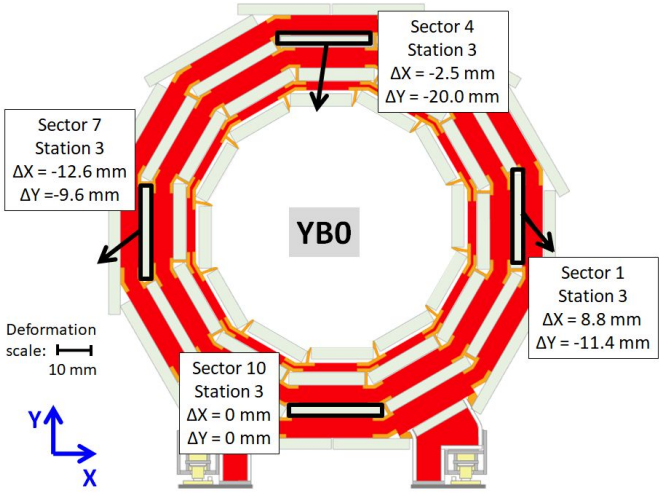

Figure 9.1. Chamber shifts in YB0 due to wheel deformation (the scale of the deformation is indicated in the drawing).

To see the difference between the nominal and real positions of the barrel muon chambers the station 3 chamber origos were compared. The nominal values are taken from the design database, the real chamber positions are the results of run 6382 taken at 3.8 T on the 21st of March 2015. The

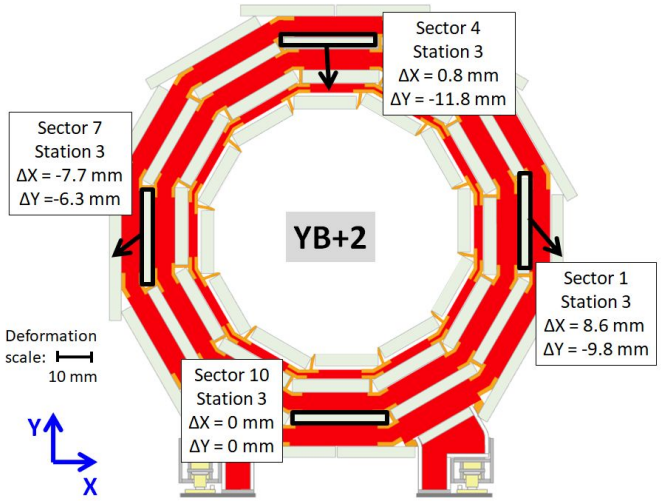

Figure 9.2. Chamber shifts in YB+2 due to wheel deformation (the scale of the deformation is indicated in the drawing)

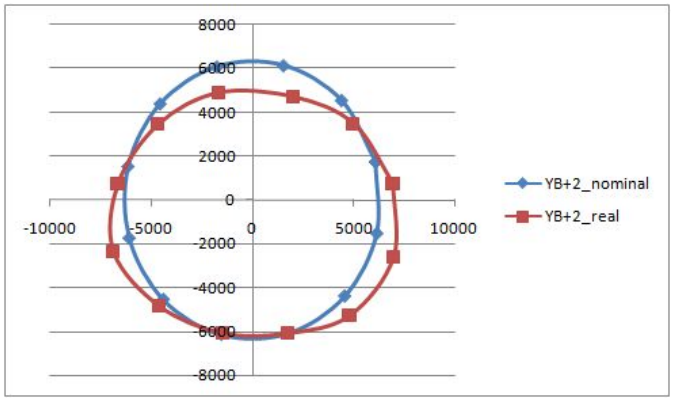

Figure 9.3. Comparison of the real and nominal MS3 chamber positions on the YB+2 wheel. The differences are enlarged by a factor of 100 for better visibility.

two data sets were fitted to each other in a way that the bottom chamber (chamber in sector 10 station 3) firmly supported by the wheel feet was regarded as fixed (free from deformation).

The difference between the nominal and the real positions of the DT chamber origos for the sectors 1, 4, 7, 10 of the central (YB0) and the

YB+2 wheels are shown in figs 9.1 and 9.2. A more complete picture of the deformation for the YB+2 is given in fig 9.3 where the differences are enlarged by a factor of 100 for better visibility.

Comparing figures 9.1, 9.2 and 9.3 to fig. 4.1 we see that the wheel deformation is roughly twice as much as that calculated by the finite element analysis for the gravity alone. The left-right asymmetry follows the asymmetry of the wheel design.

9.2 Influence of the enviromental parameters

During the CMS design and construction the preliminary calculations including the cavern geometry, the ventillation, the heat produced by the electronic devices and the efficiency of different cooling systems could not exclude high (8-10 ^{o}C) temperature differences between the bottom and top part and considerable humidity variations during the operation. Large temperature changes cause termal dilatations in the DT chambers made largerly of aluminium with dilatation coefficient of 26 μm/m/degree. For the largest (4190 mm wide) chambers at the MB4 station 10 degree change can lead to dilatation of $\sim$1 mm which is comparable with the required precision of the Position Monitoring System. The humidity changes do not affect directly the precision of the Barrel Muon Position Monitoring System as the MAB material chosen is not too sensitive to humidity unless the relative humidity is reaching extreme (close to saturated) values for very long time (several months) but it should be made sure that this does not happen.

As it was mentioned in subsection 4.3.3 the MABs are equipped with Temperature and Relative Humidity (T&RH) sensors. These sensors (4/MAB, located near the DT chambers) are producing a quite detailed map of the T and RH parameters in the full volume of the barrel muon system. As an example, a snapshot taken on the 4th of November 2009 is shown in figs 9.4 and 9.5.

In figs 9.6 and 9.7 the change of the enviromental parameters can be seen during one year running period (between two winter shutdows) in 2010.

From these pictures we can deduce the conclusion that the enviromental changes can cause small but measurable deformations [57] that remain below the level of the requested accuracy of the position monitoring system.

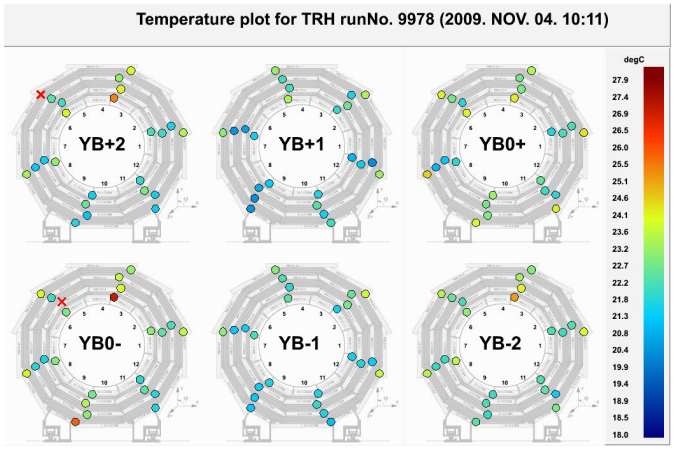

Figure 9.4. Example of the Temperature distribution in the CMS barrel muon region measured by the T&RHsensors on the MABs (4th November 2009).

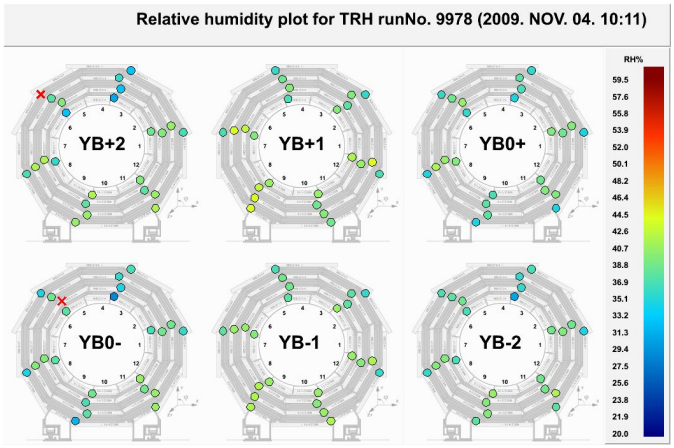

Figure 9.5. Example of the Relative Humidity distribution in the CMS barrel muon region measured by the T&RHsensors on the MABs (4th November 2009).

9.3 Z-bar measurements

As it was discussed in subsection 4.2.2 the Z-bars are performing a direct measurement of the shift of the outer wheels along the beam direction w.r.t. the central wheel caused by the magnetic field. In fig. 9.8 the magnet

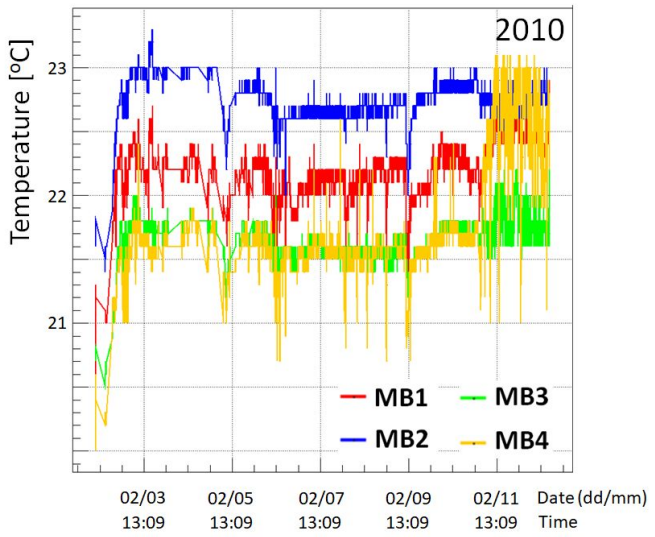

Figure 9.6. Yearly change of the Temperature measured on the MAB+3_11 in 2010

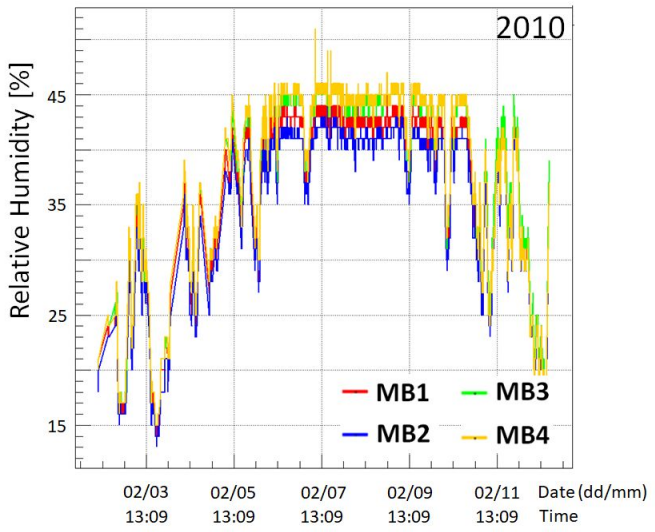

Figure 9.7. Yearly change of the Relative Humidity measured on the MAB+3_11 in 2010

current is shown during the first few days of the run period in 2010 (18000 A corresponds to 3.8 T). The related shifts for wheels YB+/-2 measured

by the 12 Z-bars are given in fig. 9.9. In fig. 9.10 the observed shifts during the whole 2010 run containing several magnet cycles are shown.

The barrel compression was already observed during the 2006 magnet test for the bottom part of the barrel which was equipped to test the hardware alignment system [51]. After the completion of the system the effect was observed and measured for the whole barrel [52].

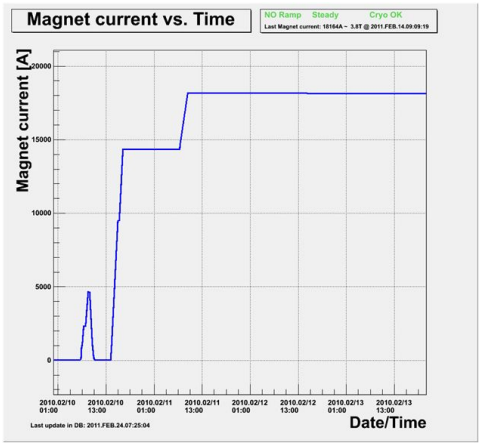

Figure 9.8. The magnet current during the first days of the run period in 2010 (18000 A corresponds to 3.8 T).

Already at the first glance it can be seen that the order of magnitude of the shifts is few (1 to 5) mm. This value is exceeding the tolerable uncertainity and has to be taken into account during the physics analysis. A closer look to the figures can lead us to several interesting and important conclusions:

- The shift during the first magnet operation is in general larger than the shifts during the running period ("nonelastic" shift).

- The shifts are following the changes of the magnet current (more exactly the changes of the magnetic field) during the run period. The wheels are returning to the previous values after the change of the magnetic field ("elastic" behaviour).

- The wheel positions in Z are quite stable if there is no change in the magnetic field.

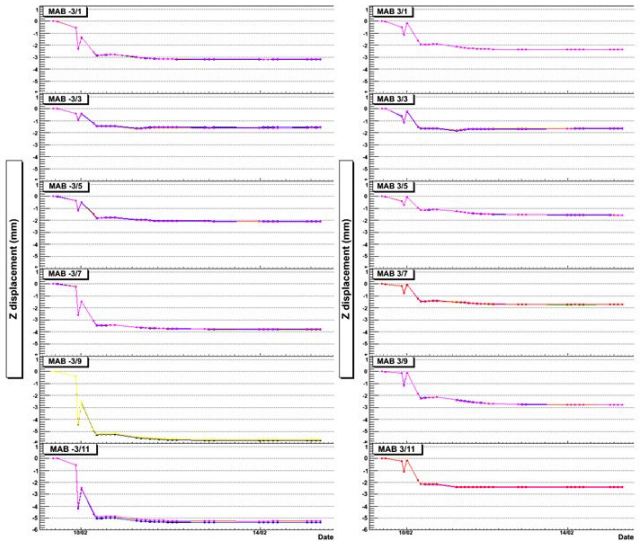

Figure 9.9. Shifts of the outer wheels measured by Z-bars during the first days of the run period in 2010.

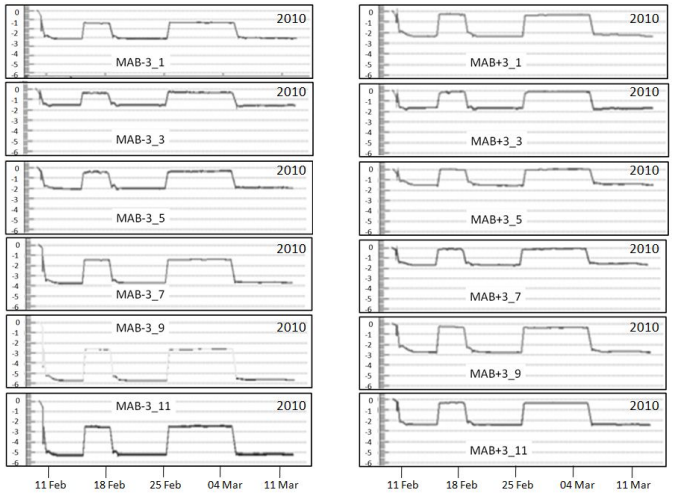

Figure 9.10. Z-bar measurements during the whole run period in 2010.

9.4 Chamber part measurements

Studies described in this section are based on the comparison of the barrel muon chamber positions measured at different times and conditions. In

most of the cases it is enough to compare the chamber origos not taking into account the angular positions. Still, the number of data to be compared is large and it is not easy to demonstrate the studied effects. In this section we characterize the changes by the mean value and the standard deviation of the differences between the runs compared.

9.4.1 Statistical error of the measurement

The statistical error of a measurement or of a measuring tool can be determined by the standard deviation of a series of measurements performed on the same object. In our case the object to be measured is the entire barrel muon spectrometer and a single measurement lasts about two hours. During this time the movement of the elements cannot be excluded but in stable conditions the changes remain small and the differences between two consecutive measurements are dominated by the statistical error of the measurement.

To study the statistical error in the sense described above two pairs of measurements were compared. For the first pair runs 8359 and 8360 have been chosen. The run 8359 started on the 10th of August 2017 at 14:16:08 and ended at 16:28:40. The run 8360 started immediately (at 16:29:01) and ended at 18:42:30. For the second pair runs 8362 and 8363 have been chosen. The run 8362 started on the 13th of September 2017 at 12:49:55 and ended at 15:17:10. The run 8363 started immediately (at 15:17:33) and ended at 17:23:50. The results are summarized in table 9.1.

Runs compared		X [mm]	Y [mm]	Z [mm]	Rot_X [mrad]	Rot_Y [mrad]	Rot_Z [mrad]
8360 vs 8359	Mean	0.048	-0.018	-0.014	-0.002	0.011	0.002
	Sigma	0.090	0.062	0.086	0.038	0.043	0.074
8363 vs 8362	Mean	-0.019	-0.024	-0.059	-0.001	-0.002	-0.010
	Sigma	0.077	0.046	0.061	0.017	0.042	0.105

Table 9.1. Mean values and standard deviations of the 6D coordinate differences between results of two pairs of successive runs.

As an example the distribution of the differences in X coordinate for the runs 8359 and 8360 is shown in fig. 9.11.

Based on the results we can state that the statistical error of the measurements of the chamber 6D positions are in the order of <0.1 mm

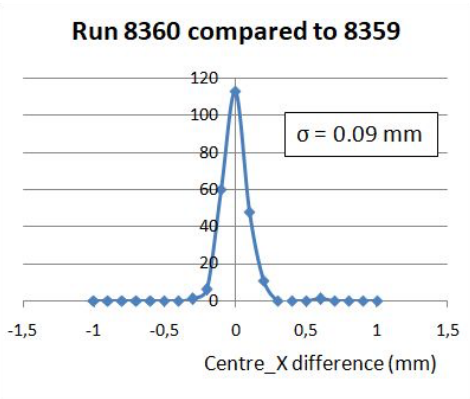

Figure 9.11. Distribution of the differences in X coordinate for the runs 8359 and 8360.

in translation and <0.1 mrad in rotation. This result becomes important for the studies described in the following subsections as all of them are based on comparisons of different runs. In these comparisons the systematic errors are dropped out so any differences above the mentioned statistical errors are significant for the given study.

9.4.2 Precision of the CMS closing procedure

During the longer shutdown periods the CMS detector is opened for maintenance (see section 2.2). At the end of the shutdown the detector is closed again and the large barrel and endcap modules are locked to each other. Though this procedure is controlled by survey and additional measuring tools, and executed with millimeter accuracy, the new position will surely differ from the previous opening-closing. The achievable accuracy of the closing procedure is demonstrated by comparing runs 6149 and 6325.

The run 6149 was taken on the 11th of April 2014 during the Long Shutdown 1 (LS1) period when the detector was closed for a magnet test. After the magnet test the positive side of CMS was partially opened again. In the barrel part only the wheel YB+2 was opened, the rest remained closed. The detector was fully closed again at the end of LS1. After the closure of YB+2 a survey measurement was performed to locate the wheel in the CMS system and check the difference between the old and new YB+2 positions [46], [48]. The run 6325 was taken on 16th of March 2015 at fully closed detector before the first magnet operation.

The results of the comparison of the two runs are presented in table 9.2. The comparison procedure is not trivial and needs some explanation. In the case of the survey both measurements located the YB+2 wheel in the same (global CMS) coordinate system so the results could directly be compared and shown in row 1 named "Survey". On the contrary, the monitoring system is using a coordinate system fixed to one of the elements so they can slightly differ from run to run. Therefore first the results of run 6325 have to be fitted to run 6149 and then the differences can be compared. The final result is shown in row 2 named "Monitoring".

As the new position of wheel YB+2 different, the chamber positions will also differ. The question is whether the difference is caused by the wheel movement only or the chambers were also moving relatively to the wheel and each other during the opening-closing. To get the answer the chamber positions in YB+2 obtained by run 6325 were directly fitted to those of run 6149. The results are shown in table 9.3.

	Mean	X [mm]	Y [mm]	Z [mm]	rotX [mrad]	rotY [mrad]	rotZ [mrad]
Survey	Mean	1.5	-0.7	-0.2	0.010	0.010	-0.440
Monitoring	Mean	1.886	-0.583	0.068	0.010	0.014	-0.430

Table 9.2. Position differences of the YB+2 wheel between two different CMS-closings.

	X [mm]	Y [mm]	Z [mm]
Mean	-0.006	-0.003	-0.003
Sigma	0.174	0.136	0.094

Table 9.3. Mean values and standard deviations of the differences between results of runs taken after two different CMS closings: fitted YB+2 chamber center comparison (see text)

Several conclusions can be deducted from the table:

– In the investigated case the wheel YB+2 was repositioned with a difference of ∼+1.8 mm in X and ∼-0.6 mm in Y w.r.t. the previous closing. Also, the rotation difference around the CMS Z (the CMS-axis) is showing the limits of the accuracy of the shimming at the CMS-feet. The repositioning in Z and the two other rotations are more accurate due to the fixed Z-stops between the wheels.

– The good agreement between the survey and monitoring measurements is an additional validation of the monitoring system.

– The chamber positions remained stable during the wheel movement. This fact leads us to the assumption that the chamber position changes in CMS are due to the wheel movements rather then the local movements of the chambers themselves.

9.4.3 Stability inside one magnetic cycle

The behaviour of the barrel muon system during a single full field period is very important from the point of view of the applicability and precision of the track based alignment as the system stability during the collection of the track used for alignment is essential. In the table 9.4 a comparison of two runs (8346 and 8364) performed at 3.8 T at different times but still inside the same magnetic cycle is shown. The run 8346 was taken on the 8th of July 2017, the run 8364 more than two months later, on the 13th of September 2017.

	X [mm]	Y[mm]	Z[mm]
Mean	0.002	-0.011	0.005
Sigma	0.133	0.120	0.117

Table 9.4. Mean values and standard deviations of the 3D differences between chamber origos of two runs inside the same magnetic cycle. The two runs compared (8346 and 8364) are separated in time by 97 days.

As it was already seen in section 9.3 the sytem can be considered stable in the Z-direction. The results of the comparison presented in table 9.4 are extending the validity of this statement to X and Y directions as the changes are close to the measurement accuracy. Chamber position differences exceeding the statistical error are real -though little- movements due to thermal and mechanical stress effects causing small inelastic deformations in the barrel structure.

9.4.4 Behaviour between magnetic cycles

During the run period the magnet is switched on and off several times. It is important to know how the elements of the system are moving and if they are returning to the same position when the magnetic field is back again. The Z-bar measurements (in section 9.3) have already shown that the

outer wheels are returning to the Z-position they occupied at the previous "magnet on" period.

To check the validity of this statement for X and Y two runs (8312 and 8346) were compared. The run 8312 was taken on the 7th of May 2017 at 3.8 T during the first magnetic cycle of the 2017 run period. The run 8346 was taken at 3.8 T on the 8th of July 2017 during the second magnetic cycle (this run was already used for comparison in subsection 9.4.3.)

The results of the comparison are shown in table 9.5.

	X [mm]	Y[mm]	Z[mm]
Mean	0.037	0.016	0.002
Sigma	0.245	0.187	0.210

Table 9.5. Mean values and standard deviations of the chamber coordinate differences between results of runs taken at 3.8 T in two different magnetic cycles.

Looking at the numbers we can deduce that the chambers are basically returning to the positions they occupied during the previous magnetic cycle. The standard deviations are still small but higher then in the case of the comparison inside the same magnetic cycle (see table 9.4). This fact shows that the wheel movements in Z during the field changes might generate small but measurable irreversible movements in X and Y directions.

9.5 Muon barrel spectrometer deformation studies: conclusions

In this chapter different studies concerning the behaviour of the Barrel Muon Spectrometer are described. The results can be summarized as follows:

- The real form of the barrel wheels is different from the designed (ideal) shape. The difference (shrinking in height, expansion on the sides) is roughly twice as much as the value predicted by finite element analysis during the design of the magnet.
- The statistical error of the chamber positions measured by the Position Monitoring System can be characterized by the standard deviation of the differences between two consecutive runs. This value is in the order of 100 μm for translations and 100 μrad in rotation.

Standard deviations exceeding these values are results of real chamber displacements.

- The accuracy of the CMS closing procedure is at the mm level in X and Y.
- At the first magnet operation after closure the barrel wheels are moving towards the IP (interaction point). This movement can reach up to several mm-s for the outer wheels.
- During the consecutive magnet cycles the wheels are moving in Z but roughly returning to the position they occupied at the previous cycle.
- The positions of the chambers in the Barrel Muon spectrometer can be regarded as stable inside a magnetic cycle (when the field is permanently on). Very small displacements are possible most probably due to thermal effects. Consecutive magnetic cycles are causing slightly bigger displacements but the chambers are remaining in positions close to those during the previous magnetic cycle.

It should be noted that the statements in the previous list are describing the global behaviour of the Barrel Muon Spectrometer using the standard deviations of the positions of 250 chambers measured in two compared runs. This was the aim of the studies described in this chapter. The displacements of some chambers are obviously exceeding the level of the standard deviations and can reach the value already important for physics analysis. Therefore the exact positions of all the chambers are permanently measured, recorded and provided to the CMS community.

Summary

The aim of the present document was to describe my work on the position monitoring (called also alignment) system of the Barrel Muon Spectrometer of the CMS experiment located in the P5 experimental hall of the CERN LHC accelerator. The task of this system is to permanently measure the 6D positions of 250 large scale barrel muon chambers distributed over a huge (14 m long, 14 m in diameter) cylinder with submillimeter and submilliradian accuracy. The position data provided to the CMS community is used for corrections during physics analysis.

This very complex and innovative position monitoring system which is the result of a teamwork lasting more than ten years was introduced (chapter 1) and reviewed at the necessary detail in chapters from 2 to 4. The subsequent chapters describing the work in which my contribution was determinative could be devided into three parts. The first part presented my activity on the construction of the system (chapters 5, 6 and 7). Once the construction had been completed the next task was to validate the full system (chapter 8). Finaly, data supplied for the CMS experiment allowed us to study the behaviour of the barrel muon structure during different phases of operation (chapter 9).

During the construction the first work performed under my responsability was the quality control and selection of the videosensors used in the camera-boxes, which are the active elements in the chamber position measurements. The task involved the measurement of the following parameters:

– the gain uniformity (in other words the fluctuation of the gain from pixel to pixel at homogenous illumination),

– the dark current (in other words the detected signal for each pixel when there is no illumination),

– the defected pixels (in other words the number and position of pixels with zero or maximum output independently of the incident light).

– Establish the criteria for selection of sensors as “passed” and “to be rejected”.

This task was solved in the following way:

– As the first step these error sources were studied by simulation and the criteria for the tolerance against these factors were formulated.

– As the second step a calibration bench was constructed to measure these parameters for each sensor. The construction of the bench and the DAQ and data storage allowed us to measure a large quantity (over 700) sensors.

– As the third step all the sensors were measured and the measured data evaluated.

– As the fourth step sensors fulfilling the criteria formulated during the first step were selected for further usage.

The second task was the calibration of the assembled camera-boxes. The reason of this step was the need to determine the internal parameters of the boxes (lens-sensor distance and the perpendicularity of the videosensors to the optical axis of the camera-box) with the precision (<10 μm and <3 mrad respectively) that could not be guaranteed by production. Here the approach was similar to that at the first task. First the required accuracy was studied and determined. Then the calibration bench was designed and constructed. Finally the calibration measurements were performed and the data stored in the CMS Alignment database.

The third task was the calibration of the assembled MABs. During this step the 6D positions of the camera-boxes had to be measured in the MAB coordinate system using the already measured internal parameters of the camera-boxes. Here again the method used was similar to the previous tasks, taking, however, into account the logistic aspects of the large objects to be calibrated and handled. After the definition of the requirements the bench was constructed and then all the 36 MABs calibrated. The calibration results were stored in the CMS Alignment database.

The fully installed Barrel Muon Position Monitoring system became operational in 2008 and was able to provide position data. The system is very complex and the output data is the result of an opto-geotmetric

calculation of a large quantity (above 30000) input parameters consisting of calibration constants and measurements. In other words, the result is obtained in a quite indirect way. Therefore it is very important to validate the system, i.e. carefully check the output results. This work was done by comparison of the results with direct position measurements provided by the CERN-Survey group. Three different studies were performed. Altogether 51 points (153 coordinates) were compared and the standard deviations were below 1 mm for the differences between the two independent measurements. Taking into account the errors of both measurements the agreement is convincing and we can declare the system validated.

The system is operational up to today and providing position data to CMS. So far more that 8000 runs (full measurements) have been performed. Beyond the primary task this large quantity of data also allowed us to perform special studies to understand the behaviour of the barrel muon system as a mechanical unit. These targeted studies have led us to the following conclusions:

- Comparing the nominal (ideal, designed) and real muon chamber positions it was shown that the difference due to gravity is twice as much as the value predicted by an early finite element analysis but still remains in the tolerable range. It was also shown that the closing procedure of the CMS barrel is in the mm range but correctly detectable by the monitoring system. Both conclusions could be directly verified also by Survey measurements providing another evidence of the system validity.

- Comparing two consecutive alignment runs it was shown that the statistical error of the measurements is below 0.1 mm and 0.1 mrad.

- Analysis of the environmental (temperature and relative humidity) sensors have shown that the change of these parameters are not exceeding the measurable but small (not relevant for physics) level.

- The Z-bar measurements have shown that after the shutdown maintenance the barrel system is shrinking at the first magnet operation and the movement of the wheels can reach several mm-s.

- Important conclusion is that the barrel muon system is stable during the period when the magnetic field is present. When the field is off the position changes but the barrel chambers are basically returning to the positions when the magnet is back again. Small (submillimeter)

deviations are detected. The most probable reason of these deviations is the nonelastic deformation at the numerous joints of the system due to the inter-cycle movements and thermal effects.

Összefoglalás

A dolgozat célja a CERN LHC gyorsítójának P5-ös pontjában telepített CMS kísérlet Barrel Müon Spektrométere helyzet meghatározó rendszerével kapcsolatos munkám ismertetése volt. Ennek a rendszernek a feladata a hatalmas (14 m hosszú, 14 m átmérőjű) hengerben elosztott 250 nagyméretű barrel müon kamra 6D pozíciójának folytonos mérése milliméter és milliradián alatti pontossággal.

Ennek a nagyon bonyolult és innovatív helyzetmeghatározó rendszernek, amely egy munkacsoport több, mint tízéves munkájának az eredménye, a bevezetés (1. fejezet) után a szükséges mélységű leírása található a 2-4. fejezetekben. A következő fejezetek, amelyeknek anyaga a saját munkámra támaszkodik, három részre tagolható. Az első rész a rendszer építésével kapcsolatos munkámat ismerteti (5., 6. és 7. fejezet). Az építés befejezése után a következő feladat volt a teljes rendszer hitelesítése (8. fejezet). Végül, a CMS kísérlet részére szolgáltatott adatok lehetővé tették, hogy tanulmányozzam a barrel müon rendszer viselkedését az üzemelés különböző fázisaiban (9. fejezet).

Az építés során az első saját feladatom a müonkamra pozíció mérés aktív elemeinek, a kamera-dobozok video-szenzorainak a minőségellenőrzése és a megfelelő szenzorok kiválasztása volt. Ez a feladat a következő paraméterek mérését jelenti:

- az erősítés egyenletességét (más szóval az erősítés fluktuációját celláról cellára homogén megvilágítás mellett),

- a sötétáram mértékét (más szóval a mért jelet minden cellában, megvilágítatlan szenzor esetén),

– a hibás cellákat (más szóval azoknak a celláknak a számát és helyét, amelyek nulla vagy maximum kimenő jelet adnak a megvilágítástól függetlenül),

– felállítani és számszerűsíteni azokat a követelményeket, amelyek alapján a szenzorok szelekcióját el lehet végezni az alkalmazhatóság szempontjából.

A feladatot a következőképpen oldottam meg:

– Első lépésként szimulációval tanulmányoztam ezeket a hibaforrásokat és megállapítottam a tolerálható mértékek határait.

– Második lépésként megterveztem és kiviteleztem a szenzorok mérésére szolgáló laboratóriumi berendezést. Az eszköz kialakítása és a kapcsolódó adatgyűjtő és adatrögzítő rendszer lehetővé tette a nagy mennyiségű (>700) szenzor megmérését.

– Harmadik lépésként megmértem az összes szenzort és kiértékeltem a mérési eredményeket.

– Negyedik lépésként az előre megállapított kritériumok alapján kiválogattam azokat a szenzorokat, amelyek megfelelőnek bizonyultak a további felhasználásra.

Második feladatom az összeszerelt kamera-dobozok kalibrálása volt. A kalibrációt az tette szükségessé, hogy a gyártás és összeszerelés folyamata nem tudta garantálni a kamera-dobozok belső paramétereinek (lencse-szenzor távolság, illetve a szenzor merőlegessége a kamera-doboz tengelyéhez képest) kellően pontos ismeretét (<10 μm, illetve <3 mrad). A megoldás ebben az esetben is hasonló volt az első feladathoz. Először a pontossági követelményeket tanulmányoztam és határoztam meg. Ezután megterveztem és kiviteleztem a mérési eszközt. Végül elvégeztem a kalibrációt és a mérési adatok bekerültek a CMS pozíció mérési adatbázisába.

A harmadik feladat a kamera-dobozokat hordozó struktúrák, az úgy nevezett MAB-ok kalibrációja volt. Itt a kamera-dobozok 6D koordinátáit kellett meghatározni a MAB koordinátarendszerében felhasználva a kamera-dobozok már megmért belső paramétereit. A módszer ezuttal is hasonló volt az első két feladatnál alkalmazott eljáráshoz, figyelembe véve a kalibrálandó eszközök nagy méretéből adódó logisztikai és kezelhetőségi igényeket. A követelmények meghatározása után a mérési elrendezés kialakítása és a

36 MAB kalibrálása következett. Az eredmények a CMS pozíció mérési adatbázisába kerültek.

A teljesen felépített barrel müon helyzetmeghatározó rendszer 2008 óta üzemképes és szolgáltatja a mérési adatokat. A rendszer rendkívül összetett és a kimenő adat egy opto-geometriai számítás eredménye, amely nagy mennyiségű bemenő (30000 feletti kalibrációs és mérési) adatra támaszkodik. Más szóval a végső eredmény eléggé indirekt módon jön létre. Ezért nagyon fontos a rendszer hitelesítése, azaz a kapott eredmény gondos ellenőrzése. Ezt a feladatot a kimenő adatoknak és a CERN-i földmérő csoport által szolgáltatott direkt méréseknek az összehasonlítása útján végeztem el. Három különböző módszert követve összesen 51 mérési pont (153 koordináta) hasonlítottam össze és a szórás 1 mm alatt volt a két független mérés között. Figyelembe véve mindkét mérés hibáit megállapítottam, hogy az egyezés meggyőző és a rendszer hitelesítettnek tekinthető.

A rendszer jelenleg is működik és adatokat szolgáltat a CMS számára. Eddig több, mint 8000 teljes mérés történt. Ez a nagy adatmennyiség az elsődleges feladaton, a müonkamrák helyetének meghatározásán túl lehetővé tette azt is, hogy tanulmányozzam a barrel müon rendszernek, mint mechanikai egységnek a viselkedését. Ezeknek a célorientált vizsgálatoknak az alapján az alábbi következtetéseket vontam le:

- Összehasonlítva a nominális (ideális, tervezett) és a valóságos müonkamra pozíciókat megmutattam, hogy a gravitáció okozta különbség kétszer nagyobb, mint amit a tervezés korai szakaszában a végeselem számítások mutattak, bár a különbség még így is a tolerálható határon belül marad. Megmutattam, hogy CMS bezárási eljárás pontossága a mm-es tartományban van, de egyértelműen mérhető a rendszer által. Mindkét következtetést direkt földmérési módszerekkel is kimérték, ez akár egy további hitelesítésnek is tekinthető.

- Összehasonlítva két közvetlenül egymás után következő teljes mérés eredményeit megmutattam, hogy a rendszer statisztikai hibája 0,1 mm és 0,1 mrad alatt van.

- A rendszerbe beépített környezeti (hőmérsékleti és relatív légnedvességi) szenzorok adatainak elemzésével megmutattam, hogy ezeknek a paramétereknek a változása jól mérhető elmozdulásokat

okoz, ezek mértéke azonban alatta marad a fizika számára lényeges értékeknek.

– Z-rudak mérései alapján arra a következtetésre jutottam, hogy a leállások és javítások után az első mágneses ciklus alatt a barrel zsugorodása következik be, amelynek mértéke néhány mm nagyságrendü.

– Igazoltam, hogy a barrel müon rendszer stabilnak tekinthető egy mágneses cikluson belül. A mágnes kikapcsolásakor a pozíciók megváltoznak, de a következő bekapcsoláskor a müonkamrák nagyjából visszatérnek az előző mágneses ciklus alatti helyzetbe, bár kis mértékű (szubmilliméter nagyságú) eltérések kimérhetőek. Ennek valószínű okai a rendszert alkotó vaselemek számos csatlakozási pontjában a ciklusközi mozgások okozta rugalmatlan deformáció és hőmérsékleti hatások.

Acknowledgements

Firstly I would like to thank for his extraordinary support of my supervisor Dr. György Bencze.

I am grateful for their continous support for the Muon Barrel Position monitoring project of the CERN-Survey group: Christian Lasseur, Jean-Christoph Gayde, Antje Behrens, Aurelie Maurissett, Raphael Goudard and many other surveyors who participated.

I would like to thank for their collaboration to my colleagues at the project: Dr. Zoltán Szillási, Dr. Péter Raics, Dr. József Molnár, Dr. Balázs Ujvári, Zsolt Szabó and many other technicians, engineers and physicists at Institute for Nuclear Research (Atomki) and University of Debrecen.

I would like to express my appreciation for their continous support of the project at CERN: Dr. Austin Ball (CMS technical coordinator) and Dr. Wolfram Zeuner (CMS deputy-technical coordinator), Mokhtar Alidra and Alexander Kurenkov and their team.

I am also grateful for the support at the administrative steps of my PhD defense process: Dr. László Oláh, Dr. Dóra Sohler, Dr. Beáta Király, Erzsébet Leiter.

The Muon Barrel Position monitoring project was supported by OTKA T034910, T043145, NK67974, NK81447, K109803 and K129058 grants

Bibliography

[1] http://www.cern.ch

[2] http://home.cern/topics/large-hadron-collider

[3] https://home.cern/about/experiments/atlas

[4] https://home.cern/about/experiments/lhcb

[5] https://home.cern/about/experiments/alice

[6] M. Della Negra *et al.* [CMS Collaboration], "CMS: The Compact Muon Solenoid: Letter of intent for a general purpose detector at the LHC", CERN-LHCC-92-03, CERN-LHCC-I-1.

[7] S. Chatrchyan *et al.* [CMS Collaboration], "The CMS Experiment at the CERN LHC", JINST **3** (2008) S08004. doi:10.1088/1748-0221/3/08/S08004

[8] G. L. Bayatian *et al.* [CMS Collaboration], "CMS Physics : Technical Design Report Volume 1: Detector Performance and Software", CERN-LHCC-2006-001, CMS-TDR-8-1.

[9] Widely available popular descriptions:
http://home.cern/about/experiments/cms
https://en.wikipedia.org/wiki/Compact_Muon_Solenoid

[10] CERN. Geneva. LHC Experiments Committee [CMS Collaboration], "The CMS muon project : Technical Design Report", CERN-LHCC-97-032, CMS-TDR-3.

[11] G. Acquistapace *et al.* [CMS Collaboration],
"CMS, the magnet project: Technical design report",
CERN-LHCC-97-10.

[12] G. Charpak and F. Sauli,
"Multiwire Proportional Chambers And Drift Chambers",
Nucl. Instrum. Meth. **162** (1979) 405.
doi:10.1016/0029-554X(79)90726-2

[13] G. Cerminara,
"The Drift Tube System of the CMS experiment",
Nucl. Phys. B Proc. Supp. **172** (2007) 71.
doi:10.1016/j.nuclphysbps.2007.07.016

[14] J. Frangenheim ,
"Measurements of the drift velocity using a small gas chamber for monitoring of the CMS muon system",
Diploma work at RWTH, Aachen, 2007.

[15] M. Aalste *et al.* [RD5 Collaboration],
"Measurement of hadron shower punchthrough in iron",
Z. Phys. C **60** (1993) 1.
doi:10.1007/BF01650426

[16] C. Albajar *et al.* [RD5 Collaboration],
"Electromagnetic secondaries in the detection of high-energy muons",
Nucl. Instrum. Meth. A **364** (1995) 473.
doi:10.1016/0168-9002(95)00474-2

[17] C. Albajar *et al.* [RD5 Collaboration],
"Measurement of momentum and angular distribution of punchthrough muons at the RD5 experiment",
Nucl. Instrum. Meth. A **386** (1997) 421.
doi:10.1016/S0168-9002(96)01014-5

[18] R. H. Lee,
"Simulation and study of the CMS endcap muon alignment scheme",
PhD thesis at the Purdue University, IN, USA, 2002.
doi:10.2172/1420955

[19] A. Calderón,
"Construcción, calibracirón y evaluacrón del sistema Link de

Alineamiento del Espectrrómetro de Muones del Experimento CMS", PhD thesis at the University of Cantabria, Santander, Spain, 2006 (in Spanish, with English summary)

[20] F. Matorras, T. Rodrigo,
"Measurement of muon pT in CMS and alignment errors in the barrel region",
CMS TN/94-210, 1995

[21] F. Matorras *et al.*,
"Influence of intrinsinc and alignment errors of MS on muon P_T measurement",
CMS TN/94-249, 1995

[22] F. Matorras, A. Meneguzzo,
"Requirements on the alignment errors of MS based on muon P_T resolutions",
CMS TN/95-069, 1995

[23] Z. Szillási,
"Kísérleti eszközök fejlesztése a nagyenergiájú fizika számára",
PhD thesis at the Debrecen University, Debrecen, Hungary, 2007 (in Hungarian, with summary in English)

[24] Stanley FH1011 data sheet:
http://datasheet.octopart.com/FH1011-Stanley-Electric-datasheet-5319793.pdf

[25] VV5402 video-sensor data sheet from Vision Ltd:
http://pdf.datasheetcatalog.com/datasheet/VLSIVisionLimited/mXsqqzu.pdf

[26] PC/104 embedded consortium:
PC/104 specification version 2.6 (2008)
http://pc104.org/wp-content/uploads/2015/02/PC104_Spec_v2_6.pdf

[27] C. F. Bedoya *et al.*,
"Electronics for the CMS muon drift tube chambers: the read-out minicrate",
IEEE Transactions on Nuclear Science **52** (2004) 1309.
doi:10.1109/NSSMIC.2004.1462440

[28] L. Brunel,
"SIMULGEO - Simulation and reconstruction software for opto-geometrical systems",
CMS note 1998/079, CERN, 1998

[29] P. Arce,
"COCOA - CMS Object-oriented Code for Optical Alignment",
http://cmsdoc.cern.ch/cms/MUON/alignment/software/COCOA/doc/cocoa.html

[30] P. Arce, A. L. Virto,
"CMS Object oriented Code for Optical Alignment (COCOA)",
CMS internal note, CMS IN 2002/060, CERN, 2002

[31] L. Brunel *et al.*,
"Performance test of the first prototype of 2 ways video camera for the Muon Barrel Position Monitor",
CMS note 1998/016, CERN (1998)

[32] Gy. L. Bencze *et al.*,
"Double camera test for the CMS muon barrel position monitoring system",
CMS note 2000/049, CERN (2000)

[33] V. Veszprémi,
"Helyzetmeghatározó rendszer fejlesztése és tesztelése a CERN-i CMS kísérlet müondetektorához",
Diploma work, Debrecen, 2000 (in Hungarian)

[34] N. Béni,
"Helyzetérzékeny detektorok vizsgálata - A CERN CMS müondetektor optikai pozicionáló rendszer elemeinek fejlesztése, építése, kalibrációja",
Diploma thesis, Debrecen, 2004 (in Hungarian)

[35] HFBR-1414T product description and parameters
http://www.alldatasheet.com/datasheet-pdf/pdf/112117/HP/HFBR-1414T.html

[36] J. F. Fuchs *et al.*,
"CMS Alignment camera-box bench",
EDMS document No.703522, 2006
https://edms.cern.ch/document/703522/1

[37] L. Brunel,
"CMS Simulation of the Full Barrel Muon position monitoring system",
Unpublished work, the results presented in internal workshops

[38] D. Pugnat,
"Close Plate Metrology",
EDMS document No. 702183, 2006
https://edms.cern.ch/document/702183/1

[39] D. Glaude,
"Far and Z Plate Metrology",
EDMS document No. 804150, 2006
https://edms.cern.ch/document/804150/1

[40] A. Behrens *et al.*,
"CMS - ISR: MAB Calibration, Photogrammetric measurements Campaign 1: MAB_001 – MAB_012",
EDMS document No. 732397, 2006
https://edms.cern.ch/document/732397/1

[41] A. Behrens *et al.*,
"CMS - ISR: MAB Calibration, Photogrammetric measurements Campaign 2: MAB_013 – MAB_024",
EDMS document No. 732397, 2007
https://edms.cern.ch/document/732397/1

[42] A. Lippitsch *et al.*,
"CMS - ISR: MAB Calibration, Photogrammetric measurements Campaign 3: MAB_025 – MAB_048",
EDMS document No. 847500, 2007
https://edms.cern.ch/document/847500/1

[43] J. Maillefaud, R. Goudard, A. Maurisset,
"CMS barrel yoke YB0, Muon chambers, HBs, OVT and MAB coordinates",
EDMS document No. 836406, 2008
https://edms.cern.ch/document/836406/2

[44] R. Goudard, J. Maillefaud
"CMS barrel yoke YB0 Z- and Z+ sides photogrammetry muon chambers and MABs coordinates",
EDMS document No. 1012370, 2009
https://edms.cern.ch/document/1012370/1

[45] A. Maurisset *et al.*
"CMS – YB0 photogrammetry of the MABs and of the DT mouns chambers on Z-/Z+ sides",
EDMS document No. 1489857, 2014
https://edms.cern.ch/document/1489857/1

[46] A. Maurisset *et al.*
"CMS - YBs position of YB0, YB+/-1, YB+/-2 after closure"
EDMS document No. 1447137, 2014
https://edms.cern.ch/document/1447137/1

[47] A. Maurisset *et al.*
"CMS - MABs - Measurement of the MABs visible survey targets with CMS closed",
EDMS document No. 1521004, 2015
https://edms.cern.ch/document/1521004/1

[48] A. Maurisset *et al.*
"CMS - YBs position of YB+/-2 after magnet test and closure of YB+2 closure",
EDMS document No. 1476500, 2015
https://edms.cern.ch/document/1476500/1

[49] H. M. Durand,
"Large Volume Metrology challenges in particle accelerators",
Presented at the LUMINAR Workshop 18-19 May 2016. held at the National Physical Laboratory, Teddington, TW11 0LW, UK. under the EMRP (European Metrology Research Programme)
http://projects.npl.co.uk/luminar/news-events/20160518-19_end_workshop/05-cern.pdf

[50] S. Chatrchyan *et al.* [CMS collaboration],
"Alignment of the CMS muon system with cosmic-ray and beam-halo muons",
JINST **5** (2010) T03020
doi:10.1088/1748-0221/5/03/T03020

[51] S. Chatrchyan *et al.* [CMS Collaboration],
"Aligning the CMS Muon Chambers with the Muon Alignment System during an Extended Cosmic Ray Run",
JINST **5** (2010) T03019
doi:10.1088/1748-0221/5/03/T03019.

[52] S. Chatrchyan *et al.* [CMS Collaboration],
"Commissioning of the CMS Experiment and the Cosmic Run at Four Tesla",
JINST **5** (2010) T03001
doi:10.1088/1748-0221/5/03/T03001

[53] S. Chatrchyan *et al.* [CMS Collaboration],
"The Performance of the CMS Muon Detector in Proton-Proton Collisions at $\sqrt{s} = 7$ TeV at the LHC",
JINST **8** (2013) P11002 doi:10.1088/1748-0221/8/11/P11002

[54] D. Novák, A. Fenyvesi, J. Molnár, G. Székely, J. Végh, N. Béni, A. Kapusi, P. Raics, Zs. Szabó, Z. Szillási, Gy. L. Bencze,
"Integration study and first test results of the CMS Muon Barrel Alignment system",
10th Workshop on Electronics for LHC and Future Experiments, Boston, MA, USA, 13 - 17 Sep 2004, pp.264-267 (CERN-2004-010)
doi:10.5170/CERN-2004-010.264

[55] G. Székely, Gy. L. Bencze, J. Imrek, J. Molnár, D. Novák, P. Raics, Zs. Szabó, Z. Szillási,
"PIConNET Based Distributed System dedicated to Magnet Test of the CMS Muon Barrel Alignment",
11th Workshop on Electronics for LHC and Future Experiments, Heidelberg, Germany, 12 - 16 Sep 2005, pp.419-421 (CERN-2005-011)
doi:10.5170/CERN-2005-011.419

[56] G. Székely, Z. Szillási, Gy. L. Bencze, N. Béni, J. Imrek, J. Molnár, D. Novák, P. Raics, Z. Szabó,
"Data acquisition and management in the calibration processes of the CMS Barrel Muon Alignment system",
12th Workshop on Electronics For LHC and Future Experiments, Valencia, Spain, 25 - 29 Sep 2006, pp.525-528 (CERN-2007-001)
doi:10.5170/CERN-2007-001.525

[57] Gy. L. Bencze, N. Béni, J. Imrek, J. Molnár, D. Novák, P. Raics, V. Sass and Z. Szabó, G. Székely, Z. Szillási,
"Results and consequences of magnet test and cosmic challenge of the CMS barrel muon alignment system",
Topical Workshop on Electronics for Particle Physics, Prague, Czech Republic, 03 - 07 Sep 2007, pp.407-410 (CERN-2007-007)
doi:10.5170/CERN-2007-007.407

[58] N. Béni, J. Palinkás, P. Raics, Zs. Szabó, Z. Szillási, G. Christian, J. Imrek and J. Molnár, D. Novák, G. Székely, Gy. L. Bencze "Completion of the muon barrel alignment system and its integration into the CMS detector environment",
Topical Workshop on Electronics for Particle Physics, Naxos, Greece, 15 - 19 Sep 2008, pp.472-476 (CERN-2008-008)
doi:10.5170/CERN-2008-008.472

[59] N. Béni, on behalf of CMS experiment,
"Experiences with the Muon Alignment Systems of the Compact Muon Solenoid Detector",
Phy. Procedia **37**, (2012) 96-103
doi: 10.1016/j.phpro.2012.02.352

[60] N. Béni, Gy. L. Bencze, Z. Szillási, B. Ujvári "Validation of the Barrel Muon Position Monitoring System by N. Beni, Gy. Bencze",
CMS Detector Note CMS DN-2018/025

Appendix A

DT connection test

In this Appendix the calculations concerning the simple setup discussed in subsection 4.2.2 and shown in fig. 4.4 are explained in more detail. The same figure completed with the notation of the elements can be seen in fig. A.1.

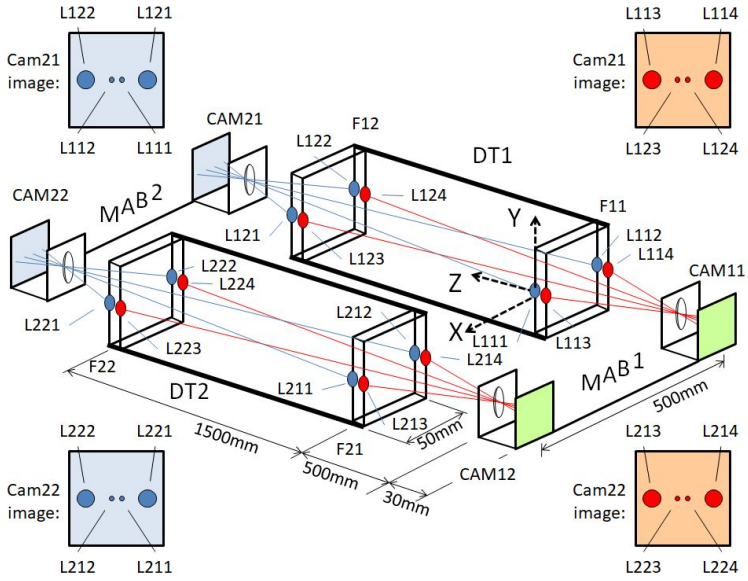

Figure A.1. Test setup to demonstrate the DT connection

As it was mentioned in subsection 4.2.2 the setup consists of four rigid elements: two DTs and two MABs. The DTs contain two forks with 4 LEDs

each (2 are seen from the left, 2 from the right). The MABs are equipped with 2 camera-boxes. The camera-box is a pinhole-sensor assembly. In the COCOA-input file the elements and their hierarchy are described in the COCOA System Tree Description of the COCOA input file:

SYSTEM_TREE_DESCRIPTION

object system setup
object setup 2 DT 2 MAB
object DT 2 fork
object fork 4 source
object MAB 2 cambox
object cambox pinhole sensor2D

Each object has its own coordinate system. The coordinate system of a complex object is determined through the embedded objects. For example, the DT1 coordinate system and the forks F11 and F12 determined in the following way:

The coordinate systems of the individual elements and and their relations are described in the SYSTEM_TREE_DATA of the COCOA input file. Also here the starting values of the 6D coordinates are defined. For example the fork F11 system is defined as follows:

The F11 origo is the L111 LED. The F11 X-axis is determined by LED 112 for which the Y and Z coordinates = 0. The orientation of the F11 Z-axis is defined by the LED113 which is laying in the X-Z plane (i.e. Y = 0 for this LED). The DT1 chamber coordinate system is defined by the F11 fork and the full setup is defined by the DT1 chamber.

The DT2 chamber is defined similarly but its 6D position in the setup is unknown and determined by the COCOA calculation from the calibrated constants and the camera-measurements.

In this example there is no real measurement data. Instead, the "simulation" option of the COCOA is used when the real measurement data is substituted by the value calculated by COCOA (the expected value following from the geometry of the setup).

The MAB1 (and analogically MAB2) coordinate system is defined by the camera-box CAM11, the box itself is by the pinhole, the sensor center and the orientation of the sensor rows and columns. The camera-box CAM12 and CAM22 are calibrated w.r.t the corresponding MAB. The 6D

coordinates for both MABs are unknown w.r.t. the setup and calculated by COCOA.

The calibration errors and the precision of the measurements (in other words the accuracy of the centroid definition) is given in the PARAMETERS section of the COCOA input file. The error-values used during the simulation of the setup are listed in table A.1. These error values are fully realistic and confirmed by the calibration and measurement practice.

Fork calibration errors, X;Y coordinates	100	μm
Fork calibration errors, Z coordinate	500	μm
Fork calibration errors, rotations	10	mrad
LED calibration errors, X;Y;Z coordinates	10	μm
Camera-box errors, X;Y coordinates	80	μm
Camera-box errors, Z coordinate	800	μm
Camera-box errors, X;Y;Z rotations	0.1	mrad
pinhole-sensor distance errors	10	μm
sensor tilt errors, X;Y rotations	3	mrad
Measurement precision	0.5	μm

Table A.1. Calibration and measurement errors used in the COCOA-simulation of the fig. A.1 setup

The technical details of the calculation exceed the frame of this description. The obtained results are summarized in table A.2.

Precision of the DT2 X coordinate	71	μm
Precision of the DT2 Y coordinate	170	μm
Precision of the DT2 Z coordinate	687	μm
Precision of the DT2 rotation around X-axis	0.11	mrad
Precision of the DT2 rotation around Y-axis	0.10	mrad
Precision of the DT2 rotation around Z-axis	0.86	mrad

Table A.2. The accuracy of the determination of the DT2 chamber position simulated by COCOA

The calculation is also providing the originally unknown MAB positions. The precision of the MAB positioning is given in tables A.3 and A.4 for MAB1 and MAB2 respectively.

Precision of the MAB1 X coordinate	39	μm
Precision of the MAB1 Y coordinate	38	μm
Precision of the MAB1 Z coordinate	240	μm
Precision of the MAB1 rotation around X-axis	0.07	mrad
Precision of the MAB1 rotation around Y-axis	0.07	mrad
Precision of the MAB1 rotation around Z-axis	0.29	mrad

Table A.3. The accuracy of the determination of the MAB1 position simulated by COCOA

Precision of the MAB2 X coordinate	141	μm
Precision of the MAB2 Y coordinate	148	μm
Precision of the MAB2 Z coordinate	518	μm
Precision of the MAB2 rotation around X-axis	0.08	mrad
Precision of the MAB2 rotation around Y-axis	0.07	mrad
Precision of the MAB2 rotation around Z-axis	0.437	mrad

Table A.4. The accuracy of the determination of the MAB2 position simulated by COCOA

Appendix B

Survey methods used in the project

The development and construction of the Barrel Muon Position Monitoring System (as the other muon alignment hardware subsystems as well) required a very close collaboration with the CERN Survey group from the beginnings to the completion and validation. Practically all the calibration steps are based on intensive use of survey methods. The task of the group is to perform large scale metrology measurements at the CERN accelerators and experiments including positioning, alignment, calibration and deformation/movement monitoring. These tasks require the most modern equipment and the knowledge of and pratice in a variety of contemporary metrology methods. A very good summary of the activity of the group can be found in [49].

In our project two methods were used, the laser tracker and photogrammetry. In this Appendix these methods are introduced very briefly.

Laser tracker was used to measure the fix installation and survey reference points in the calibration laboratories. This instrument is measuring distances and angles between points equipped with precision cornercube reflection target. The targets are put in precision target sockets allowing repositioning of the targets with micrometer precision. The sockets are part of the equipment to be measured and already considered at the design. Typical accuracy of the laser tracker measurement is 8 μm+3 μm/m in sigma giving $<$50 μm even at 10m distance. In fig. B.1 the LEICA AT 401 Laser tracker is shown with a set of targets and adaptors.

Figure B.1. The LEICA AT401 Laser Tracker in work in an experimental hall (left) and differet targets and adaptors (right).

The laser tracker is the best instrument to locate fix reference points in the lab or on the experimental setup and take an initial measurement of the survey network. In daily practice, whenever it is applicable, the photogrammetry was used. The principle is shown in fig. B.2.

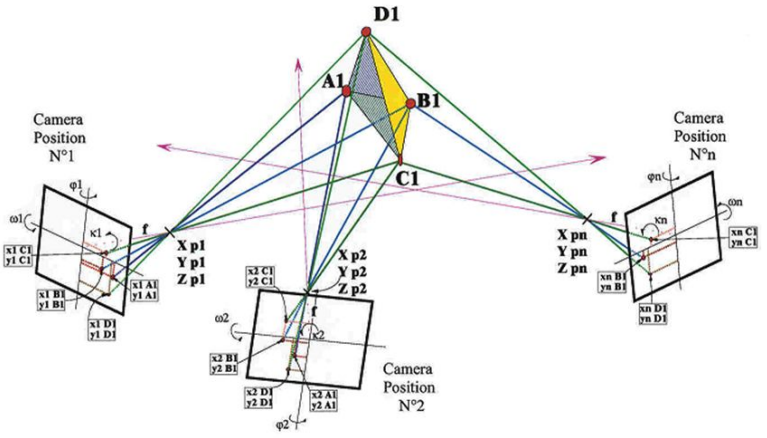

Figure B.2. Principle of photogrammetry (see text).

The task is to locate the A1, B1, C1, D1 target points on the setup. These points are equipped with retroreflective targets (fig. B.3). The setup is photographed from different directions by a camera specifically designed for metrology. The camera positions when the pictures are taken are irrelevant, they can be made by hand. The relative positions of the targets are calculated from the pictures. (As a byproduct, the camera positions are also computed.) The more the number of pictures, the higher the redundancy is so the accuracy is also increasing. The accuracy can also be increased if more points are measured. Therefore often secondary targets are added to the

setup during the photograqmmetry. The positions of these secondary targets are irrelevant, they just increase the degree of the connection network. For this purpose the coded magnetic target in fig. B.3 c) is very useful. The central part serves for the measurement itself, the peripherial ring is a code recognible by the photogrammetry data evaluation software and makes the identification of the same target on different pictures automatic.

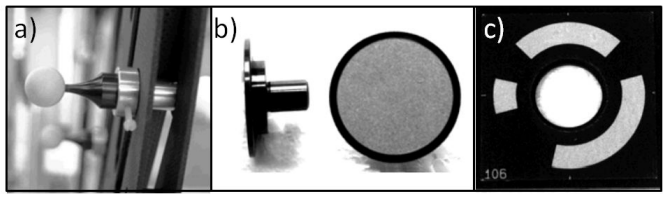

Figure B.3. Different retroreflective targets used for photogrammetry (see text).

The photogrammetry itself has no scale. It is measuring distances between points in 3D space in arbitrary unit. To give an absolute scale to the measurement a so called scale bar is added to the setup. The scale bar is a carbonfiber bar (to exclude thermal dilatation) with two retroreflective targets at precisely known distance between them.

In fig. B.4 The refelcted light on the photogrammetry targets during the MAB calibration are shown.

Figure B.4. The illuminated retroreflective targets during the MAB calibration.

Appendix C

Best fit method using COCOA

In chapter 8 the positions of the elements (chambers, MABs) of the Barrel Muon System are measured by two independent methods and the results are compared. The reference measurement (Survey in our case) is measuring n selected points from P1 to Pn (preferably spread over the system). The other measurement to be validated by Survey is the data provided by the Barrel Muon Position Monitoring System called in this Appendix as Monitor for simplicity.

For the comparison we select those points that are given also by Survey. As it is assumed (and required) that there is no movement between and during the two measurements, so that the muon barrel system is regarded as a rigid body characterized by n points measured twice. As a result we obtain two sets:

$$Pi_{\mathrm{s}}(X,Y,Z) \equiv (Xi,Yi,Zi) \quad and \quad Pi_{\mathrm{m}}(U,V,W) \equiv (Ui,Vi,Wi)$$

where (i=1,....,n), (X,Y,Z) and (U,V,W) are the coordinate systems in which the Survey and the Monitor results are expressed. These coordinate systems are fully independent. To be able to compare the two measurements the Monitor data has to be transformed in the Survey system fulfiling the commonly used least squarre criteria for which the value Q

$$Q = \sum_{i=1}^{n}[(Xi' - Xi)^2 + (Yi' - Yi)^2 + (Zi' - Zi)^2] \tag{C.1}$$

should be minimal, where

$$Pi_{\mathrm{m}}(X, Y, Z) \equiv (Xi', Yi', Zi')$$

is the i-th point of the Monitor data transformed into survey coordinate system. The parameters of the transformation are normally deduced from equation C.1.

In our case, however, the COCOA program opens a simple and elegant way to find the transformation parameters in one step without trying to solve any equation. To explain the idea we can refer to fig. C.1

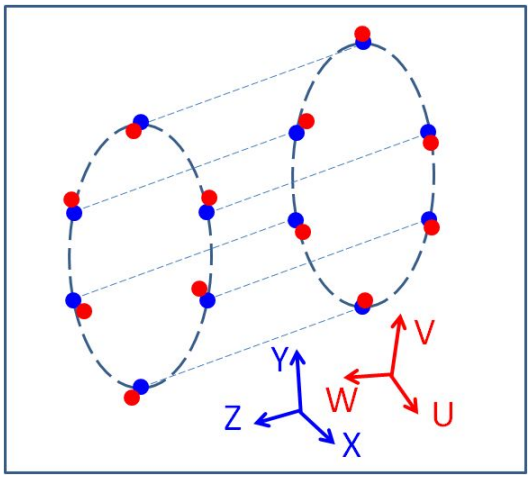

Figure C.1. Explanation to best fit.

The 12 nodes measured on the cylindrical object by Survey in the (X,Y,Z) and by the monitor in the (U,V,W) coordinate system. For simplicity we consider that the Survey measurement (blue points) perfect, the Monitor measurement (red points) is not. The COCOA model of this setup is as follows:

SYSTEM_TREE_DESCRIPTION

object system lab
object lab cylinder 12 survey_point
object cylinder 12 monitor_point
object survey_point 3 distancemeter1dim
object monitor_point 3 distance_target

As it can be seen, the survey measurements are represented by 12 independent points in the lab system called survey_point. They are set to FIX in the System_TREE_ DATA section of COCOA. We define the barrel as a rigid body called cylinder which is containing 12 monitor points. These points are FIX inside the cylinder but the cylinder itself is UNK in the lab. Each survey_point is equipped with 3 onedimensional distance meters (oriented in X, Y and Z directions respectively). Each monitor_pont is containing 3 onedimensional distance targets. In the MEASUREMENT section of COCOA the distancemeter - distance_target pairs are connected: the X-oriented meter and target of point P1 atc, 36 onedimensional measurements altogether. If both measurements were perfect then the measurement results would be zero for all the 36 cases. This is not the case but we declare the results of all the measurements as zero forcing the COCOA to find the position amd orientation of the cylinder in the lab that is closest to the ideal.

The result of the COCOA calculation is the translation and rotation to be performed with the Monitor data to fit to Survey.

Appendix D

Abbreviations used in the document

ATLAS - A Toroidal LHC Apparatus

ALICE - A Large Ion Collider Experiment

CERN - Conseil Européen pour la Recherche Nucléaire

COCOA - CMS Object-Oriented Code for Optical Alignment

CMS - Compact Muon Solenoid

DAQ - Data Acquisition

DT - Drift Tube

IP - Interaction Point

LHC - Large Hadron Collider

LHCb - LHC-beauty

LS1 - Long Shut down 1

MAB - Module for the Alignment of the Barrel

MS1 to MS4 - Muon Station 1 to Muon Station 4

P_T - transversal momentum

QC - Quality Control

RD5 - Research Development 5

USC - Underground Service Cavern

UXC - Underground Experimental Cavern

w.r.t. - with respect to

YB-2 to YB+2 - Yoke Barrel -2 to Yoke Barrel +2